AD-A121 448 ENGINEERING PROPERTIES OF CLAY SHALES REPORT 4 1/2
LABORATORY AND COMPUTATION..(U) ARMY ENGINEER WATERWAYS
EXPERIMENT STATION VICKSBURG MS D A LEAVELL ET AL.
UNCLASSIFIED SEP 82 WES/TR/S-71-6-4 F/G 8/13 NL

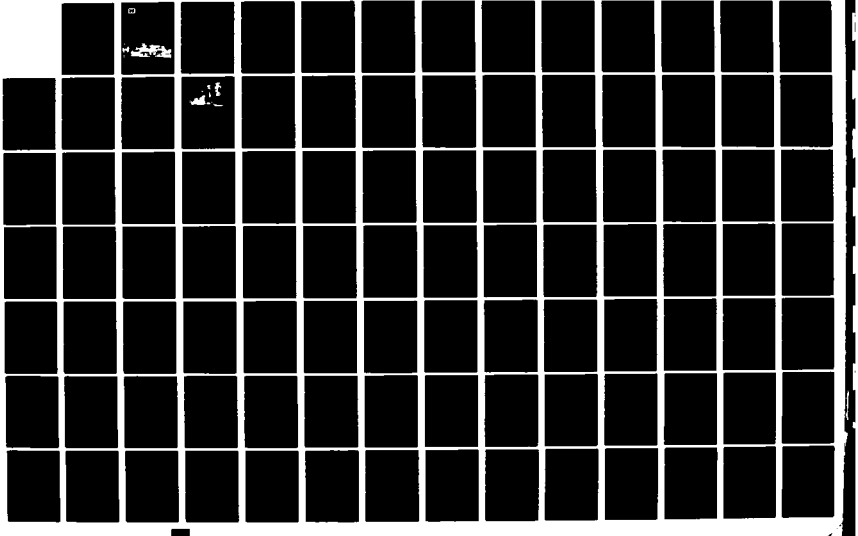

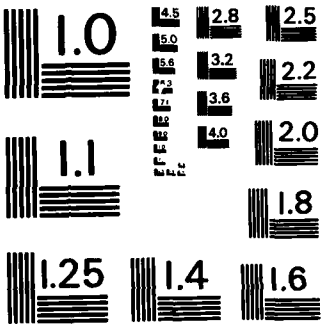

MICROCOPY RESOLUTION TEST CHART
NATIONAL BUREAU OF STANDARDS-1963-A

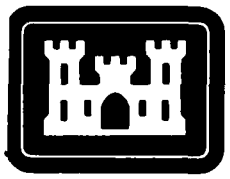

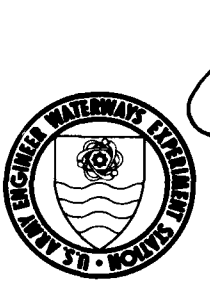

TECHNICAL REPORT S-71-6

ENGINEERING PROPERTIES OF CLAY SHALES

Report 4

LABORATORY AND COMPUTATIONAL PROCEDURES FOR PREDICTIONS OF PORE PRESSURES IN CLAY SHALE FOUNDATIONS

by

Daniel A. Leavell, John F. Peters, Frank C. Townsend

Geotechnical Laboratory
U. S. Army Engineer Waterways Experiment Station
P. O. Box 631, Vicksburg, Miss. 39180

September 1982

Report 4 of a Series

Prepared for Office, Chief of Engineers, U. S. Army
Washington, D. C. 20314

Under CWIS 31244

SECURITY CLASSIFICATION OF THIS PAGE *(When Data Entered)*

REPORT DOCUMENTATION PAGE		READ INSTRUCTIONS BEFORE COMPLETING FORM
1. REPORT NUMBER Technical Report S-71-6	2. GOVT ACCESSION NO. AD-A121448	3. RECIPIENT'S CATALOG NUMBER
4. TITLE *(and Subtitle)* ENGINEERING PROPERTIES OF CLAY SHALES; Report 4, Laboratory and Computational Procedures for Prediction of Pore Pressures in Clay Shale Foundations		5. TYPE OF REPORT & PERIOD COVERED Report 4 of a series 6. PERFORMING ORG. REPORT NUMBER
7. AUTHOR(s) Daniel A. Leavell John F. Peters Frank C. Townsend		8. CONTRACT OR GRANT NUMBER(s)
9. PERFORMING ORGANIZATION NAME AND ADDRESS U. S. Army Engineer Waterways Experiment Station Geotechnical Laboratory P. O. Box 631, Vicksburg, Miss. 39180		10. PROGRAM ELEMENT, PROJECT, TASK AREA & WORK UNIT NUMBERS CWIS 31244
11. CONTROLLING OFFICE NAME AND ADDRESS Office, Chief of Engineers, U. S. Army Washington, D. C. 20314		12. REPORT DATE September 1982 13. NUMBER OF PAGES 98
14. MONITORING AGENCY NAME & ADDRESS*(if different from Controlling Office)*		15. SECURITY CLASS. *(of this report)* Unclassified 15a. DECLASSIFICATION/DOWNGRADING SCHEDULE

16. DISTRIBUTION STATEMENT *(of this Report)*

Approved for public release; distribution unlimited.

17. DISTRIBUTION STATEMENT *(of the abstract entered in Block 20, if different from Report)*

18. SUPPLEMENTARY NOTES

Available from National Technical Information Service,
5285 Port Royal Road, Springfield, Va. 22151.

19. KEY WORDS *(Continue on reverse side if necessary and identify by block number)*

Clay shales
Pore pressure
Shales
Soil tests (Laboratory)

20. ABSTRACT *(Continue on reverse side if necessary and identify by block number)*

Design and stability analyses of structures founded on clay shales require knowledge of the pore pressure generated by applied loads. Since shales are anisotropic, heavily overconsolidated, and virtually impervious, high pore pressures can be developed that do not readily dissipate. Therefore, the objectives of this research were to (1) define the pore pressure and volume change characteristics of clay shales and (2) develop a technique for computing excess pore pressures in clay shale foundations. These
(Continued)

DD FORM 1 JAN 73 1473 EDITION OF 1 NOV 65 IS OBSOLETE

SECURITY CLASSIFICATION OF THIS PAGE *(When Data Entered)*

20. ABSTRACT (Continued).

objectives were successfully achieved by combined laboratory, analytical, and field investigations.

The laboratory tests were performed on four clay shale specimens. All four specimens were anisotropic, with a stiffness of 1.3 to 2.5 times greater in the radial plane of the specimen than in the axial plane. Skempton's pore pressure theory was shown to give a good description of pore pressure response characteristics. By treating the shales as transversely isotropic materials, Skempton's pore pressure parameters could be related to the elastic constants. From theoretical consideration, Skempton's A parameter should fall within the range of 0.5 to 0.75. This range is consistent with the pore pressure response measured in the shales tested.

Two methods were developed to compute pore pressure caused by embankment loads. The first method was implemented in the computer code CURLS and was used to predict foundation pore pressures for a Corps of Engineers dam. The second method consists of graphical construction of an influence chart and is intended for rapid field estimates of pore pressures. Both methods were shown to give a good estimate of instantaneous pore pressures. However, rapid redistribution of pore pressures during consolidation was shown to be significant, especially near embankment boundaries where pressures may be several times greater than those predicted.

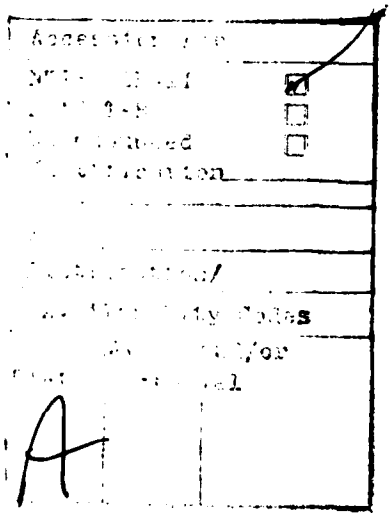

PREFACE

Laboratory investigations of the properties of clay shales by the U. S. Army Engineer Waterways Experiment Station (WES) were requested and authorized by the Office, Chief of Engineers, U. S. Army, in 1965 under Engineering Study (ES) 529 and later in FY 1968 under ES 542. The study reported herein was conducted under CWIS 31151 and CWIS 31244, "Strength and Deformation Properties of Clay Shales," during the period from 1975 to 1981.

The initial phase of the study consisted of both laboratory testing by the WES and the review of laboratory test results from other laboratories of the Corps of Engineers. Report 1 of this series, "Development of Classification Indexes for Clay Shales," which was published in June 1971, summarized existing testing procedures for evaluating the index and physical properties of clay shales and provided a basis for the adoption of standard pretreatment procedures (i.e., undried, air-dried, and blenderized) for grain-size determinations and Atterberg limits tests on clay shales.

The second phase involved classification indexes, mineralogy, and residual shear strength testing of a number of different clay shales. Report 2 of this series, "Residual Shear Strength and Classification Indexes of Clay Shales," which was published in August 1974, compares various laboratory procedures and equipment used for determining the residual strength of clay shales, and the effects of procedures developed in Report 1 on the classification indexes.

The third phase concerned the concepts and laboratory evaluation of (a) temperature change as it affects the development of pore pressures in clay shale, (b) changes in pore pressure under incremental isotropic and axial stress changes in triaxial test specimens, and (c) effects of sample anisotropy on pore pressure development. Report 3 of this series, "Preliminary Triaxial Test Program on Taylor Shale from Laneport Dam," which was published in September 1976, summarizes the triaxial testing program results, the problems encountered in testing clay shales, and the concepts used in analyzing the clay shale triaxial test data.

This report, phase four of the study, consists of defining the pore pressure and volume change characteristics of clay shales and developing a technique for computing excess construction pore pressures in clay shale foundations through the use of laboratory, analytical, and field investigations. The laboratory testing was conducted by Mr. P. A. Gilbert of the Soils Research Facility (SRF), Soil Mechanics Division (SMD), Geotechnical Laboratory (GL), WES. The analysis of the laboratory and field data was conducted by Messrs. D. A. Leavell and J. F. Peters, SRF. The laboratory testing procedures and theoretical concepts used in data analysis evolved from contributions by Dr. R. H. G. Parry in the third phase of the study. The computer program CURLS and the influence chart were developed by Mr. Peters. The field data for Hillsdale Dam were obtained from the U. S. Army Engineer District, Kansas City. Mr. Rollie Fehrman, Foundations and Materials Branch, Kansas City District, assisted in the interpretation of these field data. Mr. Ralph R. W. Beene was technical monitor throughout this investigation. From his engineering experience in the behavior of clay shales he has continually provided technical guidance for this study.

This report was prepared by Messrs. Leavell and Peters and Dr. F. C. Townsend, former employee of the WES, under the general supervision of Mr. C. L. McAnear, Chief, SMD; Mr. J. P. Sale, former Chief, GL (retired); and Dr. W. F. Marcuson III, Chief, GL.

COL John L. Cannon, CE, COL Nelson P. Conover, CE, and COL Tilford C. Creel, CE, were the Commanders and Directors of the WES during the conduct of this investigation and preparation of this report. Mr. Fred R. Brown was the Technical Director.

CONTENTS

CONVERSION FACTORS, U. S. CUSTOMARY TO METRIC (SI) UNITS OF MEASUREMENT

U. S. customary units of measurement used in this report can be converted to metric (SI) units as follows:

Multiply	By	To Obtain
degrees (angular)	0.01745329	radians
Fahrenheit degrees	5/9	Celsius degrees or Kelvins*
feet	0.3048	metres
inches	25.4	millimetres
miles (U. S. statute)	1.609347	kilometres
pounds (force) per square foot	47.88026	pascals
pounds (force) per square inch	6894.757	pascals
pounds (mass) per cubic foot	16.01846	kilograms per cubic metre

* To obtain Celsius (C) temperature readings from Fahrenheit (F) readings, use the following formula: $C = (5/9)(F - 32)$. To obtain Kelvin (K) readings, use: $K = (5/9)(F - 32) + 273.15$.

ENGINEERING PROPERTIES OF CLAY SHALES

LABORATORY AND COMPUTATIONAL PROCEDURES FOR PREDICTION OF PORE PRESSURES IN CLAY SHALE FOUNDATIONS

PART I: INTRODUCTION

Background

1. Design and stability analyses of structures founded on clay shales require knowledge of the magnitude of pore pressures induced by applied loads (Beene 1967, and Jasper and Peters 1979). Many clay shales are anisotropic and virtually impervious. These two factors in combination often lead to the development of high pore pressures that do not readily dissipate. As shown in Report 2 of this series (Parry 1976), the pore pressure response of clay shales can be predicted from the theory of transverse isotropic elasticity by assuming the clay shale to be undrained. Further, preliminary test data from a dam of moderate height suggest that the elastic pore pressure response is valid for applied stresses considerably greater than those imposed by the embankment.

2. The construction failure of the Waco Dam provides an excellent example of the problems associated with embankment construction on clay shales. The failure resulted from block sliding within the Pepper shale formation, which caused a slide within the embankment (Beene 1967, and Little 1968). The failure zone was evidently an inherently weak horizontal seam within the shale foundation. From piezometers installed after the failure, it was observed that excess pore water pressures were on the order of 70 to 100 percent of the added embankment load (Beene 1967). Results of stability analyses indicate that high induced pore water pressure contributed to this slide (Beene 1967, and Little 1968). As noted by Parry (1976), the pore water pressure may not have been generated within the failure zone but within the surrounding intact shale. For example, Beene (1967) reported that piezometers located outside the failure area

showed the pore pressures induced beneath the stable area of the dam were 100 percent of the embankment load. Therefore, these observed pore pressures were a result of the elastic or nearly elastic response of the clay shale.

3. To establish a procedure to predict pore pressure response in clay shale a laboratory investigation was performed on the Taylor shale from Laneport Dam, Texas (Parry 1976). One of the major findings in this investigation was that when loaded within the elastic range, this material displayed transverse isotropic elastic behavior. Further, by relating the pore pressure response to the elastic behavior of the clay shale, the predicted pore pressure response was found to compare favorably with that measured during undrained loading. The subsequent work described herein has been directed toward developing general procedures for evaluating pore pressure response in clay shales.

Purpose and Scope

4. The purpose of this investigation is to characterize the pore pressure and volume change response of clay shales and develop a technique for predicting pore pressure response in the field.

5. This report presents theoretical concepts and supporting laboratory and field data necessary for relating laboratory behavior to measured field pore pressures induced by changes in loading conditions. Changes in loading conditions caused by excavation and embankment placement were of primary interest; however, laboratory loadings up to failure are also presented.

6. To verify the theoretical concepts and obtain background data, four different clay shales were subjected to cycles of loading and unloading. A simplified procedure was employed to compute the changes in loading caused by excavation and embankment placement. This procedure combined with the laboratory pore pressure response was used to predict field pore pressure behavior. Theoretical concepts were used to assess the probable accuracy of this prediction technique. A detailed correlation was made between the predicted and the observed pore pressure response using piezometric data from the Hillsdale Dam project.

PART II: TESTING PHILOSOPHY AND THEORETICAL CONCEPTS

General Approach

7. The method used to evaluate pore pressure response is based on the pore pressure parameter concept. A pore pressure parameter is a numerical constant that relates the change in pore pressure to a change in applied total stress. In an elastic material, the complete pore pressure response can be adequately defined by two parameters (Skempton 1954) as follows:

$$\Delta u = B[\Delta\sigma_3 + A(\Delta\sigma_1 - \Delta\sigma_3)] \quad (1)$$

where

Δu = change in pore pressure

B = Skempton's B parameter

A = Skempton's A parameter

$\Delta\sigma_1$, $\Delta\sigma_3$ = principal stress change (total stress)

Both the A and B parameters can be measured directly in a triaxial compression test, but it is important to note that under the assumption of no drainage, they can also be related to the elastic properties of the material. For an anisotropic material, such as clay shale, the A parameter depends on the orientation of the sample with respect to the applied principal stresses. To determine the A parameter in the laboratory for general loading conditions numerous laboratory tests would be required. However, the A parameter can be related to the anisotropic elastic constants. An appropriate value of A can be determined for any loading case encountered in the field provided the elastic constants are known. Thus, emphasis has been given to laboratory determination of both pore pressure parameters and anisotropic elastic constants.

Elastic Constant Determination

8. The philosophy of the testing program was to subject a specimen to a variety of loadings for the complete determination of its elastic properties under triaxial stress conditions. The need for data from

multiple-load applications can best be understood from Figure 1a, which depicts the assumed anisotropic nature of the clay shales tested. In general, five independent constants are needed to characterize a transversely isotropic material completely (Figure 1a). For the typical field problem in which plane strain is assumed (Figure 1b), only four independent constants are necessary since two constants can be expressed as a ratio. However, for the triaxial text, only three constants can be measured independently (Figure 1c), since two of the applied stresses are equal. As shown in Appendix A (Equation A13), the elastic constants measured in the triaxial test can be related by

$$\Delta\varepsilon_v = \Delta\bar{\sigma}_a C_{aa} + 2(\Delta\bar{\sigma}_a + \Delta\bar{\sigma}_r)C_{ar} + 2\Delta\bar{\sigma}_r C_{rr} \tag{2a}$$

$$\Delta\varepsilon_a - \Delta\varepsilon_r = \Delta\bar{\sigma}_a C_{aa} + (2\Delta\bar{\sigma}_r - \Delta\bar{\sigma}_a)C_{ar} - \Delta\bar{\sigma}_r C_{rr} \tag{2b}$$

where

$\Delta\varepsilon_v = \Delta\varepsilon_a + 2\Delta\varepsilon_r$ = change in volumetric strain

$\Delta\varepsilon_a$ = change in axial strain

$\Delta\varepsilon_r$ = change in radial strain

$\Delta\bar{\sigma}_a$ = change in axial effective stress

$\Delta\bar{\sigma}_r$ = change in radial effective stress

C_{aa} = constant relating purely axial stress to axial strain

C_{ar} = constant relating purely axial stress to radial strain

C_{rr} = constant relating purely radial stress to radial strain

Equations 2a and 2b involve three constants; thus some combinations of three equations from at least two independent loading increments are required for their determination.

9. The typical loading procedure used to determine the elastic constants is depicted by the stress path in Figure 2. The sample was first subjected to isotropic drained loading (initial consolidation) as

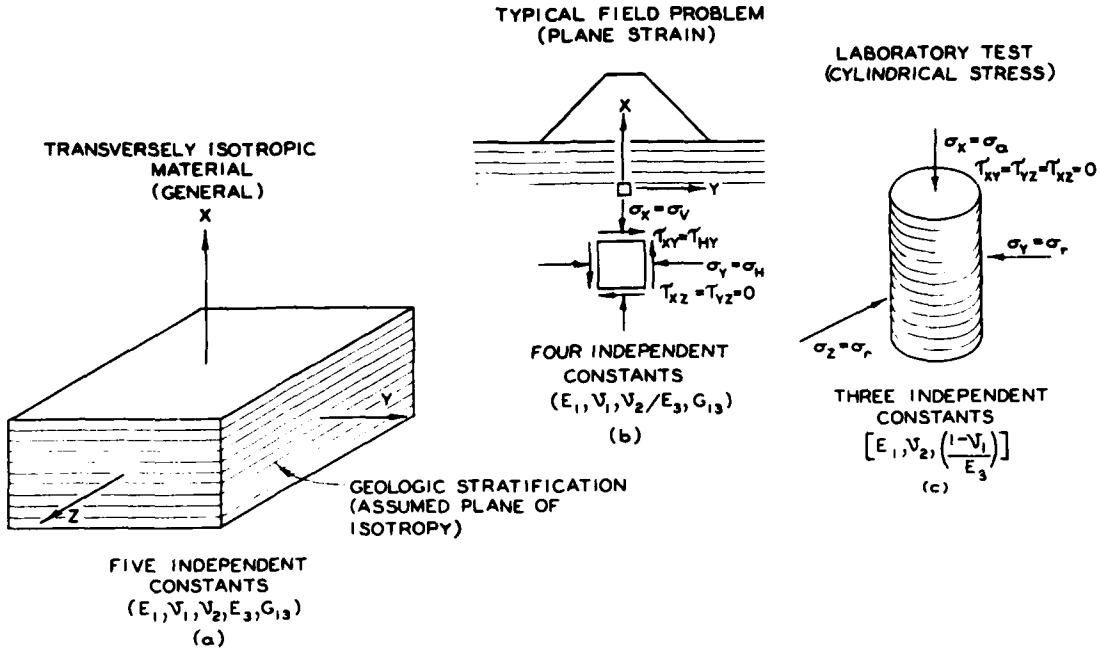

Figure 1. Elastic constants required to characterize clay shale behavior for field and laboratory loadings

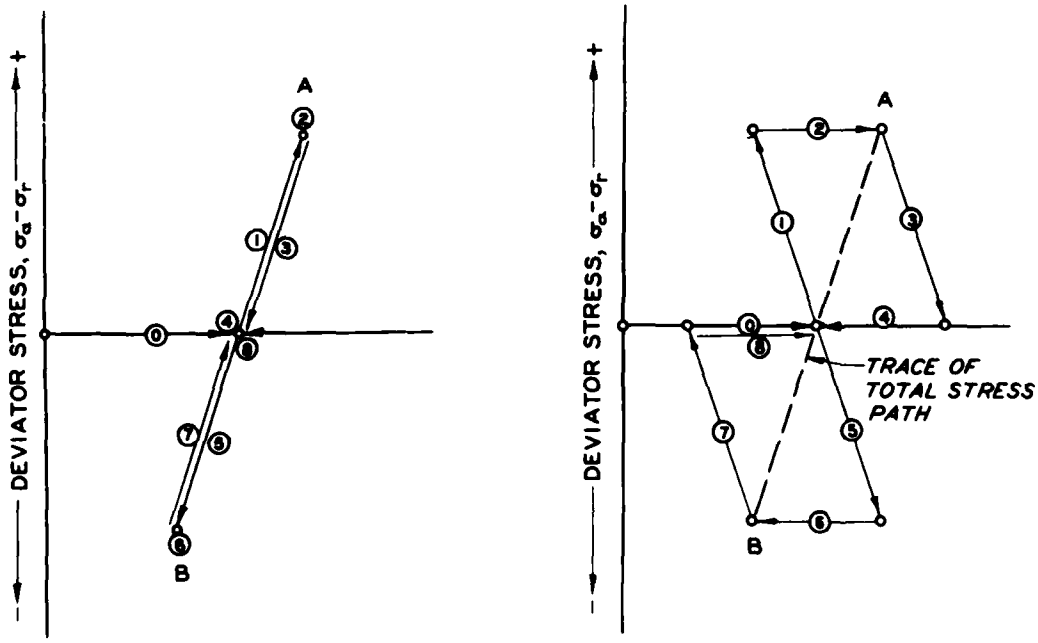

a. Total stress $(\sigma_a + 2\sigma_r)/3$ b. Effective stress $(\bar{\sigma}_a + 2\bar{\sigma}_r)/3$

Figure 2. Idealized stress paths used to test clay shale specimens

shown by increment 0. The specimen was next loaded axially undrained as indicated by increment 1. Increment 2 represents subsequent consolidation of the sample as shown by the horizontal effective stress path and unchanging total stress. An undrained increment followed by an increment of consolidation will be referred to as a loading step throughout this report. Numbers 3 through 8 along the path represent similar increments of undrained axial loading followed by consolidation under constant total stress.

10. Each of the undrained and drained increments of the stress path yields the two independent equations (2a and 2b). Thus, each set of undrained and drained increments provided sufficient data to evaluate the three elastic constants. For example, using Equation 2a for an undrained increment ($\Delta\varepsilon_v = 0$) and Equations 2a and 2b for a drained increment results in three independent equations with three unknown constants. Following this procedure for each pair of increments in the stress path gives the constants for each step. If the specimen was purely elastic, the constants would be the same for each step. However, it was found that the elastic constants varied, sometimes systematically, throughout the cycle of loading and unloading. Thus, some judgment is required to determine which measured value is most representative of the expected field behavior.

Pore Pressure Parameter Determination

11. The pore pressure parameters were obtained from the pore pressure induced during each undrained increment. The B parameter was generally on the order of 1.0; thus the A parameter could be determined directly from Equation 1, that is

$$A = \frac{\Delta u - \Delta\sigma_r}{\Delta\sigma_a - \Delta\sigma_r} \tag{3}$$

The A parameter is uniquely defined by the elastic constants and should therefore be the same for any loading. However, as in the case of the elastic constants, small variations in the A parameter were observed for each step of the loading cycle.

PART III: DESCRIPTION OF TESTING PROGRAM

Equipment

12. Triaxial tests were performed in the stress-controlled systems shown in operation in Figure 3. The specimen was loaded axially from the top by a double-acting pneumatic loading system. The top platen was rigidly connected to the loading rod to permit loading in either compression or extension. Cell pressure was also controlled pneumatically, with silicon oil used as a confining fluid to protect internal instrumentation.

13. The back pressure system is shown schematically in Figure 4. Diffusion of compressed air into the back pressure system in tests of long duration caused degradation of the B value; therefore, an air barrier was necessary to isolate the back pressure system and the saturation fluid. The air barrier for the saturation reservoirs consisted of an impervious steel membrane with O-ring seals. The burette fluid was separated from the air by a 1- to 2-in.* mercury barrier. The mercury barrier was separated from the water in this burette by dyed kerosene to facilitate accurate volume change measurements. Also, a similar air barrier was used to isolate the confining fluid from the pneumatic pressure system. This system evolved during the testing program and all these features were operational only during the testing of Pierre and Bearpaw shales.

14. Instrumentation consisted of (a) an externally mounted load cell, (b) linear variable differential transformer (LVDT) clamps, located at specimen one-third points, for measuring axial and radial deformations, (c) an external LVDT to provide axial deformation measurements, (d) three pore pressure transducers (high compliance) monitoring pore pressures at the top, bottom, and interior of the specimen, (e) a pressure transducer measuring chamber pressure, and (f) a digital clock. Data from the LVDT's and time were recorded on a Digitrend 40-channel

* A table of factors for converting U. S. customary units of measurements to metric (SI) units is presented on page 5.

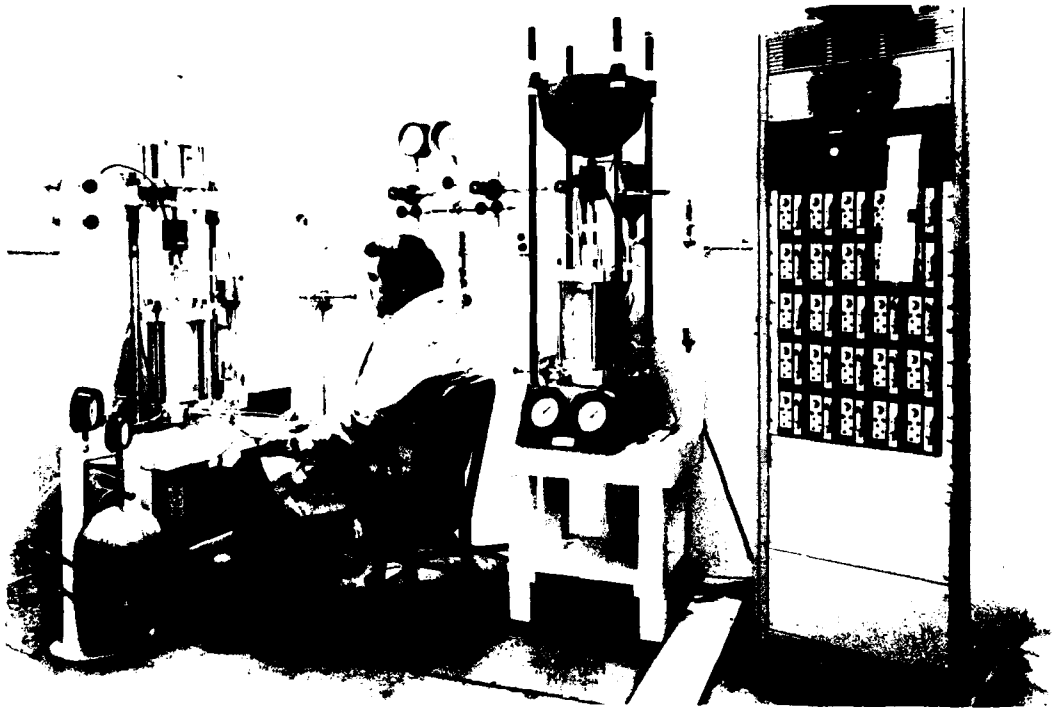

Figure 3. Laboratory equipment in operation

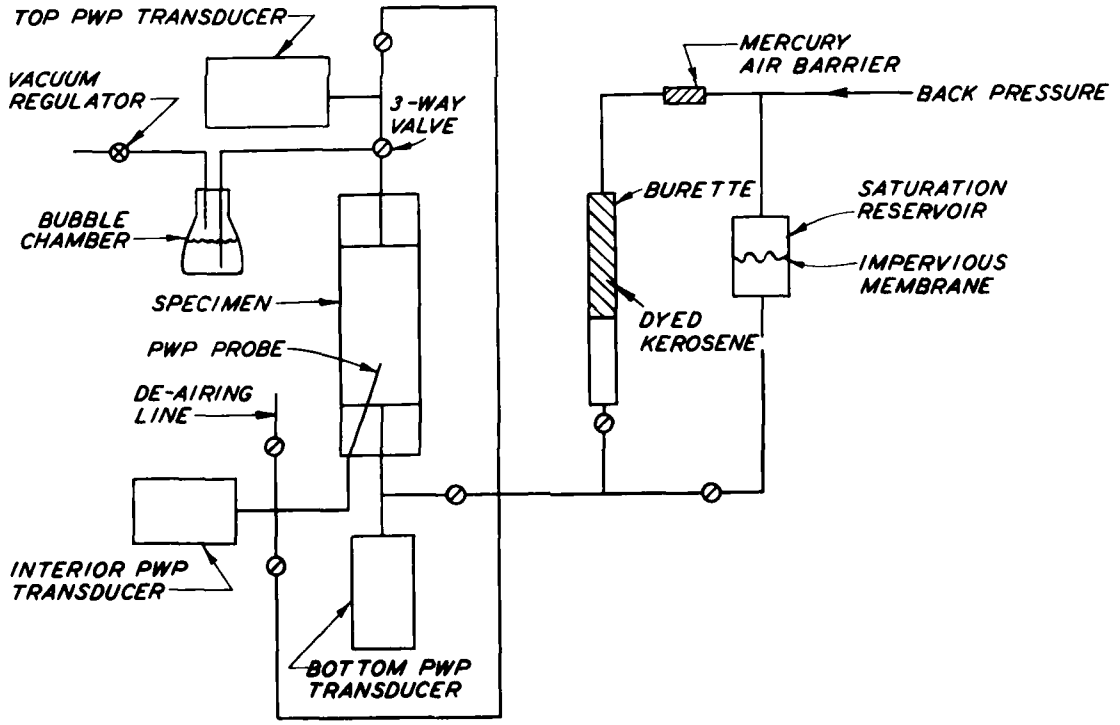

Figure 4. Schematic diagram of pore water pressure (PWP)/drainage system

digital printer. Volume changes were measured during consolidation using a small bore burette read by a vernier cathodometer to the nearest 0.0026 cc.

15. Previous work on clay shales (Parry 1976) indicated that changes in temperature severely influence pore pressure measurements, therefore testing was performed in an environmental room (±1°F) to minimize temperature effects.

Materials Tested

16. The four shales used in this study and their source locations are: (a) Bearpaw, Billings, Montana; (b) Kincaid, Cooper Dam, Northeastern Texas; (c) Pierre, Limon, Colorado; and (d) Quivira, Hillsdale Dam, Kansas.

17. The Bearpaw and Pierre shales were sampled for the Federal Highway Administration expansive soil investigation described by Snethen (1979). Their source locations correspond to Sites 19 and 14, respectively, in Snethen's report. The Kincaid shale was obtained from a piezometer boring in the spillway of Cooper Dam, northeastern Texas. The Quivira shale was sampled from the cutoff trench of Hillsdale Dam, Kansas, at sta 99 + 50. The physical characteristics of these shales are summarized in the following tabulation. Each shale was classified as either soft or stiff based on a visual inspection. Bearpaw and Kincaid shales appeared stiff, whereas Pierre and Quivira shales were comparatively soft.

Shale	Blenderized LL	Blenderized PL	Blenderized PI	G_s	w_{nat} percent	γ_d pcf	e_o
Bearpaw	58	24	34	2.74	16.6	116.0	0.47
Kincaid	85*	20*	65*	2.72*	19.5	103.0	0.67
Pierre	58	18	40	2.66	22.9	101.0	0.63
Quivira	51	24	27	2.80	14.8	121.0	0.44

Note: The definitions of the characteristics are: LL = liquid limit, PL = plastic limit, PI = plasticity index, G_s = specific gravity of solids, w_{nat} = natural water content, γ_d = dry unit weight, and e_o = initial void ratio.

* Average values (U. S. Army Engineer District, New Orleans 1977).

Test Procedures

18. Preparation of triaxial test specimens consisted of (a) trimming the specimen, (b) inserting the interior pore pressure probe, (c) assembling the triaxial chamber, (d) back pressure saturation, (e) consolidation, and (f) stress path loading.

19. The specimens were removed from their protective shipping containers and roughly trimmed to their approximate final dimensions using a band saw. The finished 2.8-in. specimen diameter was obtained by hand trimming with knives and straightedges using a soil trimming lathe. The specimen ends were trimmed perpendicular to the specimen sides in a miter box to the final 6-in. length. All final trimming was performed in a humidity-controlled room to preserve the specimen's water content.

20. The pore pressure probe was fabricated from a 1/16-in.-outside-diam stainless steel tube. The tip of the tube was shaped into a point and covered with a protective coat of epoxy. The probe tip was then finished by cutting small grooves into the sides of the tip. To prevent splitting, the specimen was confined in a split mold before the internal pore pressure probe was inserted. A pilot hole was drilled in the specimen at a 60-deg angle, to within 1/2 in. of the final probe depth, using a 1/16-in. standard metal drill bit. The probe was carefully pressed to its final depth of 1.5 in. from bottom of specimen. The shank of the probe was sealed with epoxy to the base platen as the specimen was mounted in the cell.

21. The specimens were set up by a procedure similar to that outlined for $\bar{R}$ tests in EM 1110-2-1906 (Dept. of the Army, Office, Chief of Engineers, 1970). One notable addition to the standard procedure was the placement of LVDT measurement clamps at specimen one-third points. The clamps were positioned and epoxied to the membrane after a vacuum had been applied to the specimen. The standard procedures for saturation and consolidation were used.

Interpretation of Test Data

22. The parameters measured in this study varied with time as the

sample reached an equilibrium after each load application. Often fluctuations within the pressure system created small variations in the applied loading during the period required for the equilibrium to be obtained. Therefore, some judgment was involved in selecting the best data for use in the analyses.

23. The test data from a load increment on the Pierre Shale give a good example of typical fluctuations in measured parameters with time (Figures 5, 6, and 7). Figure 5 shows that the pore water pressure reached an equilibrium within 2 min at the top and bottom of the specimen but required approximately 60 min to attain an equilibrium at the center of the specimen. Also, even with fluctuations in the axial and radial stresses, the pore water pressure (Figure 5) and the A parameter (Figure 6) were not significantly affected. The strains in Figure 7 did not reach an equilibrium as rapidly as the pore water pressure and A parameter. The dashed lines in Figures 5, 6, and 7 denote a loss of system pressure. Even though a permanent volumetric strain was induced into the specimen by this pressure loss, the A parameter remained in the 0.7 to 0.8 range.

24. The reliability of the strain data was also of considerable importance; therefore, several redundant measurements were used. The axial strain was measured both on the specimen and by the deflection of the loading rod. Further, the volumetric strain during the drained loading step could be determined directly from burette readings or computed from the radial and axial strains. Figure 8 presents a comparison of the volumetric strain, computed from axial and radial strain, and the volumetric strain determined from the burette reading. Note that the volumetric strains computed from linear strain measurements agree quite well with the measured volume changes. Further, axial strains computed from the exterior LVDT data agree well with the computed strains using the interior LVDT data.

25. Where inconsistencies were noted in redundant measurements, the following order of preference was used:

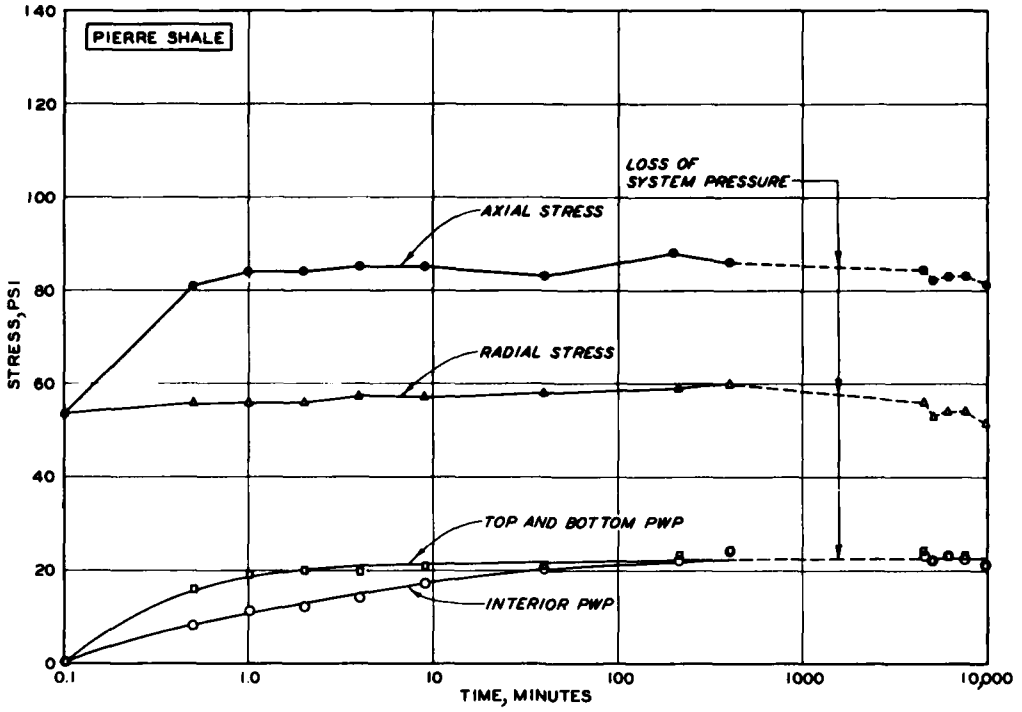

Figure 5. Applied stress and pore water pressure (PWP) versus time after stress application

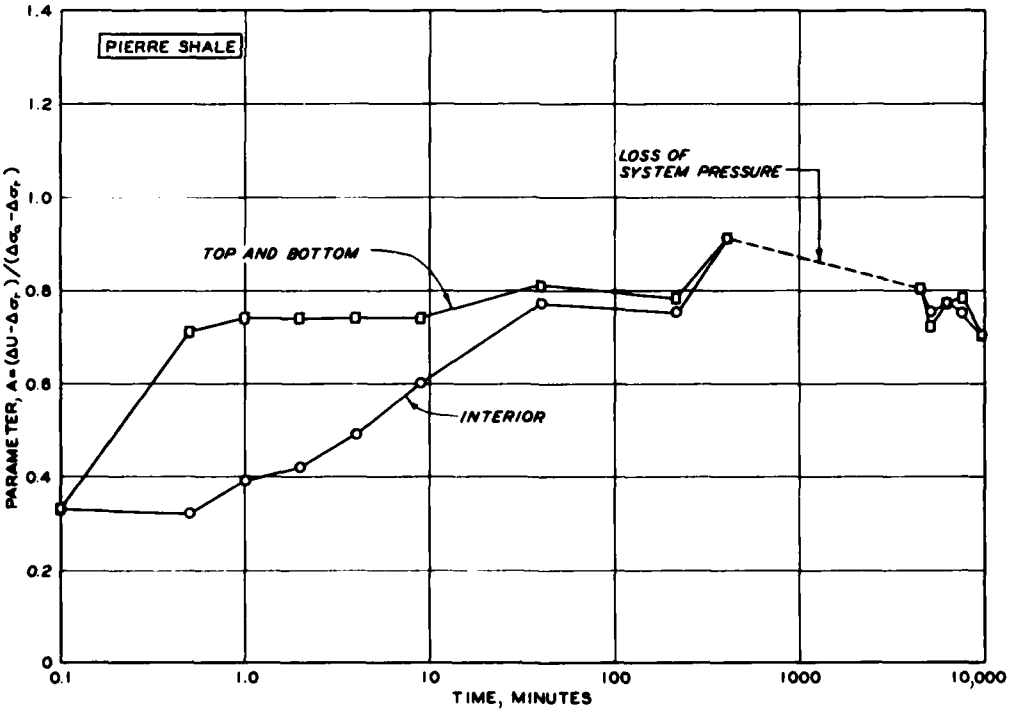

Figure 6. A parameter versus time after stress application

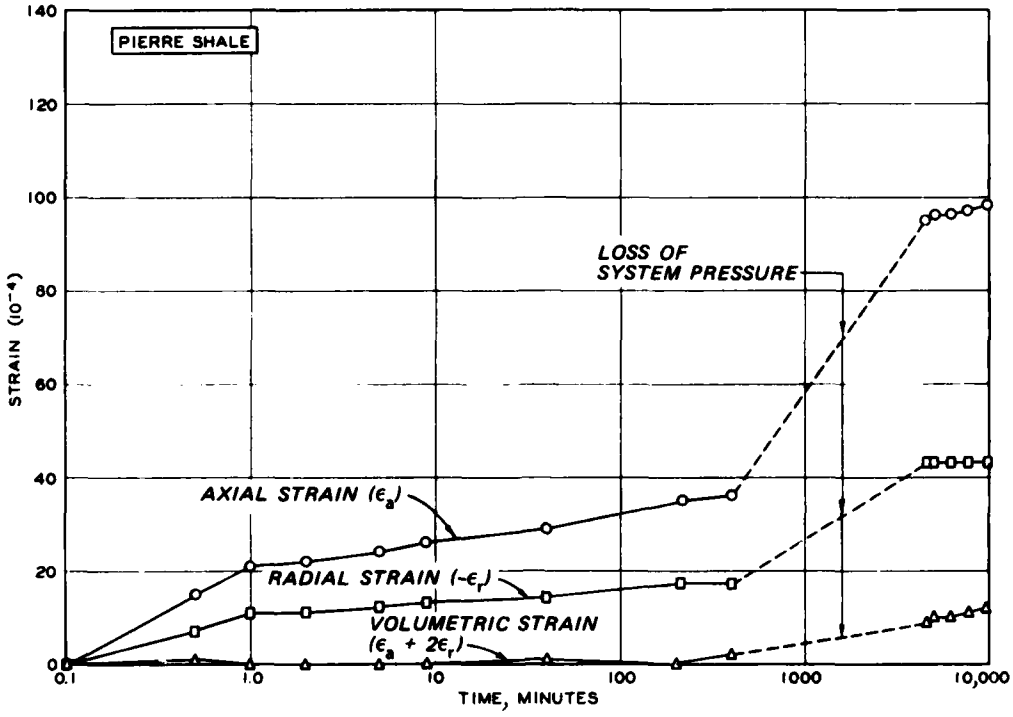

Figure 7. Strains versus time after stress application

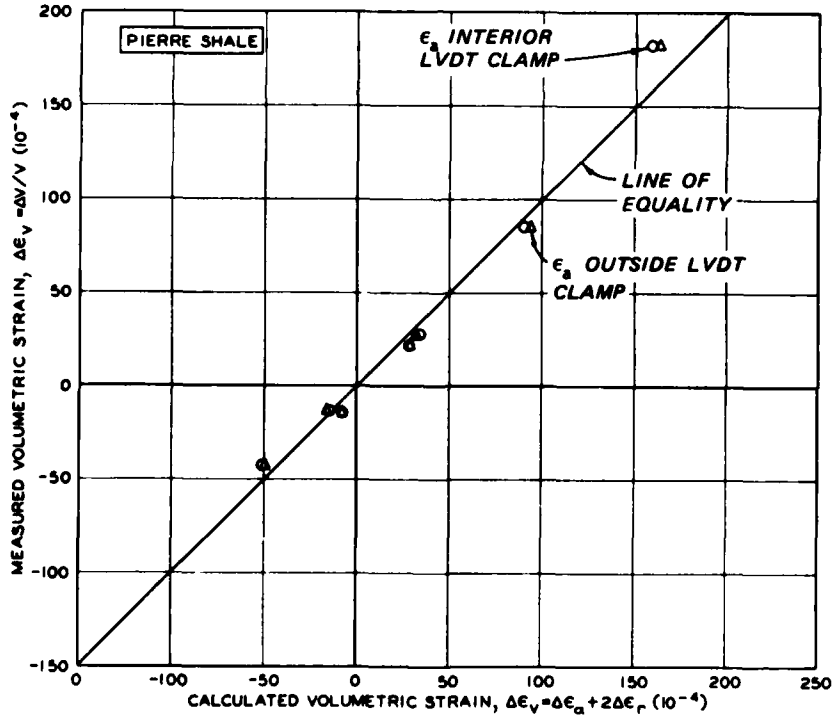

Figure 8. Burette reading versus deformation measurements for volumetric strain calculations during drained increments

Measurement	Preferred Order of Reliability
Axial strain	Outside LVDT Inside LVDT clamp
Volumetric strain	Burette Computed from axial and radial strains
Radial strain	Computed from burette and axial strain Inside LVDT clamp
Pore pressure	Bottom stone Top stone Probe

26. Another factor requiring some judgment was the selection of the loading step to use in determining the elastic constants. Any given increment would provide only two of the three independent equations required for calculating the constants. For a linear elastic material, there is no such difficulty since the elastic properties would be the same for all steps. However, for the soft clay shales, the repeated loadings tended to induce nonrecoverable strains (Figure 9). Particular difficulty was encountered when attempting to incorporate data from the initial isotropic consolidation step into the calculation process. For this reason, the data from an undrained increment were combined with the data from the subsequent drained increment to determine all three constants reliably. Figure 10 shows that this problem is not as severe in the stiff shales.

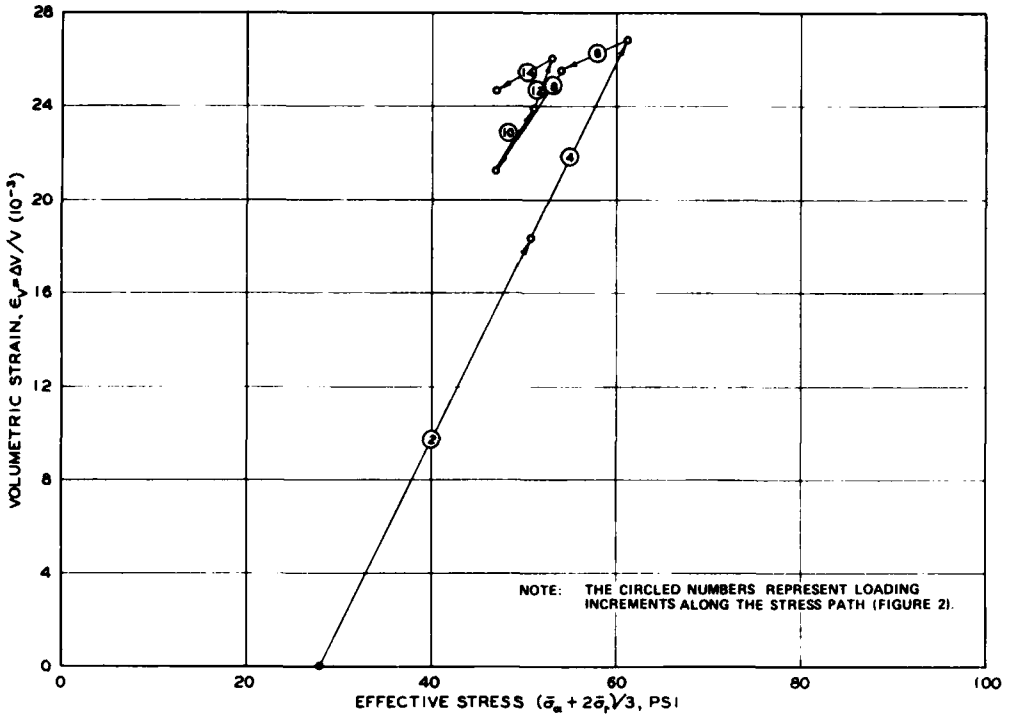

Figure 9. Accumulated volumetric strain for all drained loading increments on Pierre shale after completion of isotropic consolidation

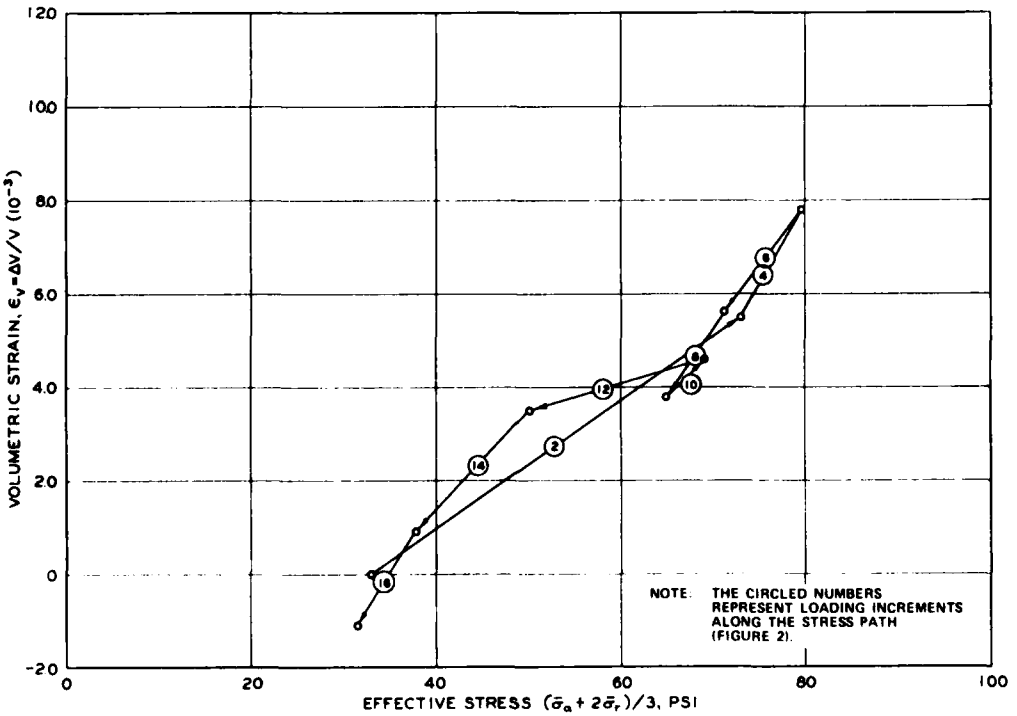

Figure 10. Accumulated volumetric strain for all drained loading increments on Bearpaw shale after completion of isotropic consolidation

PART IV: TEST RESULTS

Determination of Elastic Constants

27. The data for the triaxial tests on the four clay shales are presented in Tables 1-4. The values given for stress, strain, and the A parameter represent values obtained after the specimen reached an apparent equilibrium. The axial strain data and pore pressure data, which were measured at various locations on the specimen (see paragraph 14), are the values considered to be the most accurate based on the order of preference in paragraph 25 and are not averages of all values measured.

28. The procedure used to compute the elastic constants can best be illustrated by performing an example calculation. In Table 3, the following data are given for Pierre shale:

Increment 3 (Undrained)	Increments 3 and 4 (Drained)
$\Delta\bar{\sigma}_a = 6.9$ psi	$\Delta\bar{\sigma}_a = 32.0$ psi
$\Delta\bar{\sigma}_r = -23.0$ psi	$\Delta\bar{\sigma}_r = 1.0$ psi
$\Delta\varepsilon_a = 0.0096$	$\Delta\varepsilon_a = 0.0145$
$\Delta\varepsilon_r = -0.0044$	$\Delta\varepsilon_r = -0.0027$
$\Delta\varepsilon_v = 0$ (assumed)	$\Delta\varepsilon_v = 0.0085$

Equation 2a for the undrained quantities and Equations 2a and 2b for the drained quantities give the following three independent equations with three unknowns:

$$\begin{aligned} 6.90C_{aa} - 32.20C_{ar} - 46.00C_{rr} &= 0 \\ 32.00C_{aa} + 66.00C_{ar} + 2.00C_{rr} &= 0.0085 \\ 32.0C_{aa} - 62.00C_{ar} - 1.00C_{rr} &= 0.0172 \end{aligned} \tag{4}$$

These equations give these constants:

$$C_{aa} = 452.80 \times 10^{-6} \text{ (1/psi)}$$

$$C_{ar} = -94.82 \times 10^{-6} \text{ (1/psi)}$$
$$C_{rr} = 134.18 \times 10^{-6} \text{ (1/psi)}$$

This procedure was used to determine the anisotropic elastic constants presented in Table 5.

Comparison of Computed and Measured Pore Pressure Parameters

29. According to the elastic theory, Skempton's A parameter for an anisotropic material should be related to the elastic constants by (see Equation A15)

$$A = \frac{C_{aa} + 2C_{ar}}{C_{aa} + 4C_{ar} + 2C_{rr}} \tag{5}$$

Thus, the theoretical pore pressure response is subject to verification by a comparison of the measured and predicted A parameters. Unfortunately, the procedure used to compute the elastic constants makes use of pore pressure values that, in turn, are used to predict the A parameter. It can be shown that the A parameters computed from the data given in Table 5 are numerically equal to the corresponding measured A parameters regardless of the actual material behavior. Therefore, to obtain an independent verification of theoretical concepts, an A parameter must be computed using data only from drained loading increments.

30. To compute the elastic constants, it is necessary to load the specimens in both axial and radial directions. Therefore, data from two independent drained increments are required. However, as discussed in paragraph 26, the absolute stiffness of the soft shales was altered with each load cycle so that measurements from one drained step were not compatible with those of other drained steps. Indeed, the value of using both drained and undrained increments to evaluate elastic constants is derived from the ability to obtain three independent relationships within a single load step.

31. As an alternative to Equation 5 for verification of the theory, the A parameter was computed using the relative strains measured

during the initial isotropic consolidation. As shown in Appendix A (Equation A26),

$$A = \frac{m}{(m + 2)} \tag{6}$$

in which m equals $\Delta\varepsilon_a/\Delta\varepsilon_r$ (measured during isotropic consolidation).

32. The advantage of Equation 6 is that it does not depend on the absolute stiffness of the clay shale. The A values determined by this equation should be comparable to those measured throughout the subsequent undrained loading increments provided the ratio of stiffness in the axial and radial directions is not altered.

33. A value of m was obtained for each shale by plotting ε_r versus ε_a (Figure 11). During the initial consolidation for each shale, the value m represents the slope. A comparison of the calculated A value with the average measured value is given in the tabulation below. Note that agreement was generally good although the measured A values tend to be somewhat variable for the soft shales as indicated by the standard deviation.

Shale	Classification	$\frac{\Delta\varepsilon_a}{\Delta\varepsilon_r} = m$	Calculated A	Measured	
				A	Standard Deviation
Bearpaw	Stiff	2.5	0.56	0.60	0.05
Kincaid	Stiff	2.5	0.56	0.53	0.07
Pierre	Soft	3.0	0.60	0.57	0.14
Quivira	Soft	4.0	0.67	0.70	0.13

34. As shown in Appendix A (Equation A15), the maximum theoretical B value that can be measured is given by

$$B = \frac{C_{aa} + 4C_{ar} + 2C_{rr}}{\frac{n}{K_w} + C_{aa} + 4C_{ar} + 2C_{rr}} \tag{7}$$

where

n = porosity of soil

K_w = bulk modulus of water

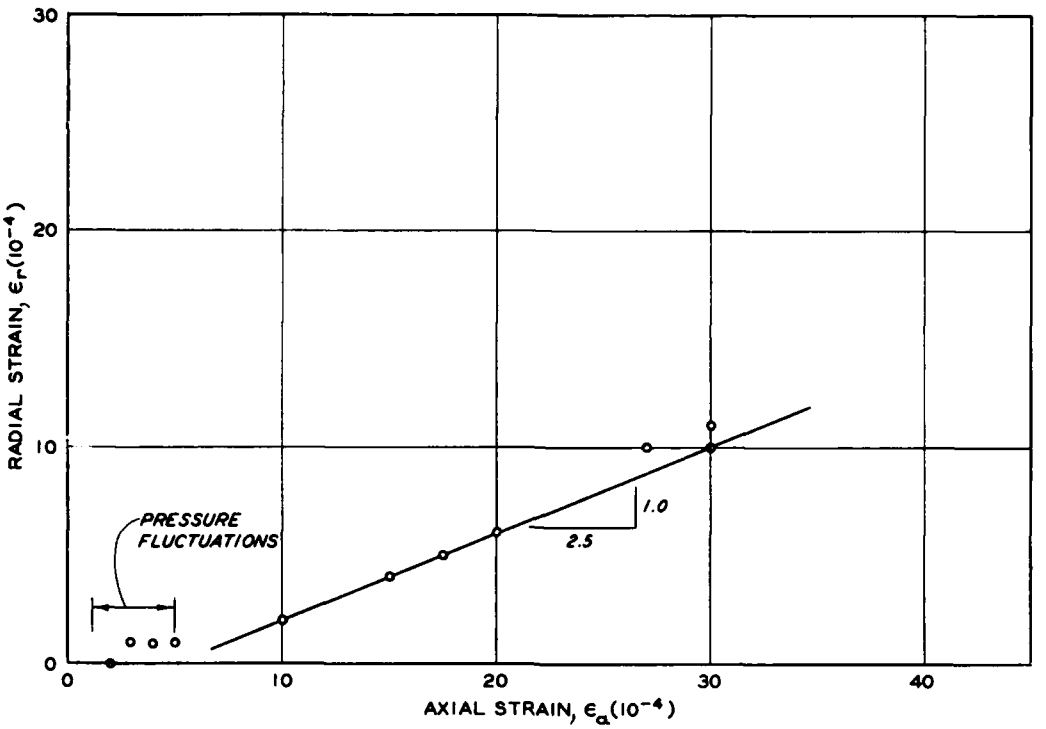

a. Bearpaw shale

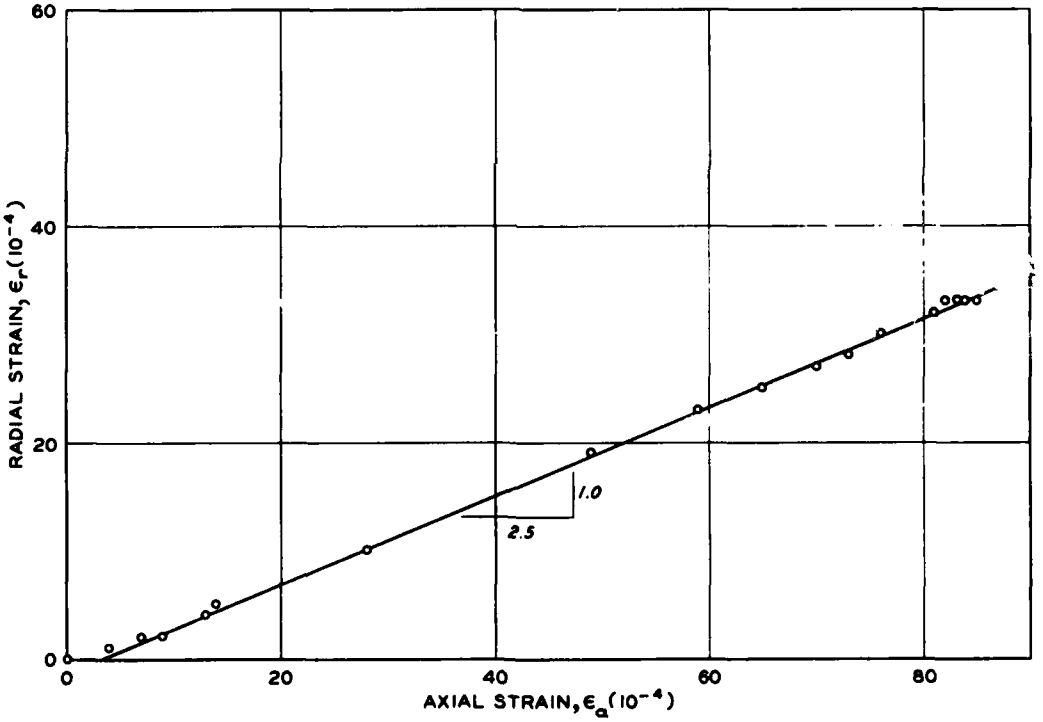

b. Kincaid shale

Figure 11. Radial strain versus axial strain during isotropic consolidation (Continued)

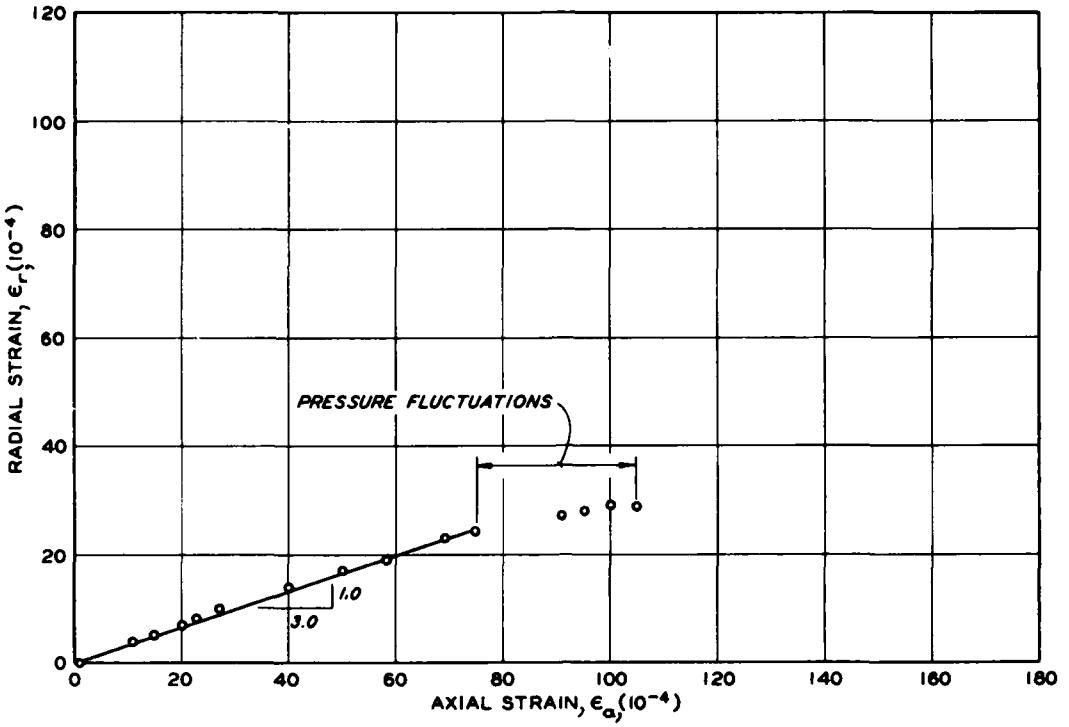

c. Pierre shale

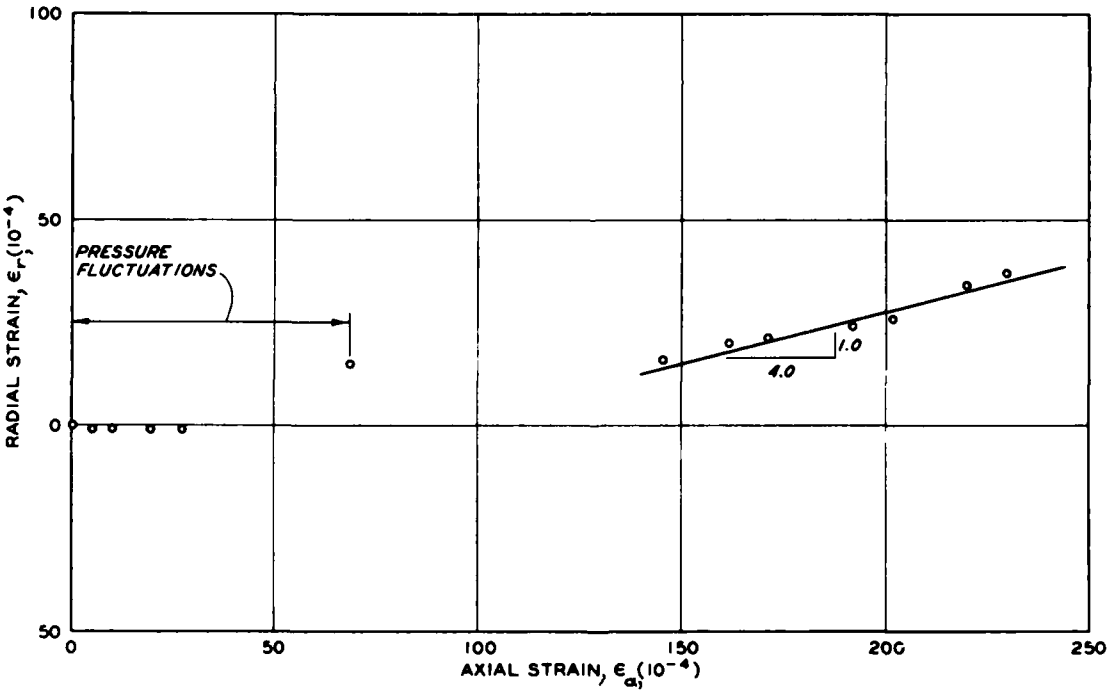

d. Quivira shale

Figure 11. (Concluded)

Smaller values of B might be measured if the specimen is not fully saturated. The theoretical and measured B values are listed in the tabulation below. The initial B values indicate that all samples were saturated. Although the duration of the tests was long (6 months to 1 year), the specimens remained reasonably saturated as indicated by the final B value.

Shale	n	B Theoretical Maximum	B Measured Initial	B Measured Final
Bearpaw	0.319	0.991	1.00	0.89
Kincaid	0.400	0.997	1.00	0.98
Pierre	0.385	0.996	1.00	--
Quivira	0.306	0.996	1.00	0.96

Note: K_w is assumed to be 314,000 psi.

Failure Characteristics

35. At the conclusion of the stress path tests, the clay shale specimens were loaded to failure in undrained compression, then unloaded. The failure stress-strain curve in Figure 12 is typical for the stiff shales. The stress-strain curve displays a slight break at a deviator stress of 50 psi but remains approximately linear up to 140 psi. Figure 13 is typical of the stress-strain curve for the soft shales. In contrast to the stiff shale, the soft shales did not display a distinct break in the stress-strain curve before failure. The failure characteristics of the clay shales tested are summarized as follows:

Shale	$\sigma_a - \sigma_r$* psi	ε_a* percent	$\sigma_a - \sigma_r$ psi	ε_a percent	A Initial	A** Final
Bearpaw	55	0.15	160	1.4	0.61	0.0
Kincaid†	60	0.30	145	1.5	0.59	0.34
Pierre	50	0.60	86	4.0	0.53	0.32
Quivira	70	0.65	110	1.8	0.70	0.20

Note: Strain measured from beginning of final loading.
* At initiation of specimen dilation.
** Based on initial and failure pore pressures.
† Not taken to failure (maximum values obtained).

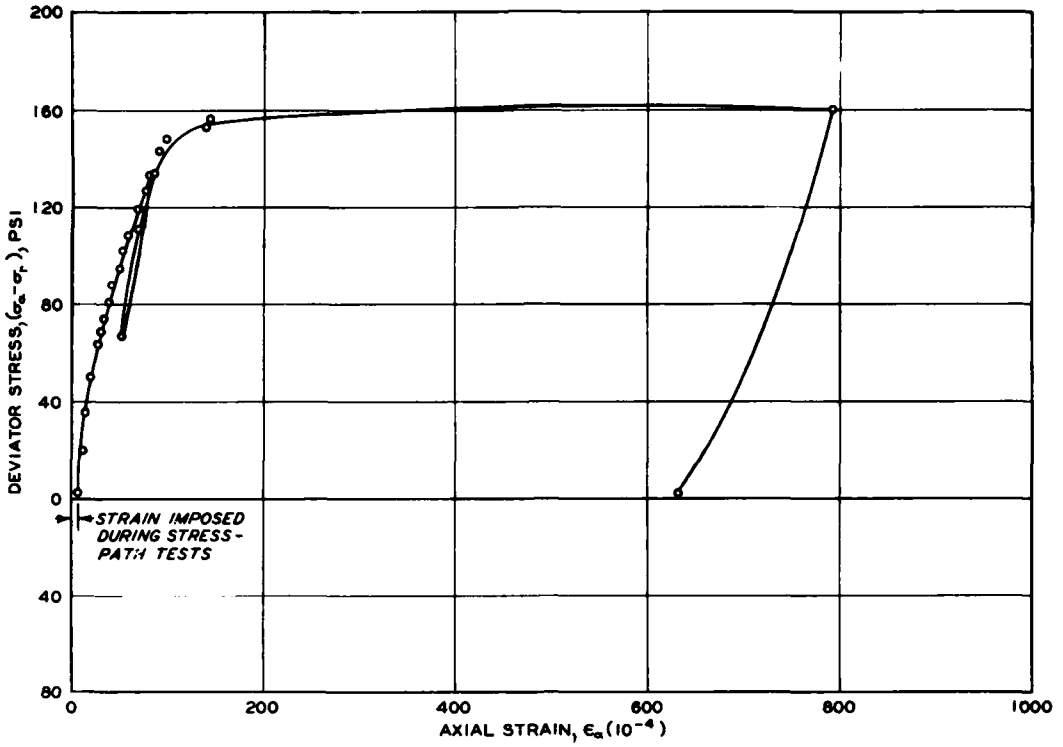

Figure 12. Deviator stress versus axial strain for loading of Bearpaw shale to failure

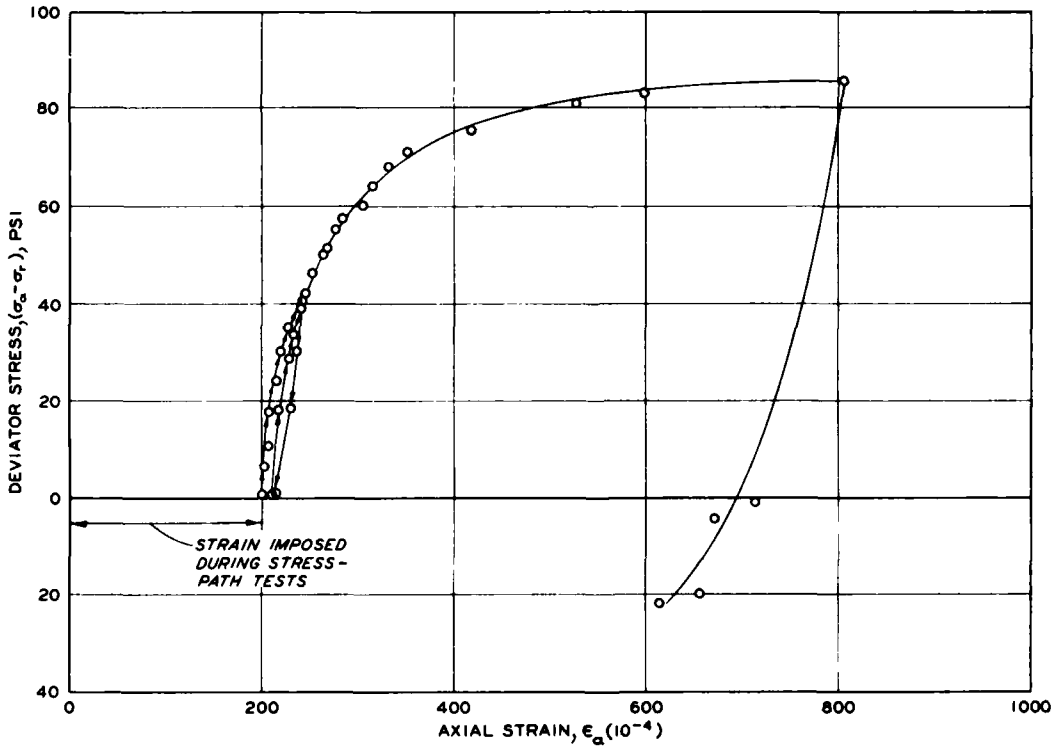

Figure 13. Deviator stress versus axial strain for loading of Pierre shale to failure

36. The A parameters for both the stiff and soft shales decrease in value as failure approached as indicated in the tabulation above. A stress-path plot is shown for the stiff shales in Figure 14 and for the soft shales in Figure 15. Note that for an isotropic elastic material the effective stress path for undrained loading would be a vertical straight line; thus the initial slope reflects the higher stiffness radially rather than axially (see Appendix A). Above a deviator stress $(\sigma_a - \sigma_r)$ of 60 psi the trend of the curves reverses because of the more dilatant nonelastic behavior of the clay shales. Interestingly, the deviator stress $(\sigma_a - \sigma_r)$ at which the effective stress paths exhibited dilatant behavior was nearly the same for all four shales even though the ultimate strengths were much greater for the stiff shales. It is important to note that the elastic theory cannot be used to predict pore pressure response beyond the point where the stress path displays dilative behavior (i.e. has positive slope).

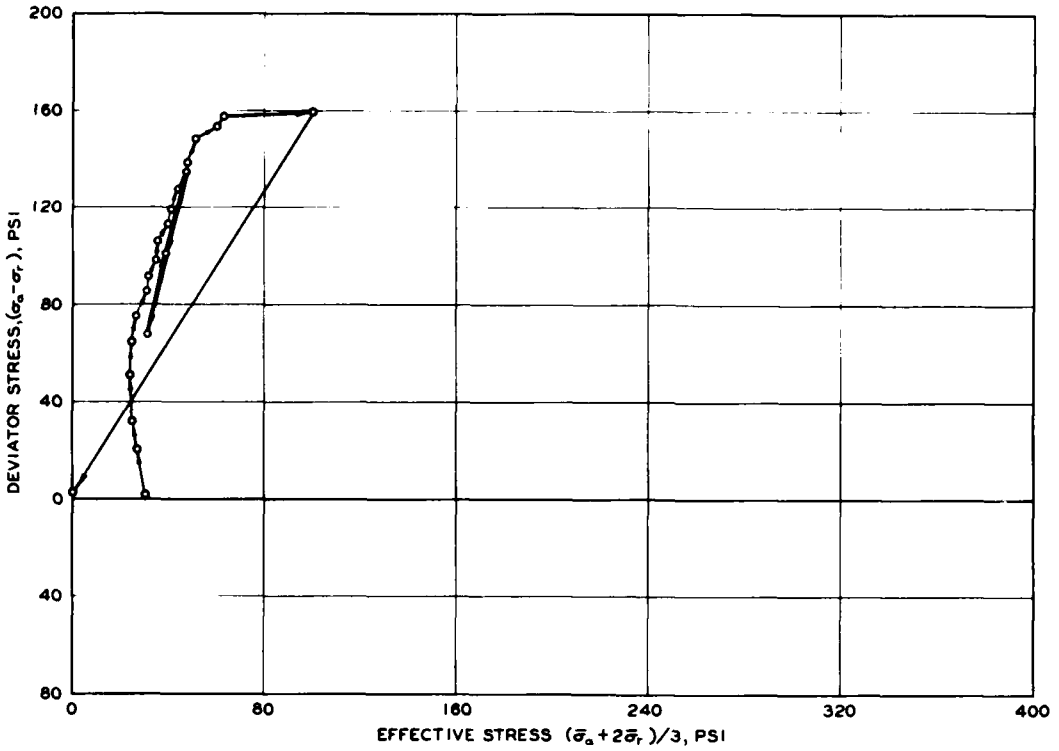

Figure 14. Stress path for loading of Bearpaw shale to failure

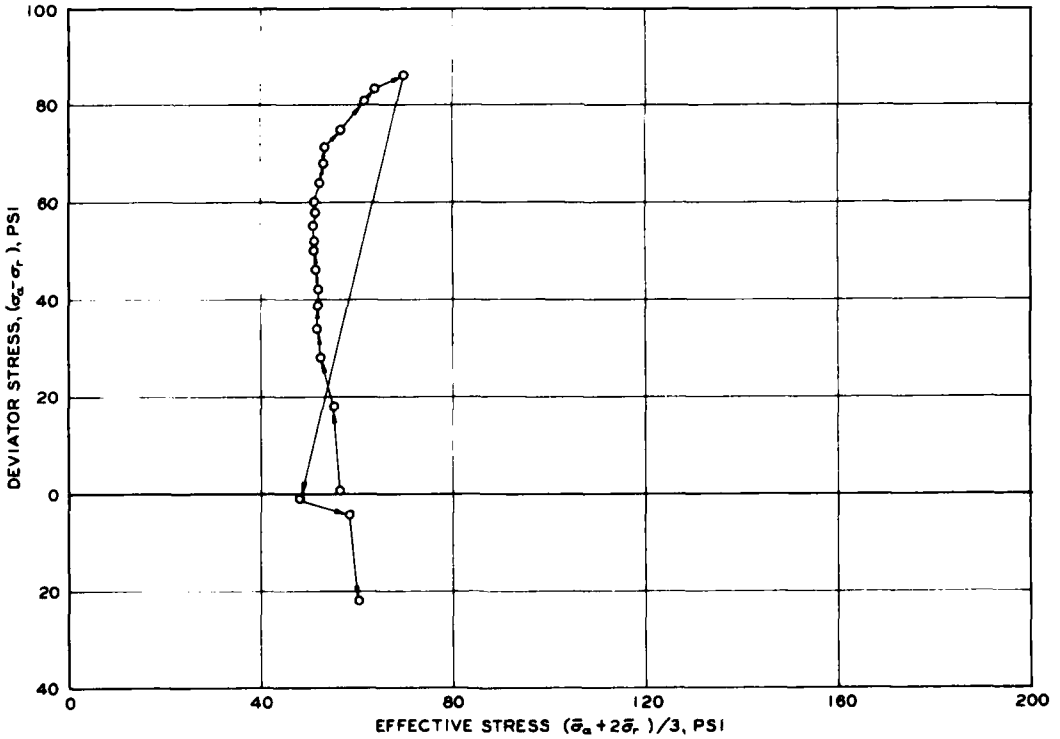

Figure 15. Stress path for loading of Pierre shale to failure

PART V: DISCUSSION OF LABORATORY RESULTS

Elastic Properties

37. The consistency of the computed elastic constants presented in Table 5 suggests that they represent actual material behavior. The greatest variation in properties appears to occur in the calculated axial stiffness (E_1) of the Pierre shale. A detailed analysis of the variation in stiffness with respect to load step indicates that the differences in stiffness are the result of the inherent behavior of the shale and not the result of random error. For example, the apparent uniaxial stress-strain behavior can be constructed from the values of E_1 in Table 5. From the reconstructed stress-strain curve for the Pierre shale (Figure 16), two features are at once apparent. First, considerable hardening occurred during step 2 that made it difficult to incorporate data from the initial loadings into subsequent computations (see paragraph 26). Second, when the specimen is subjected to a cycle of loading and unloading, the shale exhibits a distinct hysteresis, which results in a different modulus for each drained increment. Note, however, that for equivalent steps 3 and 7 in Figure 16 the moduli values are nearly equal, thus suggesting that the hysteretic behavior of the material is repeatable and indicating that the shales are not perfectly elastic. The reconstructed stress-strain curve for the Bearpaw shale (Figure 17) shows that in contrast to the softer Pierre shale, the Bearpaw shale displayed little variability in the axial stiffness with the exception of step 5.

38. Because of the loading program used, the data obtained for the Quivira and Kincaid shales were not suitable for analysis of the hysteretic behavior. However, the plastic deformation induced into both shales when subjected to a cycle of undrained loading indicates a hysteretic loop might have been observed for drained increments of loading (similar to the Bearpaw and Pierre shales). While it is apparent that the shales are not perfectly elastic, the inelasticity will not affect the pore pressure response provided the shale does not become

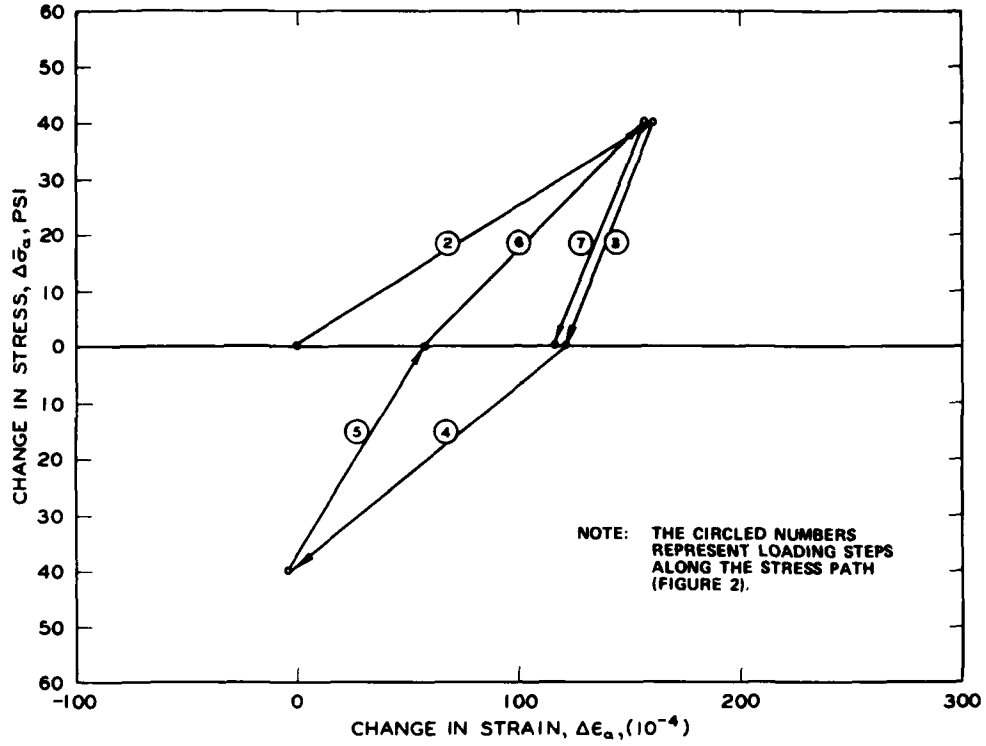

Figure 16. Elastic behavior of Pierre shale under triaxial loading

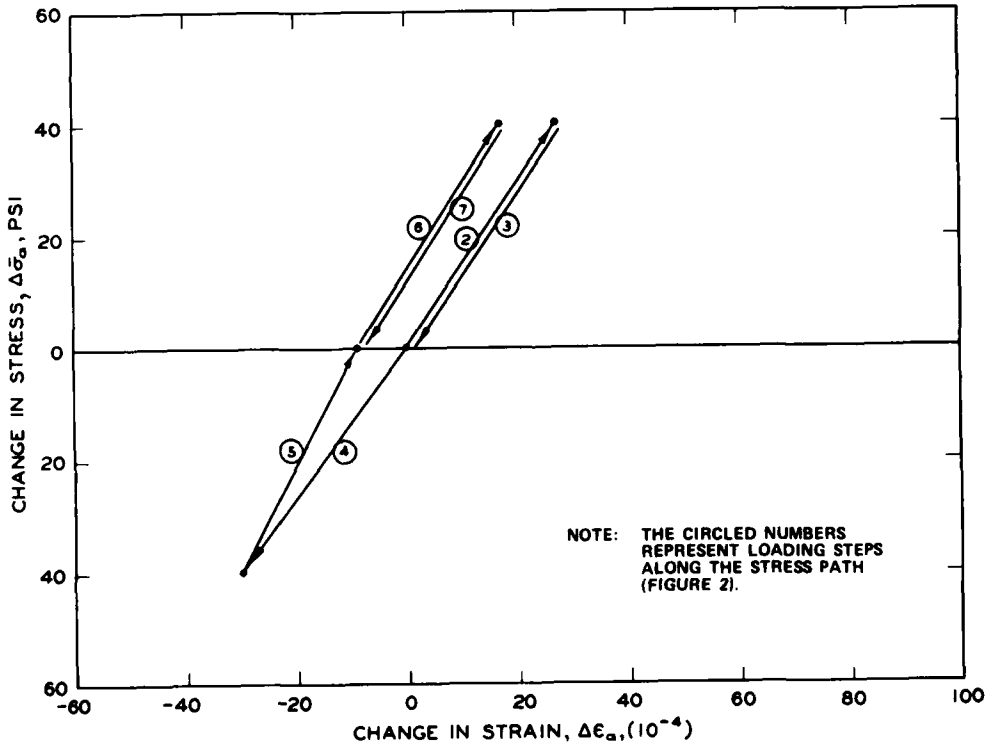

Figure 17. Elastic behavior of Bearpaw shale under triaxial loading

dilative (see paragraph 36). Further, the behavior of the clay shales should be amenable to analysis techniques based on the elastic analysis provided monotonic loadings are considered. Significantly, it is evident that much of the variation in the calculated elastic properties is related to the actual material behavior and that the testing methodology is therefore reliable.

39. One feature of the calculated elastic parameters presented in Table 5 is the degree of anisotropy they exhibit. A good measure of anisotropy is the constant η, which is the ratio of radial stiffness E_3 to axial stiffness E_1 since for an isotropic elastic material they must be equal. While it is impossible with the tests performed to uncouple ν_1 and E_3/E_1, some indication of the relative values of E_1 and E_3 can be obtained by assuming a value of ν_1. The value of ν_1 reflects the coupling of strains in the radial direction and is therefore not affected by the anisotropy. It is, in effect, an isotropic value (Parry 1979*). Assuming $\nu_1 = 0.25$, the following values of E_3/E_1 are obtained.

Shale	$E_1/E_3(1 - \nu_1)$**	η† $= E_3/E_1$
Bearpaw	0.33	2.3
Kincaid	0.56	1.3
Pierre	0.53	1.4
Quivira	0.30	2.5

** Average values obtained from Table 5.
† Value of ν_1 assumed to be 0.25.

These values suggest that the ratio of E_3 to E_1 ranges from about 1.3 to 2.5 for these four shales. It is important to note that if the maximum possible value of ν_1 (0.5) was used in the analysis above, the shales would still appear highly anisotropic.

40. The anisotropy of the shales is comparable to the value of

* R. H. G. Parry. 1979. "Pore Pressure in Clay Shales," Letter Report, Geotechnical Laboratory, U. S. Army Engineer Waterways Experiment Station, CE, Vicksburg, Miss.

2.0 determined by Parry (1976) for the Taylor shale. Also, the ratio η determined for these shales is comparable to typical published values for other geologic materials (Gerrard 1977, Gerrard et al. 1972, and Gibson 1974). Further, the values of η given in the tabulation below can be corroborated with the strain ratio data obtained from the isotropic consolidation. In Appendix A it is shown that

$$\eta = \frac{m(1 - v_1)}{1 + v_2(m - 2)} \tag{8}$$

Using Equation 8 and assuming $v_1 = 0.25$, the following values of η can be calculated:

Shale	m*	v_2**	η
Bearpaw	2.5	0	1.9
Kincaid	2.5	0.04	1.8
Pierre	3.0	0.20	1.9
Quivira	4.0	0.08	2.6

* Values obtained from Figure 11.
** Average values listed in Table 5.

The calculated values of η appear to be similiar to those obtained directly from the tabulation in paragraph 39.

Pore Pressure Parameters

41. The most striking aspect of the pore pressure response for the four shales is that in spite of the large differences in stiffness among the shales, they all exhibit A values on the order of 0.6 to 0.7. These values support the finding of Parry (1976) who suggested that the magnitude of the pore pressure response exhibited by many clay shales may be the result of elastic anisotropy. Also, Parry's conclusion is strongly supported by the correspondence between the parameter m and A (see tabulation in paragraph 33).

42. The similarity in pore pressure response among such diverse materials is best explained by considering the relationship between elastic properties and A parameters. The A parameter was determined within load ranges for which the shales are essentially elastic. From Equation 5, it is noted that A is a ratio of elastic constants. In terms of the engineering constants from Appendix A (Equation A10a) the equation becomes

$$A = \frac{1 - 2\nu_2}{1 - 4\nu_2 + 2\,\dfrac{(1 - \nu_1)}{\eta}} \qquad (9)$$

Inasmuch as Poisson's coefficients, v1 and v2 are within a relatively narrow range, A essentially depends on the constant η, which is the ratio of axial to radial stiffness. Therefore, the many factors that influence stiffness do not affect the A parameter. That is, two clay shales with drastically different stiffness and strength properties could have the same A parameter.

43. The possible numerical value of the A parameter is further limited by Equation 9. For an isotropic material, $\eta = 1.0$, $\nu_1 = \nu_2$, and $A = 1/3$. As the degree of anisotropy becomes greater, so does η. Parry (1976) showed that as η attains a value of 2.0, the A parameter will be on the order of 0.55. For an η of 5.0, A will be on the order of 0.80 where the maximum value of A would be 1.0. It would appear that for an intact (unfractured) shale with significant anisotropy A would be expected to fall within the limited range of 0.5 to 0.7.

44. Note that the above analysis assumes the specimen is oriented with the highest stiffness occurring in the radial direction. If the specimen is oriented differently, the A parameter would exhibit different limits. The relationship between the orientation and the A parameter is given in Appendix A where it is shown that the specimen orientation used in this study gives the maximum obtainable A value.

PART VI: DETERMINATION OF CONSTRUCTION-INDUCED, PORE WATER PRESSURE

Analysis of the Embankment Construction Problem

45. The pore water pressure induced in foundation materials can be related to total stress changes by Equation 1. Therefore, to determine the excess pore water pressure caused by embankment construction, it is necessary to compute changes in the total stress state associated with excavation and fill operations. While a number of analytical and numerical procedures are available for stress analyses, two important aspects of the problem must be considered. First, the geometric condition should not be overly simplified. Embankment construction does not proceed uniformly across a site, and piezometers are often located near the edges and corners of fill sections. An analysis based on the assumption of plane stress, plane strain, or axisymmetric conditions does not accurately account for these edge and corner effects. Second, the method should be easily adapted for field use where frequent comparison of observed and predicted piezometer levels are a part of construction monitoring. A compromise between these two conflicting criteria was obtained by modelling the true shape of the loaded area and by simplifying assumptions on the manner in which the embankment transmits loads to the foundation.

46. The basic problem shown in Figure 18a is to determine the change in pore pressure at point A resulting from the application of an arbitrary layer of fill. To use the procedure developed for this analysis, the problem was simplified by making the following assumptions (Figure 18b):

a. Homogeneous transversel, isotropic elastic material through depth Z .

b. Infinite loading surface.

c. Nonrigid fill layer acting as independent point loads.

d. Undrained response at point A.

e. Superposition of effects of all loads.

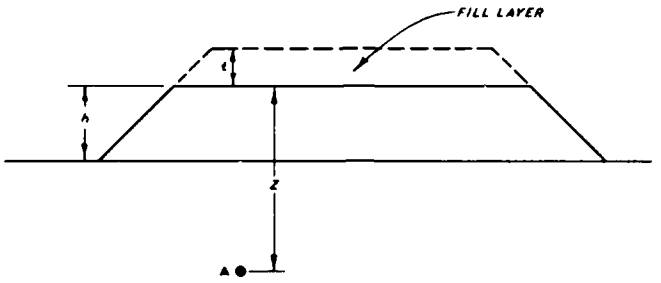

a. Basic problem

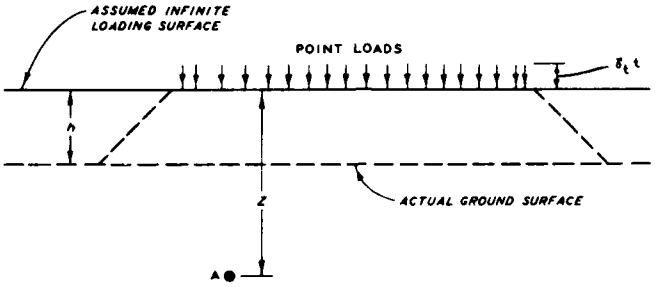

b. Assumed problem

Figure 18. Simplification of embankment problem

47. The first assumption combines the existing fill, overburden, and rock foundation layers into an equivalent transversely isotropic but homogeneous material. The second assumption gives the previously placed fill layers the capability to transfer the load as though it extended laterally to infinity, while the third assumption ignores the influence of the rigidity of the newly placed fill layers on the stress distribution. The fourth assumption requires that no pore water pressure dissipation occur during the load increment application which, when combined with the first assumption, permits superpositions of effects of all loads (fifth assumption). While it is possible to speculate on the relative error introduced by each assumption, the reliability of the computational procedure based on these assumptions must ultimately be based on comparisons with field observations.

48. The interpretation of the problem shown in Figure 18 reduces its mathematical formulation to two fundamental steps. First, the pore

water pressure induced by an individual point load must be expressed as a function of its location relative to point A. Second, the point load function must be integrated over the loaded area. Several theoretical formulas have been developed to determine the stress distribution in an anisotropic media for a point load (Gerrard and Wardle 1973). The derivation of a pore pressure distribution function is relatively straightforward. The integration of the distribution function is, however, made difficult by complex fill shapes and in general must be performed numerically. All pore pressure predictions presented in this report were based on the computer program CURLS developed to integrate the distribution function over arbitary trapezoidal-shaped fill areas. As an aid to general design computations, the program was also used to develop an influence chart (Figure 19) for a graphical determination of pore pressures. Appendix B presents a description of the development and use of the influence chart; Appendix C input instructions, a program listing for CURLS, and examples of its use.

Example Analysis - Hillsdale Dam

49. The construction and piezometer data of Hillsdale Dam were used to verify the methodology developed for predicting construction-induced pore pressures. The Hillsdale Dam construction involved several embankment segments, built at various rates over six construction seasons (1976-1981). Further, the piezometers were located at the center line, edge, and corners of fill segments, providing data for a comprehensive evaluation of the reliability of the pore pressure prediction techniques. The embankment segments analyzed are the test berms*, cofferdam, and the main embankment at sta 104+00 (Figure 20).

Description of damsite

50. The damsite is on the Big Bull Creek approximately 35 miles southwest of Kansas City and 5 miles northwest of Paola, Kansas. The 3000-ft valley section of the dam is centered between the Big Bull Creek and Little Bull Creek; their confluence lies immediately to the south of the dam (Figure 20a). The subdued upland relief necessitated

* The berm was part of first-phase construction and not intended as a test fill.

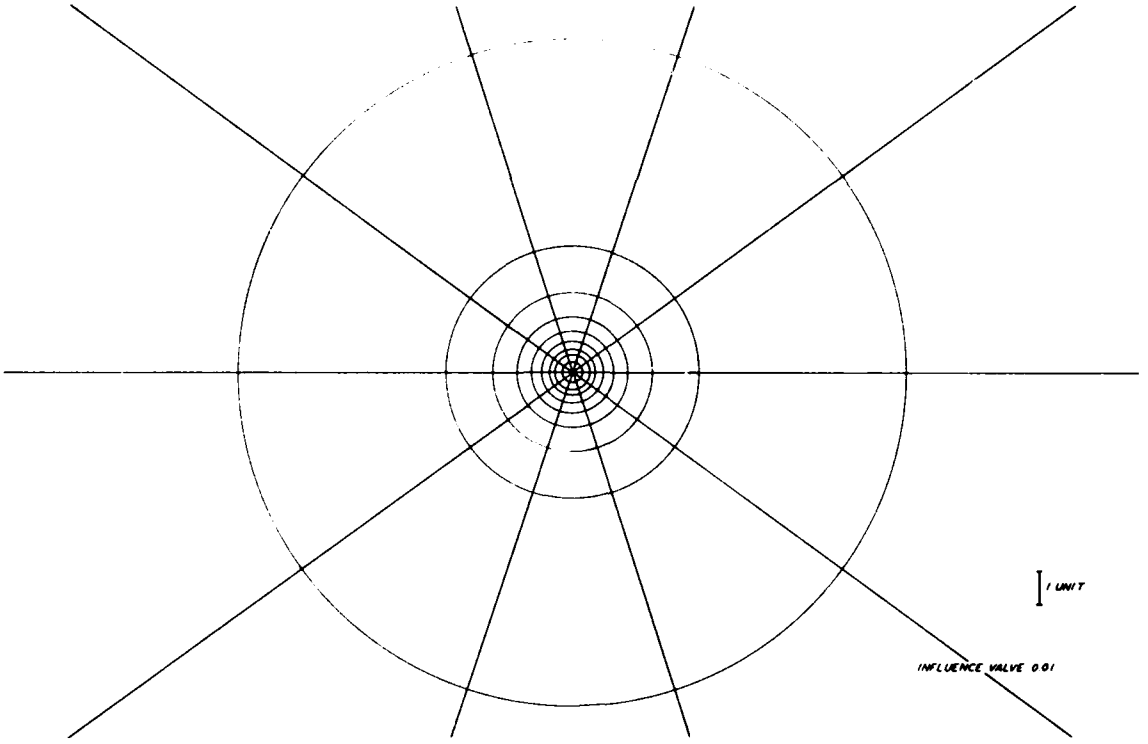

Figure 19. Influence diagram for prediction of construction-induced pore pressures in a layered foundation material ($A = 0.7$ and $\eta = 2.5$)

relatively long abutment sections extending 7900 ft to the right of Big Bull Creek and 700 ft to the left of the low bluff near Little Bull Creek. Within the valley section, the embankment obtains its maximum height of 75 ft (Figure 20b, c, and d).

51. The dam foundation shown in Figure 20b, c, and d consists of 22 to 30 ft of alluvial overburden underlain by sedimentary limestones, sandstones, and shales of the Pennsylvania-age Kansas City Group (Figure 21). The alluvium predominately consists of lean to fat clays, although up to 3 ft of clayey, gravelly sand commonly covers the bedrock surface. Within the valley section, the uppermost rock units consist of 4 ft of Drum limestone and approximately 12 ft of Quivira shale. Weathering in much of the Drum limestone has opened closely spaced, wavy shale partings and vertical joints, which in some instances extend through the limestone to the underlying Quivira shale.

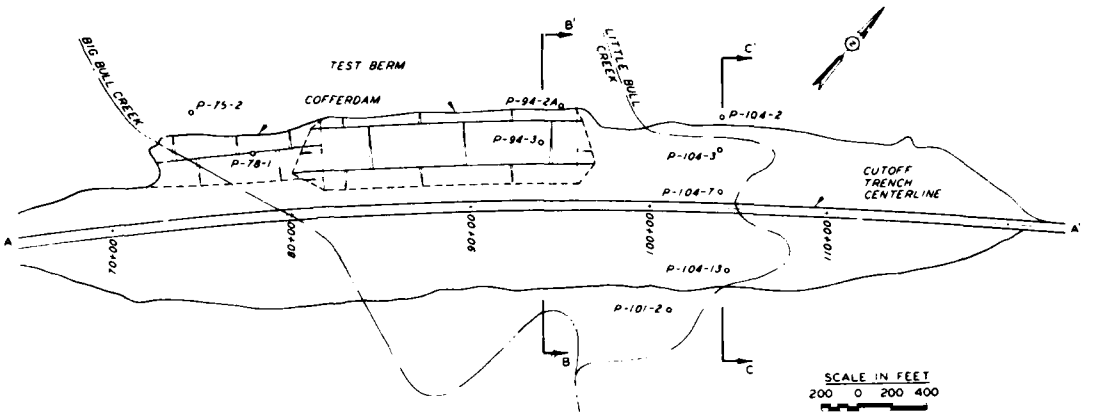

a. Plan

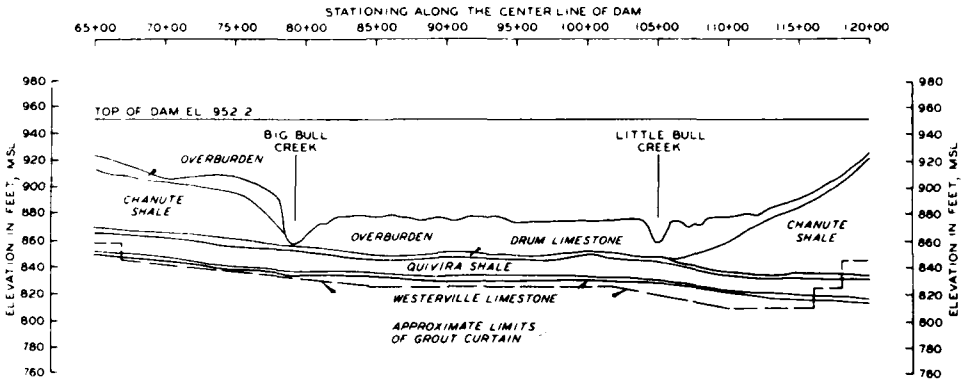

b. Section A-A'

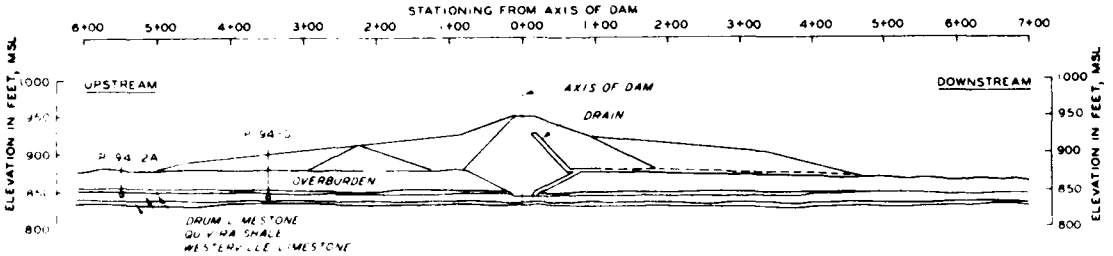

c. Section B-B'

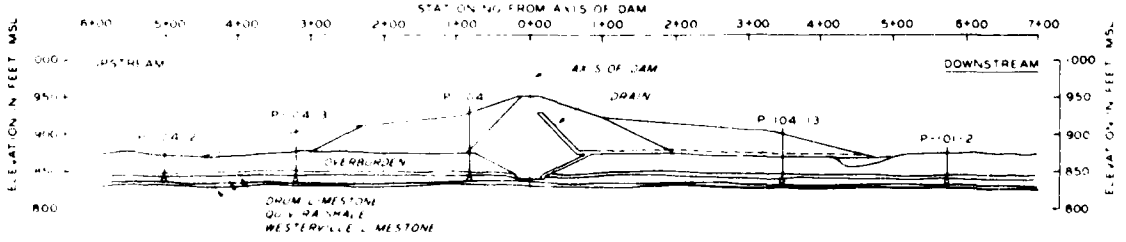

d. Section C-C'

Figure 20. Plan view and sections of Hillsdale Dam (modified from U. S. Army Engineer District, Kansas City 1971)

SYSTEM	GROUP	FORMATION	MEMBER	SYMBOL	APPROXIMATE THICKNESS	GENERAL DESCRIPTION
PENNSYLVANIAN	KANSAS CITY		LANE	La	100'	SHALE: soft to occasionally very soft, clayey to sandy, platy, grey to dark grey, with occasional carbonaceous partings and limestone nodules, upper half of formation includes: sandstone, moderately hard, fine grained, micaceous, occasionally calcareous, thin bedded, grey.
		IOLA	RAYTOWN	R_a	17'	LIMESTONE: moderately hard, dense to finely crystalline, argillaceous and fossiliferous, thin to medium wavy bedded, light bluish grey; 2 shale units separate member into 3 limestone units; shale is soft, clayey, platy, dark grey.
			MUNCIE CREEK	M_c	0.5'	SHALE: soft, clayey, platy, calcareous, occasional spherical phosphatic nodules, grey.
			PAOLA	P_a	2.5'	LIMESTONE: moderately hard, dense, fossiliferous, thick bedded, light grey.
			CHANUTE	C_n	30'	SHALE, SANDSTONE, AND SILTSTONE: lateral as well as vertical variations in lithology with sandstone and siltstone common in upper half of formation; shale is soft to moderately hard, clayey to silty, platy to massive, occasionally calcareous, dark grey to green with pinkish limestone nodules in lower portion of formation; soft shale underclay with numerous slickensides occurs in middle of formation beneath thin coal seam; sandstone and siltstone is moderately hard, very fine grained, calcareous, thin bedded, grey; siltstone often interlaminated with shale.
			DRUM	Dr	4'	LIMESTONE: moderately hard, dense to very finely crystalline, thin to medium bedded, numerous green wavy shale partings, fossiliferous, light grey.
		CHERRYVALE	QUIVIRA	Q_a	12'	SHALE AND SILTSTONE: shale is soft, clayey to silty, platy, dark grey; shale underclay, with occasional very soft partings and bands, and a thin coal seam commonly occur within the upper 4 feet of the member; in lower portion of member the shale is often interlaminated with moderately hard, light grey siltstone.
			WESTERVILLE	W_e	2.5'	LIMESTONE: moderately hard, thin-bedded, dense, argillaceous, brownish grey limestone with green shaly partings and bands, varying to a nodular limestone in a green shale matrix.
			WEA	W_a	21'	SHALE: soft to moderately hard, clayey to silty, platy, occasional calcareous and siltstone partings, dary grey to green-grey.
			BLOCK	Bl	14'	LIMESTONE: moderately hard, dense to very finely crystalline, thin wavy bedding, light brownish grey with occasional light blue mottling; with numerous dark grey, soft shale partings to beds.
			FONTANA	Fn	14'	SHALE: soft to moderately hard, clayey to silty, platy, dark grey to green-grey, with occasional siltstone partings.

Bedrock Unit Thickness	
Parting	<0.02'
Band	0.02 to 0.2'
Thin Bed	0.2 to 0.5'
Medium Bed	0.5 to 1.0'
Thick Bed	1.0 to 2.0'
Massive	>2.0'

Figure 21. Generalized stratigraphic column for rock units (modified from U. S. Army Engineer District, Kansas City 1971)

The Quivira shale consists of an upper 4-ft section of coal seams and carbonaceous shale layers with associated soft to very soft shale underclays. The remainder of the Quivera shale consists of interlaminated soft shales and moderately hard siltstones. Figure 21 describes the rock units extending below the Quivira shale, which alternately consist of limestones and shales.

52. Treatment of the foundation prior to embankment construction consisted of a grout curtain, extended into the rock units below the Quivira shale, and a cutoff trench, excavated through the permeable overburden and Drum limestone into the Quivera shale (Figure 20c and d).

Analyses of pore water pressure

53. The piezometers used in the analyses of the berm, cofferdam, and main embankment were all located within the Quivira shale adjacent to the main valley section of the embankment between Little Bull Creek and Big Bull Creek (Figure 20a). The analyses were based on the methodology described in Appendix B using the computer program CURLS listed in Appendix C. From the properties listed for Quivira shale (see paragraphs 33 and 34), pore pressure parameters A and B were chosen to be 0.7 and 0.99, respectively. The properties used to compute the stress distribution were based on the assumption that the fill, overburden, and rock collectively behaved as a transversely isotropic material with $\eta = 2.5$, $v_1 = 0.2$, $v_2 = 0.1$, and $G_{13} = 0.40E_1$. These values were determined from published literature (Gerrard 1977, and Gibson 1974) to be most representative of layered systems.

54. Test berm. The test berm (Figure 20a) was constructed prior to the main embankment during the 1976 construction season. The piezometric levels were measured before and during construction in piezometers P-94-3 and P-94-2A (Figure 22a). The construction sequence assumed for the analyses consisted of seven horizontal layers (Figure 22b). The thickness of each layer was chosen to obtain the best time sequence of construction activity as inferred from fill inspection records.

55. Excavation of the cutoff trench (Figure 22c) was initiated during the same construction season as the berm. To evaluate the

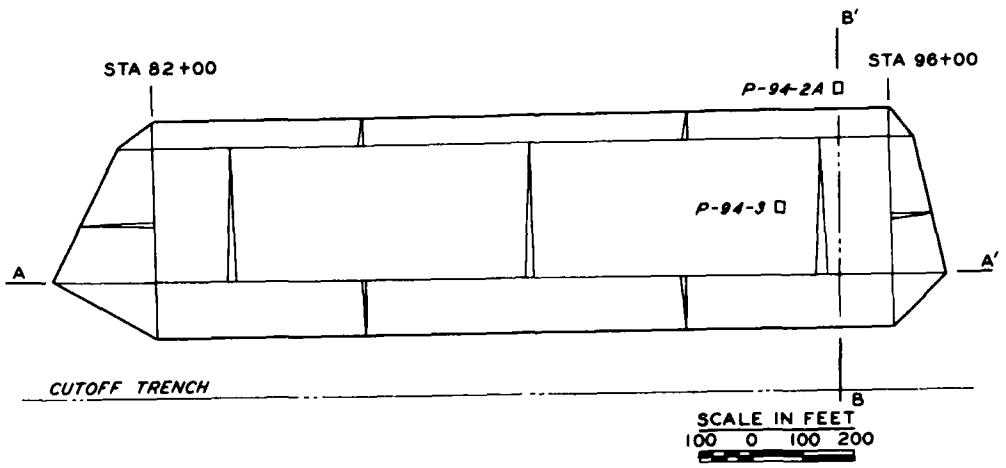

a. Plan

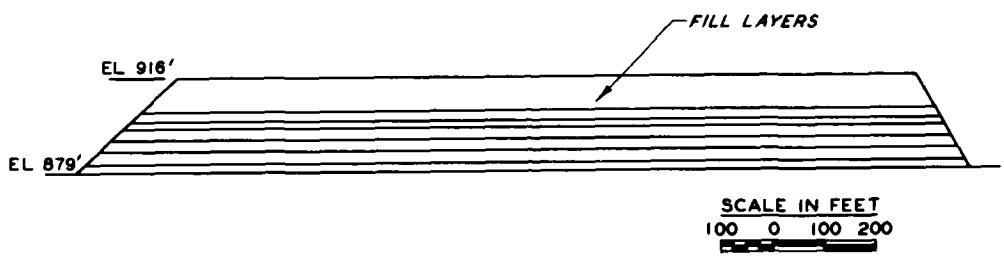

b. Section A-A'

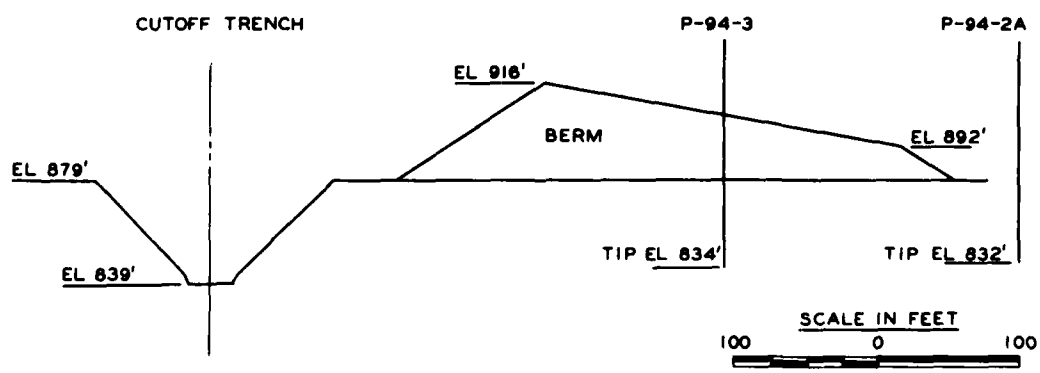

c. Section B-B'

Figure 22. Plan view and sections of test berm

influence of the trench, it was assumed that the excavated material could be modeled as negative (upward) loads. Preliminary computations indicated that unloading during trench excavation and loading during refilling of the trench had virtually no influence on the pore water pressures beneath any portion of the berm. Therefore the pore water pressures induced by the excavation and filling of the cutoff trench were not included in subsequent analyses of the berm's construction.

56. Relatively good agreement was obtained between predictions and piezometric measurements from P-94-3 at the central portion of the west end of the berm (Figure 23). However, the predicted values tended to be higher than those measured, particularly for measurements taken during September 1976 when the rate of loading was reduced. Good agreement was also obtained between predicted and observed trends for piezometer P-94-2A located near the edge of the berm (Figure 24). However, in contrast to the predictions for the central portion, predicted piezometric levels at the berm edge were lower than those measured.

57. Cofferdam. The cofferdam was constructed in a relatively short period of time, 1 month versus 3 months, and offered a good example of undrained response during rapid loading. Figure 25 shows the predicted response for piezometer P-78-1 in the center of the cofferdam to be in good agreement with the observation made near the end of construction in July 1980. The piezometric level observed in late September 1980, nearly 2 months after completion of the cofferdam, was about 4 ft lower than the maximum predicted level.

58. As predicted, the piezometric level adjacent to the cofferdam was observed in piezometer P-75-2 to have virtually no immediate response to cofferdam construction (Figure 26). However, based on the piezometer reading in September 1980, the piezometric level continued to rise after the end of construction.

59. Main embankment. The construction of the main embankment was found to be too complex to develop a time-water level prediction (similar to Figure 23) from available field data. Therefore, a comparison was made between the piezometric levels at the end of construction and the predicted distribution of piezometric levels across the axis of the

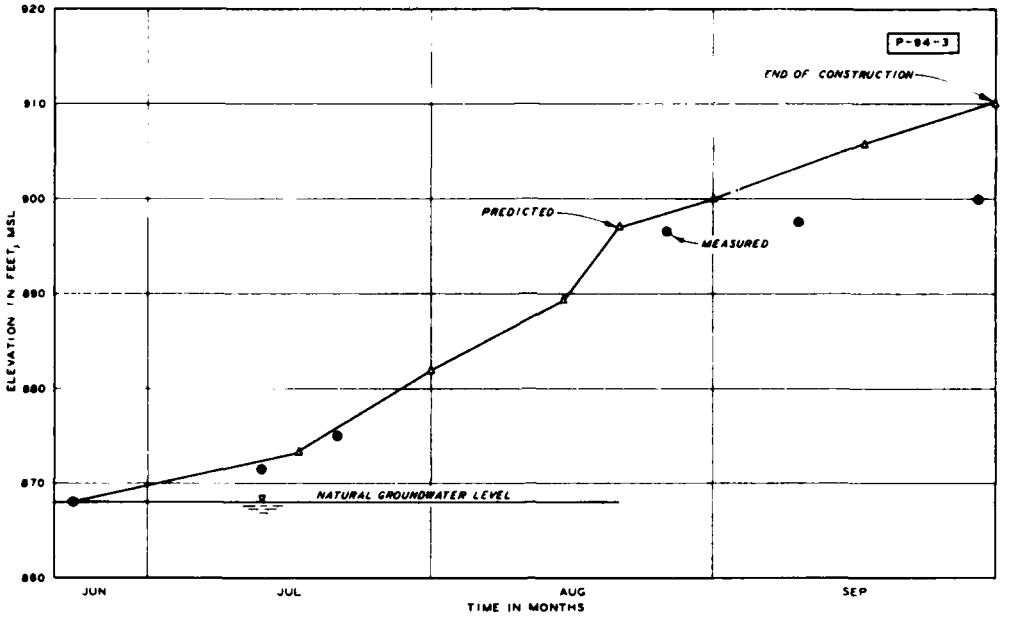

Figure 23. Predicted and measured induced piezometric pore water elevations for piezometer P-94-3

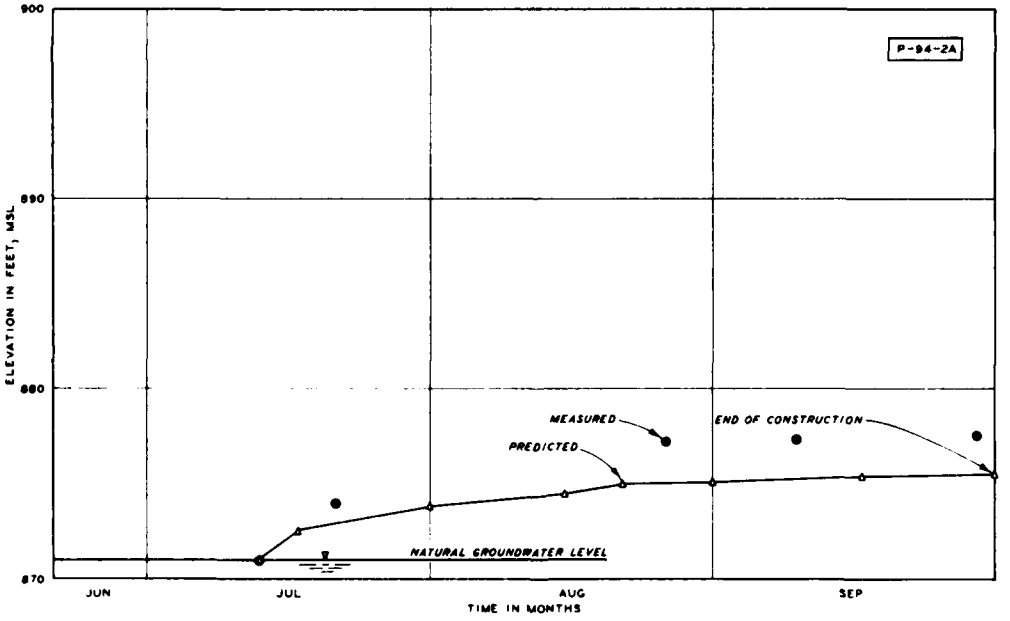

Figure 24. Predicted and measured induced piezometric pore water elevations for piezometer P-94-2A

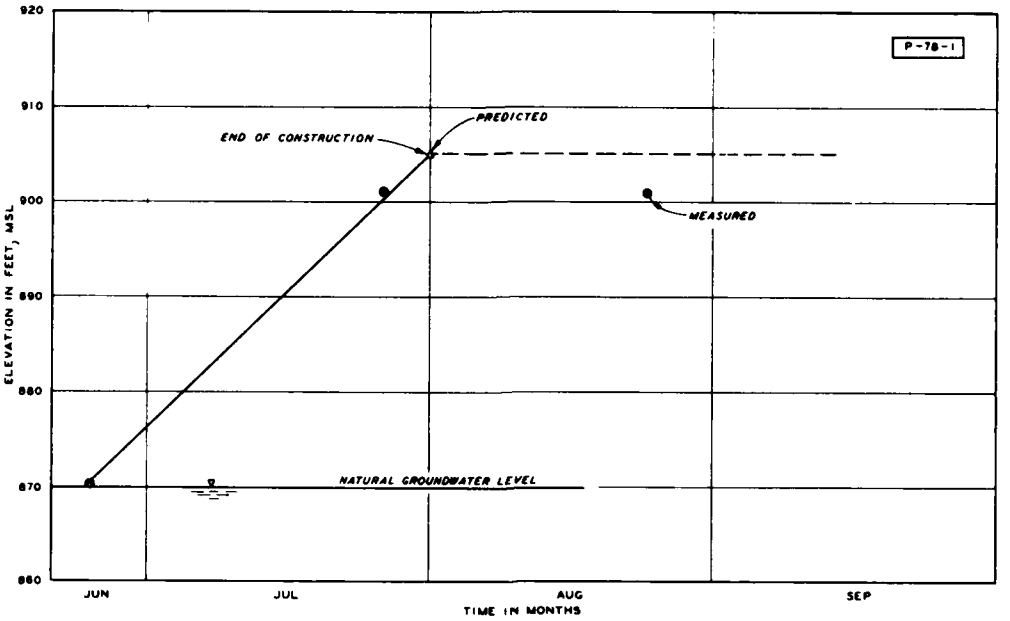

Figure 25. Predicted and measured induced piezometric pore water elevations for piezometer P-78-1

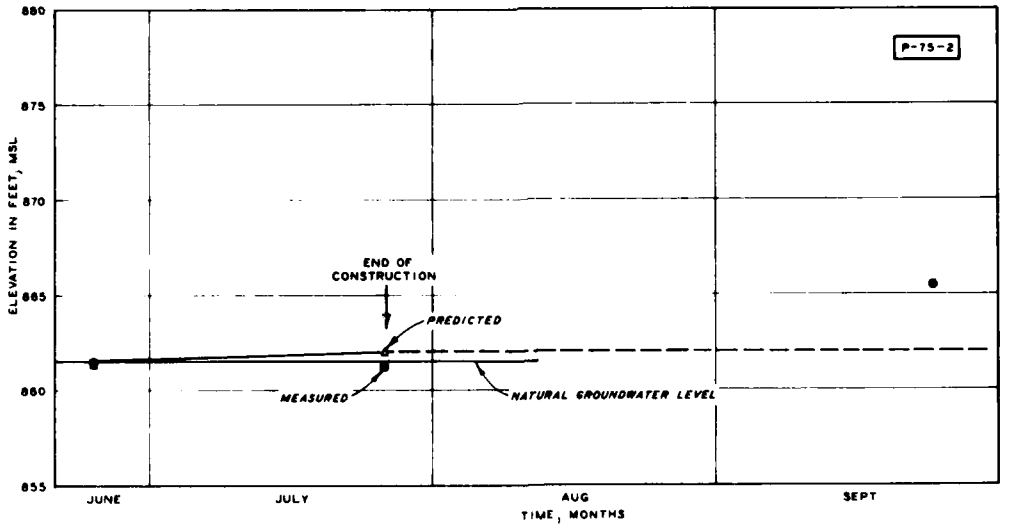

Figure 26. Predicted and measured induced piezometric pore water elevations for piezometer P-75-2

dam. The predicted levels correspond to induced heads at el 845.0 and 832.0 ft, which, respectively, correspond to the top and bottom of the Quivira shale. Table 6 presents the specific predictions made for each piezometer location.

60. The comparison of trends shown in Figure 27 reveals that near

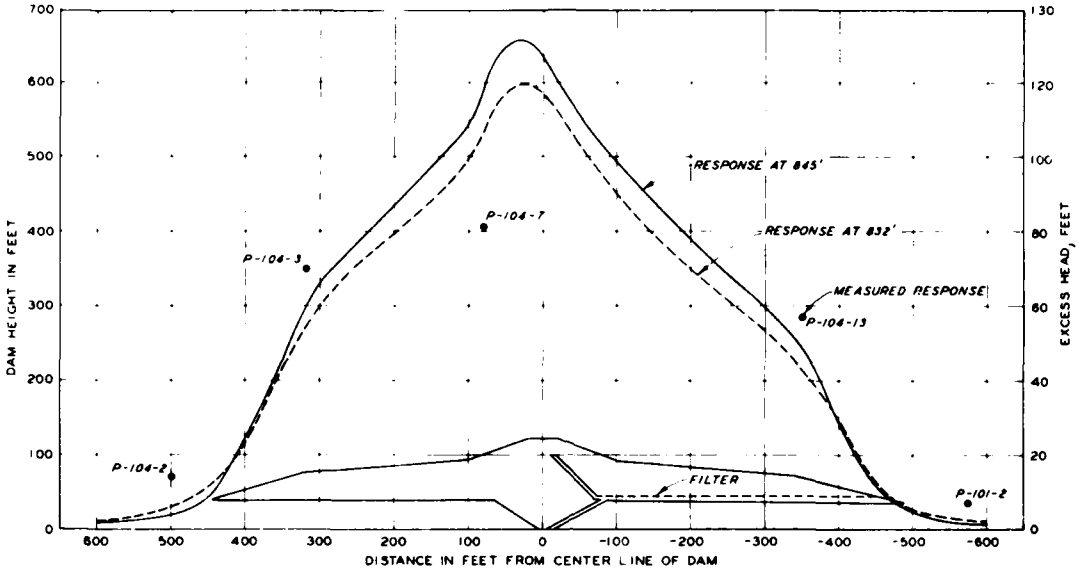

Figure 27. Predicted and measured induced piezometric pore water heads across axis of dam (η = 2.5)

the center line of the embankment, the predicted piezometric level is greater than that observed, while at the edges of the embankment the predicted is somewhat less than the observed. Therefore, the comparison corroborates the general observations made for the test berm and cofferdam that the prediction method overestimated the induced pore water pressure near the embankment center line but underestimated the pressure at the embankment fringe.

PART VII: DISCUSSION OF RESULTS

61. Comparisons between observed and predicted values of piezometric levels indicate that the proposed computational procedure gives a good general prediction of construction-induced pore water pressures. However, the general correspondence between prediction error and piezometer location relative to the embankment center line suggests the error could be attributed to some fundamental cause. Four factors can be identified that could influence the comparison of predicted and measured pore pressure changes.

a. Fluctuations in the natural groundwater level during loading.

b. Material parameters used in analysis.

c. Total stress computation procedure.

d. Dissipation of pore pressures during loading.

The potential error caused by these factors and the distribution of this error with respect to piezometer location will be discussed in the following paragraphs.

Groundwater Fluctuations

62. The groundwater fluctuations observed prior to initiation of construction were generally too small to account for the differences between predicted and measured induced pore water pressures. However, changes in the groundwater conditions caused by construction could account for some of the error. For example, the excavation and refilling of the cutoff trench was observed to cause water level fluctuations in piezometers located in the Quivira shale. Based on computations, these fluctuations were too great to be attributed to the unloading and loading associated with trench construction. Moreover, concomitant fluctuations were observed in piezometers located within the Drum limestone, which generally did not respond to loading. It was concluded that while little seepage was observed to flow into the trench excavation, trench construction did have sufficient influence on the

groundwater flow conditions to alter the piezometric surface. Thus, the cutoff trench excavation could have been responsible for the leveling off of the piezometric levels observed in P-94-3 near the end of construction (Figure 23). Trends in piezometric levels shown in Figures 24 through 27 should not have been similarly affected.

Material Parameters

63. The choice of material parameters enters into the analysis in two ways. First, the pore pressure parameter A must be properly selected to model not only the intact material as tested in the laboratory but also the in situ conditions that include large-scale structural and stratigraphic features. Second, the elastic properties used in the computation of total stress distribution must be selected to give the best representation of the various foundation materials. Neither of these factors can be evaluated solely from laboratory test data.

64. The A parameter has an influence on both the magnitude and distribution of pore water pressures. The approximate pore pressure response induced by extensive fills is shown in the following tabulation:

	$\Delta u/\gamma_t t$	
A	Embankment Center	Embankment Edge*
0.33	0.90	0.33
0.50	0.92	0.27
0.55	0.93	0.25
0.60	0.94	0.24
0.65	0.95	0.22
0.70	0.96	0.20
0.75	0.97	0.19
1.0	1.0	0.11

Note: Smallest lateral dimension of fill exceeds 50 times the depth of the piezometer.
* Distance from fill is equal to one to two times the depth of the piezometer.

For materials with an A parameter approaching 1.0, the induced pore water pressure Δu is equal to the applied vertical stress. For such materials, a fill having a lateral dimension of three to four times the piezometer depth will produce pore water pressures equal to the applied surface load $\gamma_t t$ (Table B1). For isotropic materials having $A = 0.33$, the two horizontal stresses each have an influence equal to that of the vertical stress. For such materials, an extensive fill would produce a pore water pressure of only 90 percent of the surface pressure $\gamma_t t$. Observe that for the range of A values measured for the Quivira shale (0.55 to 0.7), the error introduced by uncertainty in the A parameter is less than 5 percent.

65. The error introduced in the analysis by an incorrect value of A is considerably greater for piezometers located near the edge of an embankment than it is for an interior piezometer. For example, for piezometers located at a distance from the embankment of one to two times the piezometer depth, the induced pore water pressure would be $0.3\gamma_t t$ for an $A = 0.33$ but $0.1\gamma_t t$ for $A = 1$. Thus, the effect of reducing the A parameter on the computed pore water pressure is to decrease the computed pore water pressure near the center but increase the computed pore water pressure near the embankment edge. Thus, some improvement in the comparison between predicted and observed piezometric levels could be achieved by using a smaller A parameter in the analysis. However, the magnitude of the improvement would be insufficient to explain the high pore water pressures observed adjacent to the embankment (Figure 27). Moreover, manipulation of the A parameter to improve the comparisons for embankment edges would create a less favorable comparison for the centrally located piezometers as indicated in Figures 23 and 25.

66. The primary material property that describes the anisotropy of the foundation system is the ratio η. From the comparisons in Table 6, it is indicated that the pore water pressures computed for the isotropic case, $\eta = 1.0$, are virtually the same as for the assumed anisotropic case, $\eta = 2.5$. For the extreme anisotropic case, $\eta = 10.0$, the computed pore water pressures are about

20 percent higher than the isotropic case in the embankment centers and several times the isotropic case at the embankment edge. Thus, unless extreme degrees of anisotropy are envisioned, the induced pore water pressure is not greatly affected by anisotropy. Further, to improve the comparisons between predicted and observed pressures, a different value of η would have to be assumed for each piezometer location. In view of the correspondence between the location of the piezometer within the loaded area and the observed error, it is unlikely that random variations in anisotropic properties would fully account for differences between observed and predicted pressures.

Computation Procedure

67. The potential error created by simplification of the stress analysis is difficult to assess without invoking a significantly more sophisticated computational procedure to use as a comparison. However, the systematic nature of the error would suggest that the simplified method possibly distorts the picture of the true stress distribution. By incorporating the true embankment stiffness and the inhomogeneities of the layered foundation, the stress predictions could possibly be improved. However, since a more sophisticated analysis would also increase the number of variables to be determined (and the opportunities for data manipulation), it is doubtful that the reliability of a more sophisticated analysis could be assessed with the available data.

68. Another potential problem in the comparison of predicted and observed piezometric levels is the assumption that the piezometer acts at a distinct point within the foundation mass. In Figure 28, the pore water pressure varies by 5 to 10 percent in the vicinity of the piezometer tip, an error that exceeds those associated with the uncertainties in material properties. However, from the predicted values shown in Figure 26, the error associated with pressure differences between the top and bottom of the Quivira shale would not explain the observed difference between computed and measured pore water pressures.

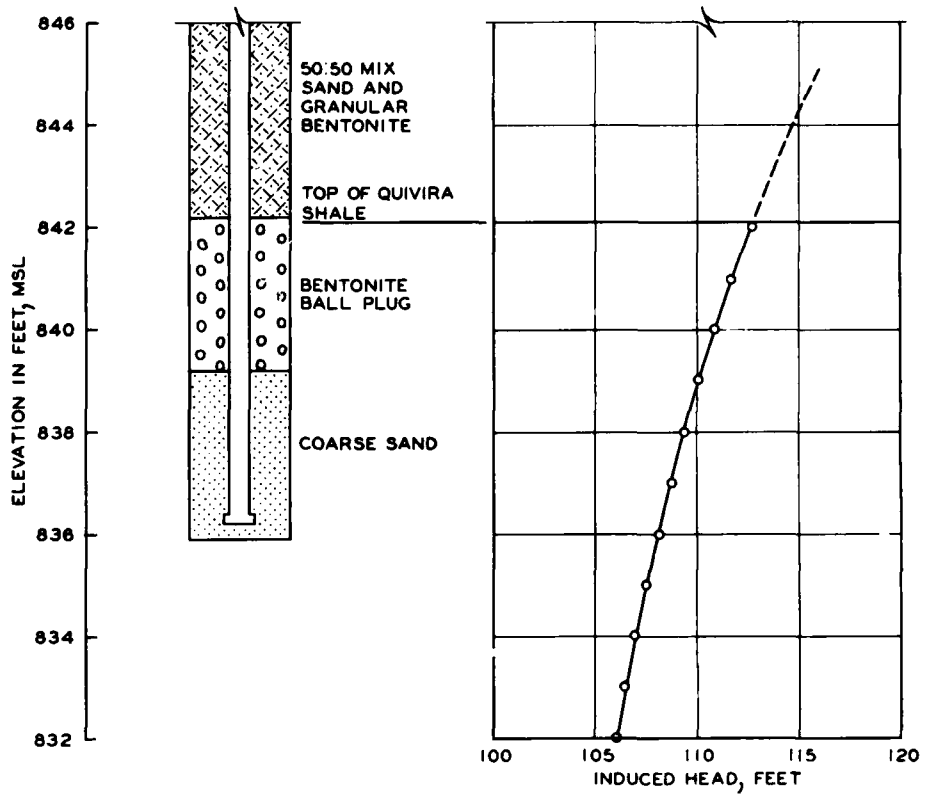

Figure 28. Comparison of typical piezometer installation with computed induced head through depth of Quivira shale

Pore Pressure Dissipation

69. In view of the pore pressure dissipation that can occur during construction, the potential error introduced by the assumption of undrained pore water pressure response can be quite significant. The magnitude of the error caused by dissipation cannot be fully assessed with the available data. However, the general influence of dissipation on the pore pressure response was observed. For example, in Figures 22 through 26, the greatest deviation between observed and predicted values occurred after construction rates were either reduced or the embankment topped out. Further, it was generally observed for all piezometers that piezometric levels lower than the predicted value tended to fall off with time, while levels higher than those predicted either continued to rise

or remained constant. In many cases, the difference in the two types of performance was quite dramatic as shown in Figures 29 and 30. The interpretation of these observations shown in Figure 31 is that while the shape of the initial undrained pore pressure distribution is similar to that of the embankment, with time the consolidation process causes a flatter distribution to develop that extends well beyond the limits of the embankment. The interpretation explains both the distribution and the magnitude of the observed error and is consistent with all piezometric data obtained at the Hillsdale damsite.

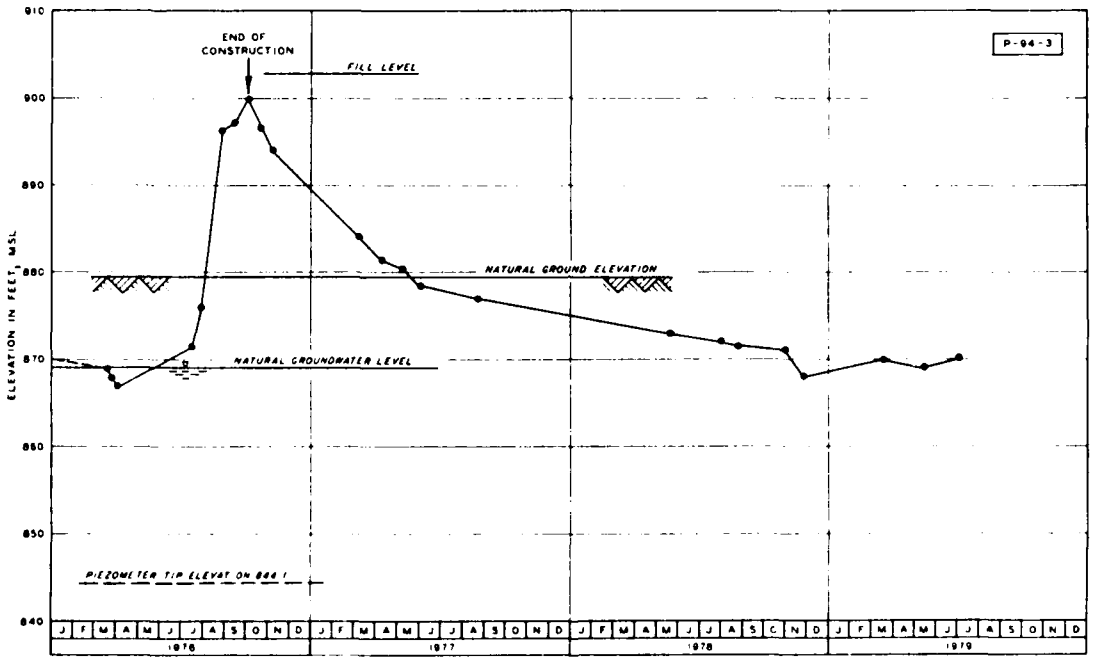

Figure 29. Piezometric pore water response after the completion of construction for piezometer P-94-3

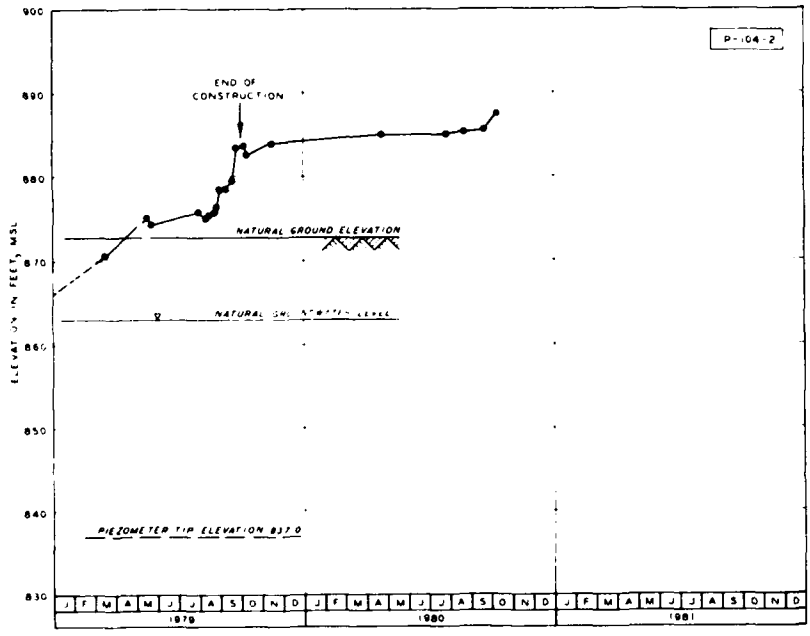

Figure 30. Piezometric pore water response after the completion of construction for piezometer P-104-2

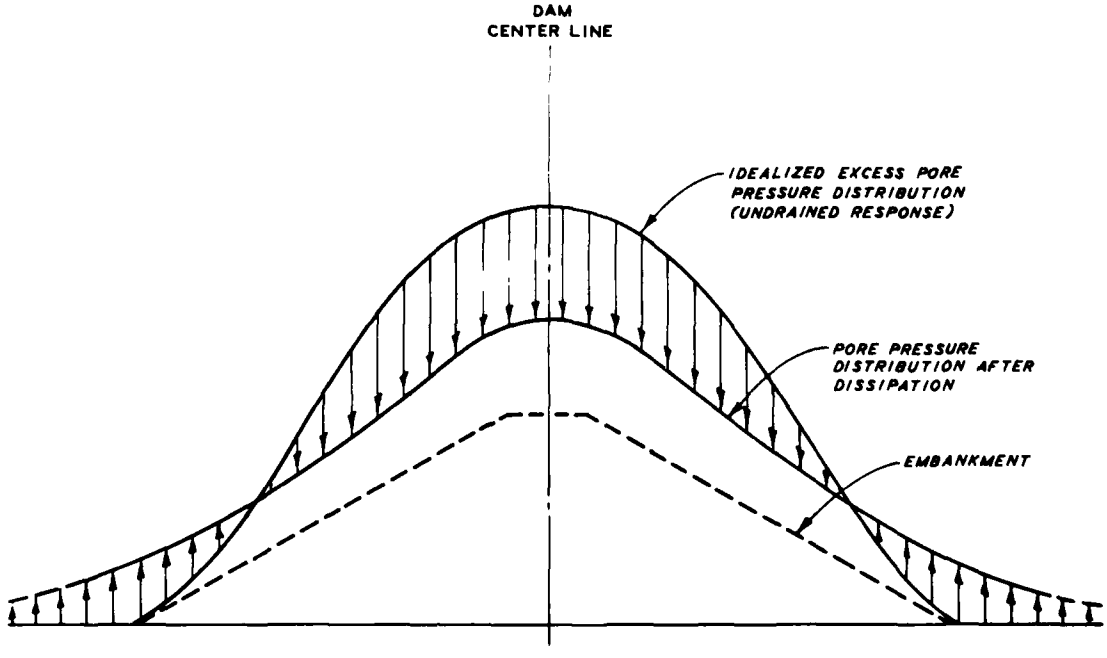

Figure 31. Conceptional view of pore pressure redistribution with dissipation

PART VIII: CONCLUSIONS

70. A combined laboratory and field investigation demonstrated the feasibility of using the theory of elasticity for undrained loading of transversely isotropic materials to predict the pore pressures induced in clay shale foundations by embankment construction.

Laboratory Investigations

71. Based on the four shales tested and a previous investigation by Parry (1976), the following conclusions are made:

a. Reliable data can be obtained from long-term triaxial tests on compact clay shales, provided special precautions are made to isolate air pressure from direct contact with saturating and confining fluids. Pore pressure B values varied from 1.0 at initial saturation to 0.9 or greater after one year of testing.

b. Although shales are not perfectly elastic, within the range of most field loadings, this inelasticity is of secondary importance, and shales can be characterized as elastic materials for prediction of construction-induced pore pressures.

c. Clay shales are markedly anisotropic, exhibiting a stiffness 1.3 to 2.5 greater in the bedding plane than normal planes (E_3/E_1 1.3 to 2.5).

d. The pore pressure during undrained loading can be related to changes in total stress by

$$\Delta u = B[\Delta\sigma_r + A(\Delta\sigma_a - \Delta\sigma_r)]$$

The pore pressure parameters A and B can be related to the anisotropic elastic constants.

e. By combining the pore pressure response for an undrained loading segment with the subsequent drained stress-strain response, a computational procedure was developed to determine three of the five elastic constants needed to describe the transverse-isotropic behavior. The remaining constants can be adequately estimated from published data.

f. Theoretical values for the pore pressure parameters,

based on the elastic properties, compared favorably with those measured in the laboratory tests. Thus, the theory of elasticity gives a reliable basis for estimating construction-induced pore pressures in clay shale foundations.

g. The pore pressure parameter A essentially depends upon the ratio of anisotropy, E_3/E_1, and not the magnitude of stiffness. For elastic materials, A ranges between 1/3 for isotropic materials to 1.0 for extreme anisotropy. Since the E_3/E_1 ratio of clay shales commonly falls within a range of 1.5 to 3.0, the A parameter for natural transversely isotropic materials tends to fall in the more restricted range of 0.5 to 0.7.

h. Near failure, the shales display inelastic dilatant behavior and the A parameter approaches zero. However, because the mode of failure in the field is controlled by the usually horizontal planes of isotropy, the shear failure induced in a triaxial specimen may not be representative of field behavior.

Pore Pressure Predictions

72. A simplified procedure was developed to compute the pore pressure induced in the foundation by fill placed at the ground surface. A comparison between predicted and observed piezometric levels indicated that the procedure gives good estimates of instantaneous pore pressure response. Conclusions on the use of the simplified procedure include:

a. The material parameters having the greatest influence on the computed pore pressures are the parameter A for the shale and the E_3/E_1 ratio for the combined foundation layers. It was determined that for the limited range of numerical values typically observed for the parameters, differences between observed and predicted pore pressures could not be attributed to uncertainties in material properties.

b. Natural and construction-related changes in groundwater levels had a relatively small influence on induced pore pressures.

c. Redistribution of pore pressures during and after construction was shown to have the greatest influence on the differences in observed and predicted pore pressures. Therefore, to evaluate the pore pressure response of

clay shale foundations better, the analysis should consider the effects of pore pressure dissipation and migration.

73. The inevitable redistribution of pore pressures has important practical implications in design and construction. It is important to recognize that pore pressure dissipation does not imply pore pressure reduction when the two-dimensional aspects of the problem are considered. At and beyond the edges of the embankment, pressures may rise with time, possibly to the detriment of foundation stability. Pore pressure measurements should be an important part of the construction monitoring program, especially in closure sections where high pore pressures can be developed before final embankment construction. Refer to EM 1110-2-1908, entitled "Instrumentation of Earth and Rock-fill Dams," part 1, paragraph 4-2, for guidance.

REFERENCES

Baker, Wallace H., and Krizek, Raymond J. 1969. "Pore Pressure Equation for Anisotropic Clays," Journal of the Soil Mechanics and Foundations Division, American Society of Civil Engineers, Vol 95, No. SM2, pp 719-724.

Barden, L. 1963. "Stresses and Displacements in a Cross-Anistropic Soil," Geotechnique, Vol 13, No. 3, pp 198-210.

Beene, Ralph R. W. 1967. "Waco Dam Slide," Journal of the Soil Mechanics and Foundations Division, American Society of Civil Engineers, Vol 93, No. SM4, Proceedings Paper 5306, pp 35-44.

Craig, R. F. 1978. "Stresses and Displacements," Soil Mechanics, 2d ed., Van Nostrand Reinhold, New York, pp 162-176.

Department of the Army, Office, Chief of Engineers. 1970. "Laboratory Soils Testing," Engineer Manual 1110-2-1906, Washington, D. C.

Gerrard, C. M. 1977. "Background to Mathematical Modelling in Geomechanics: The Roles of Fabric and Stress History," Finite Elements in Geomechanics, G. Gudehus, ed., 1st ed., Wiley, New York, pp 33-120.

Gerrard, C. M., and Wardle, L. J. 1973. "Solutions for Point Loads and Generalized Circular Loads Applied to a Cross-Anisotropic Half Space," Australian Geomechanics Journal, Paper No. 13, pp 4-5.

Gerrard, C. M., Davis, E. H., and Wardle, L. J. 1972. "Estimation of the Settlements of Cross-Anisotropic Deposits Using Isotropic Theory," Australian Geomechanics Journal, Vol G2, No. 1, pp 1-10.

Gibson, R. E. 1974. "The Analytical Method in Soil Mechanics," Geotechnique, Vol 24, No. 2, pp 115-139.

Hornbeck, R. W. 1975. "Numerical Integration," Numerical Methods, Quantum Publishers, New York, pp 144-165.

Jaspar, J. L., and Peters, N. 1979. "Foundation Performance of Gardiner Dam," Canadian Geotechnical Journal, Vol 16, pp 758-788.

Lekhnitskii, S. G. 1963. "Deformations of Solids of Revolution," Theory of Elasticity of an Anisotropic Elastic Body, J. J. Brandstatter, ed., Holden-Day, San Francisco, Calif., pp 347-397.

Little, A. L. 1968. "Discussion of Waco Dam Slide," Journal of the Soil Mechanics and Foundations Division, American Society of Civil Engineers, Vol 94, No. SM2, pp 588-590.

Parry, R. H. G. 1976. "Engineering Properties of Clay Shales; Preliminary Triaxial Test Program on Taylor Shale from Laneport Dam," Technical Report S-71-6, Report 3, U. S. Army Engineer Waterways Experiment Station, CE, Vicksburg, Miss.

Skempton, A. W. 1954. "The Pore Pressure Coefficients A and B," Geotechnique, Institution of Civil Engineers, London, Vol 4, No. 4, pp 143-147.

Snethen, D. R. 1979. "An Evaluation of Methodology for Prediction and Minimization of Detrimental Volume Change of Expansive Soils in Highway Subgrades, Vols I and II," Research Report FHWA-RD-79-49, Federal Highway Administration, Washington, D. C.

U. S. Army Engineer District, Kansas City. 1971. "Hillsdale Lake, Osage River Basin, Big Bull Creek, Kansas; Soil Data and Embankment Design," Design Memorandum No. 7, Kansas City, Mo.

U. S. Army Engineer District, New Orleans. 1977. "Red River Below Denison Dam, Cooper Lake and Channels, Sulphur River, Texas; Detail Design of Cooper Dam and Spillway," Design Memorandum No. 3, Vol 1, New Orleans, La.

Zienkiewicz, O. C. 1977. "Curved, Isoparametric Elements and Numerical Integration," The Finite Element Method, 3d ed., McGraw-Hill (UK) Limited, London, pp 179-210.

Table 1

Measured Quantities for Bearpaw Shale

Step	Increment	$\Delta\bar{\sigma}_a$	$\Delta\bar{\sigma}_r$	Δu	$\Delta\varepsilon_a$ (10^{-4})	$\Delta\varepsilon_r$ (10^{-4})	$\Delta V/V(10^{-4})$	A
1			$\bar{\sigma}_a = 28.9$	$\bar{\sigma}_r = 30.0$	$u = 109.0$			
	1	-1.4	0.0	43.0	2.0	0.0	--	--
	2	39.0	39.0	-40.0	28.0	11.0	55.0	--
2			$\bar{\sigma}_a = 69.6$	$\bar{\sigma}_r = 68.0$	$u = 112.0$			
	3	10.5	-20.0	19.0	5.0	-2.0	--	0.65
	4	19.6	21.0	-20.0	15.0	4.0	23.0	--
3			$\bar{\sigma}_a = 98.7$	$\bar{\sigma}_r = 69.0$	$u = 111.0$			
	5	-13.4	15.0	-15.0	-5.0	2.0	--	0.53
	6	-13.4	-14.0	14.0	-7.0	-1.0	-22.0	--
4			$\bar{\sigma}_a = 70.9$	$\bar{\sigma}_r = 72.0$	$u = 110.0$			
	7	-10.7	16.0	-21.0	-8.0	1.0	--	0.60
	8	-15.0	-15.0	20.0	-12.0	-1.0	-18.0	--
5			$\bar{\sigma}_a = 44.8$	$\bar{\sigma}_r = 73.0$	$u = 109.0$			
	9	12.4	-15.0	12.0	7.0	-2.0	--	0.55
	10	9.5	9.0	-12.0	6.0	1.0	8.0	--
6			$\bar{\sigma}_a = 67.4$	$\bar{\sigma}_r = 68.0$	$u = 109.0$			
	11	10.1	-19.0	-13.0	5.0	-2.0	--	0.65
	12	-10.6	-11.0	12.0	-5.0	-2.0	-11.0	--
7			$\bar{\sigma}_a = 65.9$	$\bar{\sigma}_r = 39.0$	$u = 107.0$			
	13	-11.3	18.0	-18.0	-6.0	2.0	--	0.61
	14	-17.7	-18.0	18.0	-12.0	-3.0	-21.0	--

Note: All pressures are in pounds per square inch.

Table 2

Measured Quantities for Kincaid Shale

Step	Increment	$\Delta\bar{\sigma}_a$	$\Delta\bar{\sigma}_r$	Δu	$\Delta\varepsilon_a$ (10^{-4})	$\Delta\varepsilon_r$ (10^{-4})	$\Delta V/V(10^{-4})$	A
1			$\bar{\sigma}_a = 24.7$	$\bar{\sigma}_r = 25.0$	$u = 99.0$			
	0	46.8	47.0	0.0	83.0	33.0	166.0	--
2			$\bar{\sigma}_a = 69.6$	$\bar{\sigma}_r = 70.0$	$u = 99.0$			
	1	11.5	-17.0	19.0	17.0	-6.0	--	0.60
	2	2.0	2.0	11.0	1.0	0.0	--	--
	3	-14.8	13.0	-13.0	-12.0	5.0	--	0.47
	4	0.0	0.0	-13.0	0.0	0.0	--	--
	5	-1.0	-1.0	1.0	2.0	1.0	3.0	--
3			$\bar{\sigma}_a = 69.3$	$\bar{\sigma}_r = 69.0$	$u = 101.0$			
	6	26.6	-2.0	1.0	28.0	1.0	31.0	--
4			$\bar{\sigma}_a = 97.1$	$\bar{\sigma}_r = 68.0$	$u = 102.0$			
	7	-1.3	-1.0	15.0	1.0	0.0	--	--
	8	-16.9	12.0	3.0	-7.0	4.0	--	--
	9	-1.6	-2.0	13.0	-1.0	1.0	--	--
	10	13.6	-15.0	2.0	10.0	-4.0	--	--
	11	10.9	11.0	-6.0	10.0	1.0	8.0	--
5			$\bar{\sigma}_a = 95.8$	$\bar{\sigma}_r = 67.0$	$u = 103.0$			
	12	-27.7	1.0	-1.0	-22.0	2.0	-27.0	--
6			$\bar{\sigma}_a = 35.6$	$\bar{\sigma}_r = 36.0$	$u = 99.0$			
	12A	35.7	35.0	1.0	63.0	23.0	120.0	--
7			$\bar{\sigma}_a = 71.2$	$\bar{\sigma}_r = 71.0$	$u = 100.0$			
	13	-1.5	-1.0	30.0	0.0	1.0	--	--
	14	30.6	30.0	-30.0	46.0	17.0	83.0	--
	15	-14.0	4.0	-5.0	-8.0	2.0	--	0.43
	16	1.1	-2.0	-26.0	0.0	0.0	--	--
	17	7.8	-7.5	6.5	1.0	-1.0	--	0.49
	18*	--	--	--	--	--	--	--
	19	0.1	0.5	27.5	0.0	0.0	--	--
	20	2.4	4.0	-3.0	0.0	0.0	2.0	--
	21	-27.1	-28.0	1.0	-21.0	-10.0	-46.0	--
8			$\bar{\sigma}_a = 73.1$	$\bar{\sigma}_r = 72.0$	$u = 100.0$			
	22	-15.2	-1.0	1.0	-15.0	0.0	-17.0	--
9			$\bar{\sigma}_a = 57.9$	$\bar{\sigma}_r = 71.0$	$u = 101.0$			
	23	10.8	-4.0	4.0	6.0	-2.0	--	0.58
	24	-6.4	8.0	-8.0	-6.0	1.0	--	0.56
	25	-7.8	-8.0	7.0	-5.0	0.0	-11.0	--
10			$\bar{\sigma}_a$ 7.4	$\bar{\sigma}_r = 71.0$	$u = 110.0$			
	26	9.6	-4.0	3.0	7.0	-3.0	--	0.59
	27	3.5	2.0	-3.0	2.0	0.0	1.0	--

Note: All pressures are in pounds per square inch.
* No increment.

Table 3

Measured Quantities for Pierre Shale

Step	Increment	$\Delta\bar{\sigma}_a$	$\Delta\bar{\sigma}_r$	Δu	$\Delta\varepsilon_a$ (10^{-4})	$\Delta\varepsilon_r$ (10^{-4})	$\Delta V/V$ (10^{-4})	A
1			$\bar{\sigma}_a = 28.2$		$\bar{\sigma}_r = 28.0$	$u = 90.0$		
	1	-0.6	0.0	31.0	0.0	0.0	--	--
	2	31.1	31.0	-31.0	103.0	28.0	183.0	--
2			$\bar{\sigma}_a = 53.5$		$\bar{\sigma}_r = 54.0$	$u = 95.0$		
	3	6.9	-23.0	21.0	96.0	-44.0	--	0.77
	4	25.1	24.0	-21.0	49.0	17.0	85.0	--
3			$\bar{\sigma}_a = 85.6$		$\bar{\sigma}_r = 95.0$	$u = 95.0$		
	5	-21.0	9.0	-11.0	-26.0	11.0	--	0.30
	6	-7.2	-7.0	11.0	-7.0	-2.0	-13.0	--
4			$\bar{\sigma}_a = 57.4$		$\bar{\sigma}_r = 57.0$	$u = 95.0$		
	7	-12.9	17.0	-15.0	-57.0	24.0	--	0.57
	8	-12.3	-12.0	13.0	-37.0	-1.0	-43.0	--
5			$\bar{\sigma}_a = 33.2$		$\bar{\sigma}_r = 63.0$	$u = 92.0$		
	9	14.5	-15.0	15.0	23.0	-11.0	--	0.51
	10	11.6	13.0	-17.0	23.0	4.0	27.0	--
6			$\bar{\sigma}_a = 59.3$		$\bar{\sigma}_r = 61.0$	$u = 90.0$		
	11	7.3	-12.0	-15.0	30.0	-13.0	--	0.62
	12	8.0	9.0	-8.0	18.0	3.0	21.0	--
7			$\bar{\sigma}_a = 76.2$		$\bar{\sigma}_r = 60.0$	$u = 67.0$		
	13	-9.6	6.0	17.0	-10.0	5.0	--	0.38
	14	-7.0	-7.0	7.0	-6.0	-1.0	-14.0	--

Note: All pressures are in pounds per square inch.

Table 4

Measured Quantities for Quivira Shale

Step	Increment	$\Delta\bar{\sigma}_a$	$\Delta\bar{\sigma}_r$	Δu	$\Delta\varepsilon_a$ (10^{-4})	$\Delta\varepsilon_r$ (10^{-4})	$\Delta V/V(10^{-4})$	A
1			$\bar{\sigma}_a = 22.1$ $\bar{\sigma}_r = 32.0$ $u = 98.0$					
	0	55.0	44.0	0.0	257.0	42.0	337.0	--
2			$\bar{\sigma}_a = 74.1$ $\bar{\sigma}_r = 74.0$ $u = 99.0$					
	1**							
	2	2.2	2.0	10.0	7.0	0.0	--	--
	3	-6.4	21.0	-21.0	-6.0	5.0	--	0.73
	4	0.5	0.0	-12.0	6.0	3.0	--	--
	5**							
	6	31.2	0.0	1.0	66.0	-3.0	55.0	--
3			$\bar{\sigma}_a = 73.5$ $\bar{\sigma}_r = 73.0$ $u = 110.0$					
	7	4.3	0.0	1.0	140.0	19.0	195.0	--
4			$\bar{\sigma}_a = 77.5$ $\bar{\sigma}_r = 73.0$ $u = 112.0$					
	8	4.0	-18.0	18.0	14.0	-4.0	--	0.82
	9	0.7	2.0	13.0	2.0	0.0	--	--
	10	-11.6	12.0	-11.0	17.0	2.0	--	--
	11	-20.4	-20.0	22.0	40.0	0.0	64.0	--
5			$\bar{\sigma}_a = 87.2$ $\bar{\sigma}_r = 90.0$ $u = 112.0$					
	12	-12.5	11.0	-12.0	-14.0	5.0	--	0.47
	13*							
	14	1.2	0.0	-29.0	-2.0	1.0	--	--
	15	8.5	-19.0	20.0	7.0	-1.0	--	0.69
	16	-0.2	2.0	26.0	1.0	0.0	--	--
	17	8.9	8.0	-7.0	14.0	0.0	12.0	--
6			$\bar{\sigma}_a = 90.3$ $\bar{\sigma}_r = 89.0$ $u = 113.0$					
	18	3.5	-24.0	25.0	16.0	-3.0	--	0.87
	19	7.9	21.0	-21.0	-8.0	1.0	--	0.73
	20	2.7	2.0	-3.0	-1.0	0.0	--	--
7			$\bar{\sigma}_a = 89.9$ $\bar{\sigma}_r = 91.0$ $u = 123.0$					
	20A*							
8			$\bar{\sigma}_a = 88.5$ $\bar{\sigma}_r = 88.0$ $u = 114.0$					
	21	-9.7	12.0	-11.0	-12.0	6.0	--	0.55
	22	-26.2	0.0	-1.0	-41.0	6.0	-35.0	--
9			$\bar{\sigma}_a = 65.1$ $\bar{\sigma}_r = 90.0$ $u = 113.0$					
	23	7.4	-17.0	14.0	9.0	-1.0	--	0.70
	24	23.4	-2.0	-2.0	34.0	-4.0	26.0	--

Note: All pressures are in pounds per square inch.
* No increment.
** Bad PWP data.

Table 5

Summary of Calculated Parameters

Shale	Increments*	C_{aa} 10^{-6} · 1/psi	C_{ar} 10^{-6} · 1/psi	C_{rr} 10^{-6} · 1/psi	E_1, psi	ν_2**	$\frac{E_1}{E_3}(1 - \nu_1)$
Bearpaw	3-4	65.11	5.06	14.73	15,400	-0.08	0.23
	5-6	60.06	12.46	25.56	16,700	-0.21	0.43
	7-8	75.19	-1.60	25.56	13,300	0.02	0.34
	9-10	53.21	-2.99	22.45	18,800	0.06	0.42
	11-12	64.81	1.08	16.65	15,400	-0.02	0.26
	13-14	63.15	4.59	18.19	15,800	-0.07	0.29
Kincaid	1-20	99.28	-9.88	53.59	10,100	0.10	0.54
	3-20	82.59	-1.82	45.80	12,100	0.02	0.56
	15-20	75.82	1.46	42.64	13,200	-0.02	0.56
	23-20	72.84	2.90	41.25	13,700	-0.04	0.57
	24-20	81.05	-1.07	45.08	12,300	0.01	0.56
	26-20	89.54	-5.17	49.05	11,200	0.06	0.55
Pierre	3-4	452.80	-94.73	134.18	2,200	0.21	0.30
	5-6	110.61	-27.71	92.15	9,000	0.25	0.83
	7-8	338.48	-69.01	144.95	3,000	0.20	0.43
	9-10	165.78	-27.01	80.95	6,000	0.16	0.49
	11-12	274.77	-59.54	107.09	3,600	0.22	0.39
	13-14	109.71	-16.62	77.86	9,100	0.15	0.71
Quivira	3-6	206.40	-14.97	42.20	4,900	0.07	0.20
	21-22	162.40	-10.11	67.45	6,200	0.06	0.42
	23-24	143.13	-13.78	38.94	7,000	0.10	0.27

* Increments used to calculate parameters (see Appendix B).
** Negative values imply errors in computing nearly zero values.

Table 6

Predicted and Measured Induced Piezometric Pore Water Heads

Piezometer	Location* X	Y	Elevation	Elevation of Fill at Piezometer	Predicted Isotropic $\eta = 1.0$	Predicted Anisotropic $\eta = 2.5$	Predicted Anisotropic $\eta = 10.0$	Measured
P-104-2**	2435	500	837.0	--	2.9	4.6	8.3	14.0
P-104-3	2418	320	840.0	905.0	51.9	54.1	67.7	70.0
P-104-7	2425	80	841.4	927.2	99.5	100.8	122.5	81.0
P-104-13	2457	-350	836.2	901.7	40.3	42.2	53.6	57.0
P-101-2**	2135	-575	837.2	--	1.2	2.1	4.4	7.0
P-78-1	-140	360	849.1	902.0	34.9	35.0	--	31.0
P-94-3	1380	350	844.1	902.0	46.3	46.8	--	32.0
P-94-2A**	1495	575	846.0	--	3.9	5.8	--	6.5
P-75-2**	-460	610	851.0	--	0.3	0.6	--	--

Note: All values are in feet; elevations are in feet above msl.
* Center of coordinate axes is located at x = sta 80+15 and y = dam center line.
** Piezometers are located at dam fringe.

APPENDIX A: PORE PRESSURE RESPONSE OF TRANSVERSELY ISOTROPIC MATERIALS

1. The relationship between pore pressure response and the elastic compressibility is important in two respects. First, by establishing a relationship between the elastic compressibility and pore pressure response, limits can be placed on the pore pressure response parameters by simply defining the expected range of numerical values of the elastic constants. Second, to relate the pore pressure response observed in a triaxial test to the response under more general loading conditions expected in field problems, a theoretical correspondence between the pore pressure parameters and the mechanical properties of the material is needed. In addition, it is important to establish the stress and strain limits for which the theory of elastic materials can be used to approximate pore pressure response. Thus, it is important to establish relationships between pore pressure response under undrained conditions and compressibility characteristics under drained conditions to test the theory experimentally.

Preliminary Considerations

2. The stress-strain response for linear elastic materials can be expressed in the general incremental form

$$\{\Delta\varepsilon\} = [C]\ \{\Delta\bar{\sigma}\} \tag{A1}$$

where

$\{\Delta\varepsilon\}$ = strain increments

$[C]$ = matrix of elastic coefficients

$\{\Delta\bar{\sigma}\}$ = effective stress increments

It is important to recognize that for transverse isotropy the elements in $[C]$ depend on the orientation of the reference axes relative to the transverse plane of isotropy. For development of the theory for pore

pressure response of a transversely isotropic material, it is convenient to use a reference coordinate system in which one axis is orthogonal to the plane of transverse isotropy. Thus, using the coordinate system shown in Figure 1a, $\{\Delta\varepsilon\}$, $\{\Delta\bar{\sigma}\}$, and $[C]$ can be expressed as follows:

$$\{\Delta\varepsilon\} = \begin{Bmatrix} \Delta\varepsilon_x \\ \Delta\varepsilon_y \\ \Delta\varepsilon_z \\ 1/2\Delta\gamma_{xy} \\ 1/2\Delta\gamma_{xz} \\ 1/2\Delta\gamma_{yz} \end{Bmatrix}, \qquad \{\Delta\bar{\sigma}\} = \begin{Bmatrix} \Delta\bar{\sigma}_x \\ \Delta\bar{\sigma}_y \\ \Delta\bar{\sigma}_z \\ \Delta\tau_{xy} \\ \Delta\tau_{xz} \\ \Delta\tau_{yz} \end{Bmatrix}$$

$$[C] = \begin{bmatrix} C_{xx} & C_{yx} & C_{yx} & 0 & 0 & 0 \\ C_{yx} & C_{yy} & C_{yz} & 0 & 0 & 0 \\ C_{yx} & C_{yz} & C_{yy} & 0 & 0 & 0 \\ 0 & 0 & 0 & \frac{1}{G_{xy}} & 0 & 0 \\ 0 & 0 & 0 & 0 & \frac{1}{G_{xy}} & 0 \\ 0 & 0 & 0 & 0 & 0 & \frac{1}{G_{xz}} \end{bmatrix}$$

where C_{xx}, C_{yx}, C_{yz}, C_{yy}, G_{xy}, and G_{yz} are general elastic constants. The $[C]$ matrix can also be written in terms of the engineering constants E_1, E_3, ν_1, ν_2, and G_{13}:

$$[C] = \begin{bmatrix} \frac{1}{E_1} & -\frac{\nu_2}{E_1} & -\frac{\nu_2}{E_1} & 0 & 0 & 0 \\ -\frac{\nu_2}{E_1} & \frac{1}{E_3} & -\frac{\nu_1}{E_3} & 0 & 0 & 0 \\ -\frac{\nu_2}{E_1} & -\frac{\nu_1}{E_3} & \frac{1}{E_3} & 0 & 0 & 0 \\ 0 & 0 & 0 & \frac{1}{G_{13}} & 0 & 0 \\ 0 & 0 & 0 & 0 & \frac{2(1+\nu_1)}{E_3} & 0 \\ 0 & 0 & 0 & 0 & 0 & \frac{2(1+\nu_1)}{E_3} \end{bmatrix}$$

Note that when [C] is expressed in terms of engineering constants, it can be readily observed that five independent constants are required to describe the behavior of a transversely isotropic material. If [C] is described with respect to a coordinate system (x',y',z'), the coefficient terms will not be the same as those shown above. Rather, the coefficients will be combinations of the five engineering constants and the cosines of transformation that relate (x,y,z) to (x',y',z'). Importantly, unless one of the axes is orthogonal to the plane of transverse isotropy, the shear stresses $\Delta\tau_{x'y'}$, $\Delta\tau_{x'z'}$, and $\Delta\tau_{y'z'}$ will contribute to the normal strains $\Delta\varepsilon_{x'}$, $\Delta\varepsilon_{y'}$, and $\Delta\varepsilon_{z'}$, thus implying a coupling between shear stress and volumetric strain. In view of the simplicity gained by eliminating the shear-normal coupling effect, the (x,y,z) coordinate system has a particular advantage in the derivation of the pore pressure response equations.

General Pore Pressure Response Relationships

3. The procedure used to develop the pore pressure response relationship follows the theory proposed by Skempton (1954) in which the

volumetric strain of a material is assumed to be equal to the volumetric strain of the saturating fluid within the material's pore space. Skempton's equation was derived for isotropic materials subjected to an increment of total principal stress such that $\Delta\sigma_2 = \Delta\sigma_3$ (i.e., as in a triaxial test). The form of Skempton's equation was such that a component of pore pressure was caused by a change in confining pressure $\Delta\sigma_3$, and a component caused by the stress difference $\Delta\sigma_1 - \Delta\sigma_3$. That is,

$$\Delta u = B(\Delta\sigma_3 + A(\Delta\sigma_1 - \Delta\sigma_3)) \tag{A2}$$

where A and B are Skempton's pore pressure parameters. An equation of form similar to Equation A2 was derived by Parry (1976) for a transversely isotropic material. To illustrate the application of Skempton's approach, the derivation of the pore pressure equations for transversely isotropic material is presented in the following paragraphs.

4. From Equation A1, the elastic volume change is given by

$$\Delta\varepsilon_v = \Delta\varepsilon_x + \Delta\varepsilon_y + \Delta\varepsilon_z = \Delta\bar{\sigma}_x(C_{xx} + 2C_{yx}) + (\Delta\bar{\sigma}_y + \Delta\bar{\sigma}_z)(C_{yx} + C_{yz} + C_{yy})$$

where the generalized elastic constants C_{xx}, C_{yx}, and C_{yy} are used for conciseness of expression. Note that because of the choice of the (x,y,z) coordinate system, the terms G_{xy}, G_{xz}, and G_{yz} do not appear in the expression for $\Delta\varepsilon_v$.
Let

$$a = (C_{xx} + 2C_{yx})$$

$$b = (C_{yx} + C_{yz} + C_{yy})$$

to get

$$\Delta\varepsilon_v = \Delta\bar{\sigma}_x a + (\Delta\bar{\sigma}_y + \Delta\bar{\sigma}_z)b \tag{A3}$$

If $\Delta\bar{\sigma}_x = \Delta\bar{\sigma}_y = \Delta\bar{\sigma}_z = \Delta\bar{p}$ and $\Delta\tau_{xy} = \Delta\tau_{yz} = \Delta\tau_{xz} = 0$ (hydrostatic stress increment) is applied, then the volumetric strain is given by:

$$\Delta\varepsilon_v = \Delta\bar{p}(a + 2b) = \Delta\bar{p}C_s \tag{A4}$$

where

C_s = effective stress bulk compressibility

$= C_{xx} + 4C_{yx} + 2(C_{yy} + C_{yz})$

Since $\Delta\varepsilon_v$ and $\bar{p}$ are independent of how the sample is oriented, C_s is an invariant quantity. That is, $C_{xx} + 4C_{yx} + 2(C_{yy} + C_{yz}) = C_{x'x'} + 4C_{y'x'} + 2(C_{y'y'} + C_{y'z'})$, where (x',y',z') refer to an arbitrary reference axis. The bulk modulus of the material can be defined as

$$K_s = \frac{1}{C_s} \tag{A5}$$

5. For undrained loading, if the compression of the individual grains is ignored, it can be assumed that the volume change of the pore fluid is equal to the total volume change of the material. The volume change of the fluid can be determined from the change in pore pressure as

$$\Delta\varepsilon_v = \frac{\Delta u\ n}{K_w} \tag{A6}$$

where

Δu = change in pore water pressure

n = porosity of soil

K_w = bulk modulus of water

6. By equating Equations A3 and A6 and invoking the definition of effective stress, the following equation can be written in terms of total stress and Δu :

$$\Delta\varepsilon_v = \frac{\Delta u\ n}{K_w} = a(\Delta\sigma_x - \Delta u) + \left[(\Delta\sigma_y - \Delta u) + (\Delta\sigma_x - \Delta u)\right]b \tag{A7}$$

Then solving for Δu

$$\Delta u = \frac{a\Delta\sigma_x + (\Delta\sigma_y + \Delta\sigma_z)b}{\frac{n}{K_w} + (a + 2b)} \tag{A8}$$

$$= \frac{\frac{1}{2}(a + 2b)(\Delta\sigma_y + \Delta\sigma_z) + a\left[\Delta\sigma_x - \frac{1}{2}(\Delta\sigma_y + \Delta\sigma_z)\right]}{\frac{n}{K_w} + (a + 2b)} \tag{A8a}$$

Using the definition of C_s (Equation A4), Equation A8a can be written as

$$\Delta u = \frac{C_s}{\frac{n}{K_w} + C_s}\left\{\frac{1}{2}(\Delta\sigma_y + \Delta\sigma_z) + \frac{a}{C_s}\left[\Delta\sigma_x - \frac{1}{2}(\Delta\sigma_y + \Delta\sigma_z)\right]\right\}$$

7. The above equation is in the form of Skempton's equation (Skempton 1954) for an isotropic elastic media in which the pore pressure parameters A and B are written as

$$B = \frac{C_s}{\frac{n}{K_w} + C_s}$$

$$A = \frac{a}{C_s}$$

with

$$\Delta u = B\left\{\frac{1}{2}(\Delta\sigma_y + \Delta\sigma_z) + A\left[\Delta\sigma_x - \frac{1}{2}(\Delta\sigma_y + \Delta\sigma_z)\right]\right\} \tag{A9}$$

8. Note that B is invariant and of the same form as for an isotropic material. However, the A parameter is not invariant, and Equation A9 is valid only if the coordinate axes (x,y,z) are specified relative to the plane of transverse isotropy as indicated in Figure 1a.

9. The A parameter can be written as

$$A = \frac{C_{xx} + 2C_{yx}}{C_{xx} + 4C_{yx} + 2(C_{yy} + C_{yz})} \tag{A10}$$

By dividing the numerator and denominator by C_{xx} and defining the ratio

$$\frac{C_{xx}}{C_{yy}} = \frac{E_3}{E_1} = \eta$$

Equation A10 can be expressed in terms of the engineering constants as

$$A = \frac{1 - 2\nu_2}{1 - 4\nu_2 + \dfrac{2(1 - \nu_1)}{\eta}} \tag{A10a}$$

which is identical to the anistropic A parameter derived by Parry (1976).

10. Similarly, the B parameter can be expressed in terms of the engineering constants as

$$B = \frac{1 - 4\nu_2 + \dfrac{2(1 - \nu_1)}{\eta}}{\dfrac{n\,E_1}{K_w} + \left[1 - 4\nu_2 + \dfrac{2(1 - \nu_1)}{\eta}\right]} \tag{A11}$$

which was also derived by Parry (1976). The bulk modulus can also be related to the engineering constants as

$$K_s = \frac{E_1}{\left[1 - 4\nu_2 + \dfrac{2(1 - \nu_1)}{\eta}\right]} \tag{A12}$$

11. For an isotropic material $\eta = 1$, $\nu_2 = \nu_1$ and Equations A10a and A12 reduce to

$$A = \frac{1}{3}$$

$$K_s = \frac{E}{3(1 - 2_v)}$$

which are well-known results of elastic theory.

Special Stress and Boundary Conditions

12. The relationships for anisotropic materials can be simplified for many practical problems in which special stress or boundary conditions exist. Three important special cases are the triaxial test, drained isotropic compression, and plane strain conditions.

Triaxial test

13. Triaxial test with ($\sigma_x = \sigma_a$ and $\sigma_y = \sigma_z = \sigma_r$). For this test, only two stresses are controlled independently. Thus, the stress and strain increments are related by only three constants in the following equation:

$$\begin{aligned} \Delta\varepsilon_a &= C_{aa}\Delta\bar{\sigma}_a + 2C_{ar}\Delta\bar{\sigma}_r \\ \Delta\varepsilon_r &= C_{ar}\Delta\bar{\sigma}_a + C_{rr}\Delta\bar{\sigma}_r \end{aligned} \tag{A13}$$

These constants are related to the elastic properties as follows:

$$\begin{aligned} C_{aa} &= C_{xx} = \frac{1}{E_1} \\ C_{ar} &= C_{xy} = -\frac{\nu_2}{E_1} \\ C_{rr} &= C_{xy} + C_{yy} = \frac{1 - \nu_1}{E_3} \end{aligned} \tag{A14}$$

Note that only three independent constants are involved in the triaxial test. However, C_{aa}, C_{ar}, and C_{rr} are sufficient to determine A and B since

$$C_s = C_{aa} + 4C_{ar} + 2C_{rr}$$

$$a = C_{aa} + 2C_{ar}$$

This results in

$$A = \frac{C_{aa} + 2C_{ar}}{C_{aa} + 4C_{ar} + 2C_{rr}} \tag{A15}$$

$$B = \frac{C_{aa} + 4C_{ar} + 2C_{rr}}{\frac{n}{K_w} + C_{aa} + 4C_{ar} + 2C_{rr}}$$

14. As an aid to the interpretation of test data, it is of interest to relate the direction of the effective stress path to the A parameter. First, Equation A9 must be written in terms of the effective stress and pore pressure as

$$\Delta u = B \left\{ \frac{1}{2}\left(\Delta\bar{\sigma}_y + \Delta\bar{\sigma}_z\right) + A\left[\Delta\bar{\sigma}_x - \frac{1}{2}\left(\Delta\bar{\sigma}_y + \Delta\bar{\sigma}_z\right)\right] + \Delta u \right\}$$

Then, solving for Δu, the relationship obtained is

$$\Delta u \frac{(1 - B)}{B} = \frac{1}{2}\left(\Delta\bar{\sigma}_y + \Delta\bar{\sigma}_z\right) + A\left[\Delta\bar{\sigma}_x - \frac{1}{2}\left(\Delta\bar{\sigma}_y + \Delta\bar{\sigma}_z\right)\right] \tag{A16}$$

It is immediately seen that if $B = 1.0$, the effective stresses are related by

$$\frac{1}{2}\left(\Delta\bar{\sigma}_y + \Delta\bar{\sigma}_z\right) + A\left[\Delta\bar{\sigma}_x - \frac{1}{2}\left(\Delta\bar{\sigma}_y + \Delta\bar{\sigma}_z\right)\right] = 0$$

For the triaxial test with $\Delta\bar{\sigma}_x = \Delta\bar{\sigma}_a$ and $\Delta\bar{\sigma}_y = \Delta\bar{\sigma}_z = \Delta\bar{\sigma}_r$, this relationship reduces to

$$(1 - A)\Delta\bar{\sigma}_r + A\Delta\bar{\sigma}_a = 0$$

or

$$\frac{\Delta\bar{\sigma}_a}{\Delta\bar{\sigma}_r} = \frac{A - 1}{A} \tag{A17}$$

15. The stress path plots used in this report are based on the stress difference $(\bar{\sigma}_a - \bar{\sigma}_r)$ and mean stress (1/3) $(\bar{\sigma}_a + 2\bar{\sigma}_r)$ shown in Figure 2. The slope of the stress path is given by

$$\text{slope} = 3\,\frac{\Delta\bar{\sigma}_a - \Delta\bar{\sigma}_r}{\Delta\bar{\sigma}_a + 2\Delta\bar{\sigma}_r}$$

Using Equation A17, the stress path slope is related to the A parameter by

$$\text{slope} = 3\,\frac{\frac{A - 1}{A} - 1}{\frac{A - 1}{A} + 2} = -\frac{3}{3A - 1} \tag{A18}$$

From Equation A18, it is noted that for $A > 1/3$ the slope is negative and for $A = 1/3$ (as for isotropic material) the slope is vertical. Further, since the slope of the effective stress path depends only on A in the triaxial test, the direction of the effective stress path is independent of the total stress path.

16. Triaxial test $(\sigma_x \neq \sigma_a$, $\sigma_y \neq \sigma_r$ and $\sigma_z = \sigma_r)$. If the plane of transverse isotropy is not orthogonal to the axis of a triaxial specimen, Equation A2 is not valid. For example, even though σ_a and σ_r are principal stresses, ε_a and ε_r are not principal strains since $\gamma_{ar} \neq 0$. Since the specimen depicted in Figure A1 will distort when subjected to the principal stress increments $\Delta\sigma_a$ and $\Delta\sigma_r$, the interpretation of the test is greatly complicated.

17. While distortion of the specimen limits the use of a test in which the sample axis is not orthogonal to the plane of isotropy, such a test could still be used to estimate the A parameter. Further, in

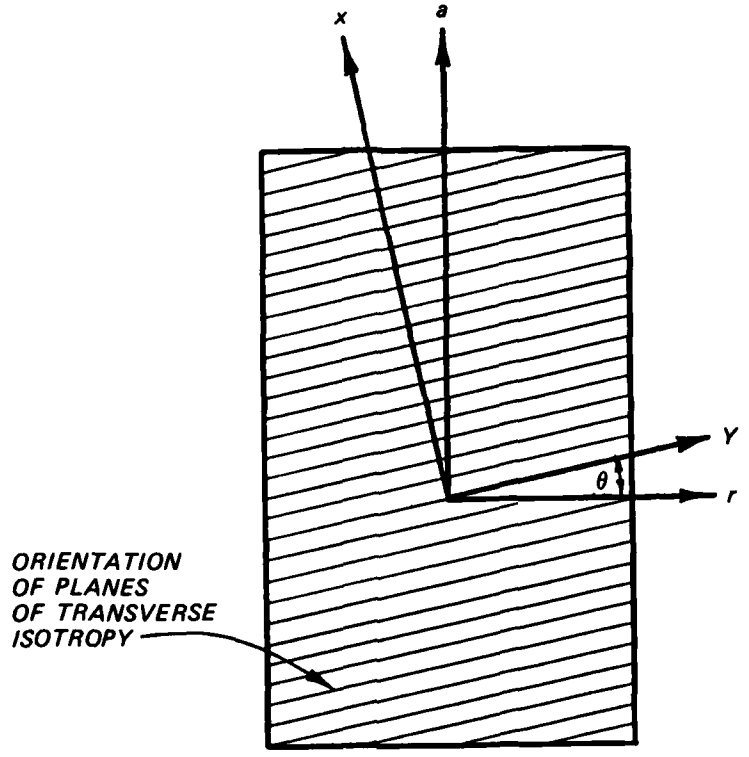

Figure A1. Relationship between transverse plane and specimen axis

practice the true orientation of the transverse isotropic plane is not known, and it is of interest to determine the effect of its orientation on the pore pressure response.

18. The influence of orientation on the A parameter can be derived in a manner similar to a more general procedure proposed by Baker and Krizek (1969). Considering the sample shown in Figure A1, $\Delta\sigma_x$, $\Delta\sigma_y$, and $\Delta\sigma_z$ can be determined from the principal stresses $\Delta\sigma_a$ and $\Delta\sigma_r$ using Mohr's circle of transformation

$$\Delta\sigma_x = \frac{1}{2}\left(\Delta\sigma_a + \Delta\sigma_r\right) + \frac{1}{2}\left(\Delta\sigma_a - \Delta\sigma_r\right)\cos 2\theta$$

$$\Delta\sigma_y = \frac{1}{2}\left(\Delta\sigma_a + \Delta\sigma_r\right) - \frac{1}{2}\left(\Delta\sigma_a - \Delta\sigma_r\right)\cos 2\theta \qquad \text{(A19)}$$

$$\Delta\sigma_z = \Delta\sigma_r$$

Let the A parameter at the reference configuration (given by Equation A15) be denoted A_o. Then since B is invariant, Equation A9 may be written

$$\Delta u_\theta = B\left(\frac{1}{2}\left[\frac{1}{2}\left(\Delta\sigma_a + \Delta\sigma_r\right) - \frac{1}{2}\left(\Delta\sigma_a - \Delta\sigma_r\right)\cos 2\theta + \Delta\sigma_r\right]\right.$$
$$+ A_o\left\{\frac{1}{2}\left(\Delta\sigma_a + \Delta\sigma_r\right) + \frac{1}{2}\left(\Delta\sigma_a - \Delta\sigma_r\right)\cos 2\theta\right.$$
$$\left.\left. - \frac{1}{2}\left[\frac{1}{2}\left(\Delta\sigma_a + \Delta\sigma_r\right) - \frac{1}{2}\left(\Delta\sigma_a - \Delta\sigma_r\right)\cos 2\theta + \Delta\sigma_r\right]\right\}\right) \quad \text{(A20)}$$

Rearranging the terms

$$\Delta u_\theta = B\left\{\Delta\sigma_r + \frac{1}{4}\left[(1 - \cos 2\theta)\right.\right.$$
$$\left.\left. + A_o(1 + 3\cos 2\theta)\right](\Delta\sigma_a - \Delta\sigma_r)\right\} \quad \text{(A20a)}$$

which is in the form of Skempton's Equation A2. Hence

$$A_\theta = \frac{1}{4}\left[(1 - \cos 2\theta) + A_o(1 + 3\cos 2\theta)\right] \quad \text{(A21)}$$

Note that for an isotropic specimen, $A_\theta = A_o = 1/3$. The maximum and minimum values of A_θ can be obtained by noting that they correspond respectively to the maximum and minimum values of Δu. Taking the derivative,

$$\frac{\partial u}{\partial \theta} = \frac{1}{2} B(1 - 3A_o)(\Delta\sigma_a - \Delta\sigma_r) \sin 2\theta \quad \text{(A22)}$$

The maximum and minimum values are given by

$$\frac{\partial u}{\partial \theta} = 0$$

which occurs when $\sin 2\theta = 0$, or

$$\theta = k\frac{\pi}{2}\ ,\ k = 0,\ 1,\ 2,\ldots$$

Hence, from Equation A18, A is a maximum at $\theta = 0$ and a minimum at $\theta = 90$ deg. The influence of θ on A can be seen from the following tabulation:

	A_θ				
θ, deg	$A_o = 0.3333$	0.50	0.60	0.70	1.0
15	0.3333	0.48	0.57	0.66	0.93
30	0.3333	0.44	0.50	0.56	0.75
45	0.3333	0.38	0.40	0.43	0.50
60	0.3333	0.31	0.30	0.29	0.25
90	0.3333	0.25	0.20	0.15	0

19. Provided the orientation of the normal to the transverse isotropic plane is within 15 deg to the specimen axis, the potential error in testing an improperly oriented specimen is relatively small. However, as θ exceeds 30 deg, the potential error in the determination of A becomes quite significant.

Drained hydrostatic compression ($\Delta\sigma_a = \Delta\sigma_r = \Delta\bar{\sigma}_a = \Delta\bar{\sigma}_r$)

20. If a transversely isotropic specimen is subjected to a hydrostatic stress increment in which $\Delta\bar{\sigma}_a = \Delta\bar{\sigma}_r$, the ratio of $m = \Delta\varepsilon_a/\Delta\varepsilon_r$ is indicative of the degree of anisotropy. For an isotropic specimen $m = 1$. For material in which $E_3/E_1 > 1$, $m > 1$. The relationship between m and A is important because it offers a means of obtaining an independent experimental verification of the relationship between the material constants and the pore pressure response.

21. The ratio of strains observed during drained isotropic compression can be related to the A parameter as follows. From Equation A13

$$\frac{\Delta\varepsilon_a}{\Delta\varepsilon_r} = \frac{\Delta\bar{\sigma}_a C_{aa} + 2\Delta\bar{\sigma}_r C_{ar}}{\Delta\bar{\sigma}_a C_{ar} + \Delta\bar{\sigma}_r C_{rr}}$$

if $\Delta\bar{\sigma}_r = \Delta\bar{\sigma}_a$

$$m = \frac{C_{aa} + 2C_{ar}}{C_{ar} + C_{rr}} \tag{A23}$$

By dividing by C_{aa} and noting $C_{ar}/C_{aa} = -\nu_2$, Equation A23 can be written as

$$m = \frac{1 - 2\nu_2}{\frac{C_{rr}}{C_{aa}} - \nu_2} \tag{A23a}$$

Solving for C_{rr}/C_{aa}

$$\frac{C_{rr}}{C_{aa}} = \frac{1 - 2\nu_2 + m\nu_2}{m} \tag{A24}$$

Similarly, from Equation A15

$$A = \frac{1 - 2\nu_2}{1 - 4\nu_2 + 2\frac{C_{rr}}{C_{aa}}} \tag{A25}$$

Substituting Equation A24 into Equation A25.

$$A = \frac{1 - 2\nu_2}{1 - 4\nu_2 + 2\left(\frac{1 - 2\nu_2 + m\nu_2}{m}\right)}$$

$$= \frac{m(1 - 2\nu_2)}{m(1 - 2\nu_2) + 2(1 - 2\nu_2)}$$

Therefore,

$$A = \frac{m}{m + 2} \tag{A26}$$

Plane strain ($d\varepsilon_z = 0$, $\sigma_y \neq \sigma_z$)

22. Plane strain conditions are often assumed to exist in problems involving long embankments. In contrast to the cases considered previously, the plane strain condition involves both stress and strain boundary conditions. Thus, to use Equation A8, $\Delta\sigma_z$ must be computed from $\Delta\sigma_x$ and $\Delta\sigma_y$ using the condition $d\varepsilon_z = 0$. From Equation A1a, $\Delta\bar{\sigma}_z$ can be computed as

$$\Delta\bar{\sigma}_z = \nu_2\eta\Delta\bar{\sigma}_x + \nu_1\Delta\bar{\sigma}_y \tag{A27}$$

Since Equation A27 is written in terms of effective stress, Equation A16 must be used. Substituting Equation A27 into Equation A16 yields

$$\frac{\Delta u(1 - B)}{B} = \Delta\bar{\sigma}_x \left[\frac{1}{2}\nu_2\eta(1 - A) + A\right] + \frac{1}{2}\Delta\bar{\sigma}_y(1 - A)(1 + \nu_1) \tag{A28}$$

Define new parameters

$$A_1 = \frac{1}{2}\nu_2\eta(1 - A) + A$$

$$A_2 = \frac{1}{2}(1 - A)(1 + \nu_1)$$

and write Equation A28 in terms of total stress

$$\frac{\Delta u(1 - B)}{B} = A_1\Delta\sigma_x + A_2\Delta\sigma_y - (A_1 + A_2)\Delta u \tag{A29}$$

Solving for Δu

$$\Delta u = B\,\frac{A_1\Delta\sigma_x + A_2\Delta\sigma_y}{(A_1 + A_2)B + (1 - B)} \tag{A30}$$

Note that for problems in which one of the strains is constrained at a constant value, the pore pressure cannot be reduced to the simple

Skempton's form (Equation A9). However, if B equals 1.0, Equation A30 can be reduced to

$$\Delta u = \Delta\sigma_y + A_{ps}(\Delta\sigma_x - \Delta\sigma_y) \qquad \text{(A31)}$$

where

$$A_{ps} = \frac{A_1}{A_1 + A_2}$$

which is in Skempton's form for $B = 1.0$. For isotropic conditions with $A = 1/3$, $\nu_1 = \nu_2 = \nu < 0.5$, and $\eta = 1$, note that

$$A_1 = \frac{1}{3}(1 + \nu)$$

$$A_2 = \frac{1}{3}(1 + \nu)$$

and

$$A_{ps} = 0.5$$

As for the A parameter (Equation A10a), the maximum value of A_{ps} is 1.0.

APPENDIX B: COMPUTATION OF PORE PRESSURES INDUCED BY EMBANKMENT LOADS

1. The computation of pore pressures induced by embankment loads is based on the assumption that the embankment can be replaced by an equivalent load distribution applied on a level, homogeneous, transversely isotropic foundation. Thus, the effect of the internal stiffness of the embankment is ignored in the analysis. The equivalent load distribution is assumed to be given by

$$P(x,y) = \gamma_t h(x,y)\, dx\, dy \tag{B1}$$

where

$P(x,y)$ = the load on the infinitesimal area $dx\, dy$ at location (x,y) on the loading surface

γ_t = total unit weight of fill material

$h(x,y)$ = height of fill at location (x,y)

The stresses induced by a surface point load can be computed by the appropriate formula and combined with Skempton's equation to give a relationship for the pore pressure induced by a point load. The pore pressure induced by the embankment is thus given by

$$\Delta u = \int_{x_1}^{x_2} \int_{y_1}^{y_2} \gamma_t h(x,y) I(x,y)\, dx\, dy \tag{B2}$$

where $I(x,y)$ equals the influence factor derived from the equations for stresses induced by $P(x,y)$.

2. The most commonly used equations for determining the influence factor $I(x,y)$ are based on the Boussinesq theory (Craig 1978), which gives for a point at (x_o, y_o, z_o)

$$\sigma_z = \frac{3P(x,y)}{2\pi z^2} \left[\frac{1}{1 + (r/z)^2}\right]^{5/2}$$

(B3)

$$\frac{1}{2}(\sigma_r + \sigma_\theta) = \frac{P(x,y)}{2\pi} \left[\frac{3r^2}{(r^2 + z^2)^{5/2}} + \frac{z(1 - 2v)}{(r^2 + z^2)^{3/2}}\right]$$

where from Figure B1

z = depth of point (x_o, y_o, z_o) below ground surface

r = radial distance from $P(x,y)$ and (x_o, y_o, z_o)

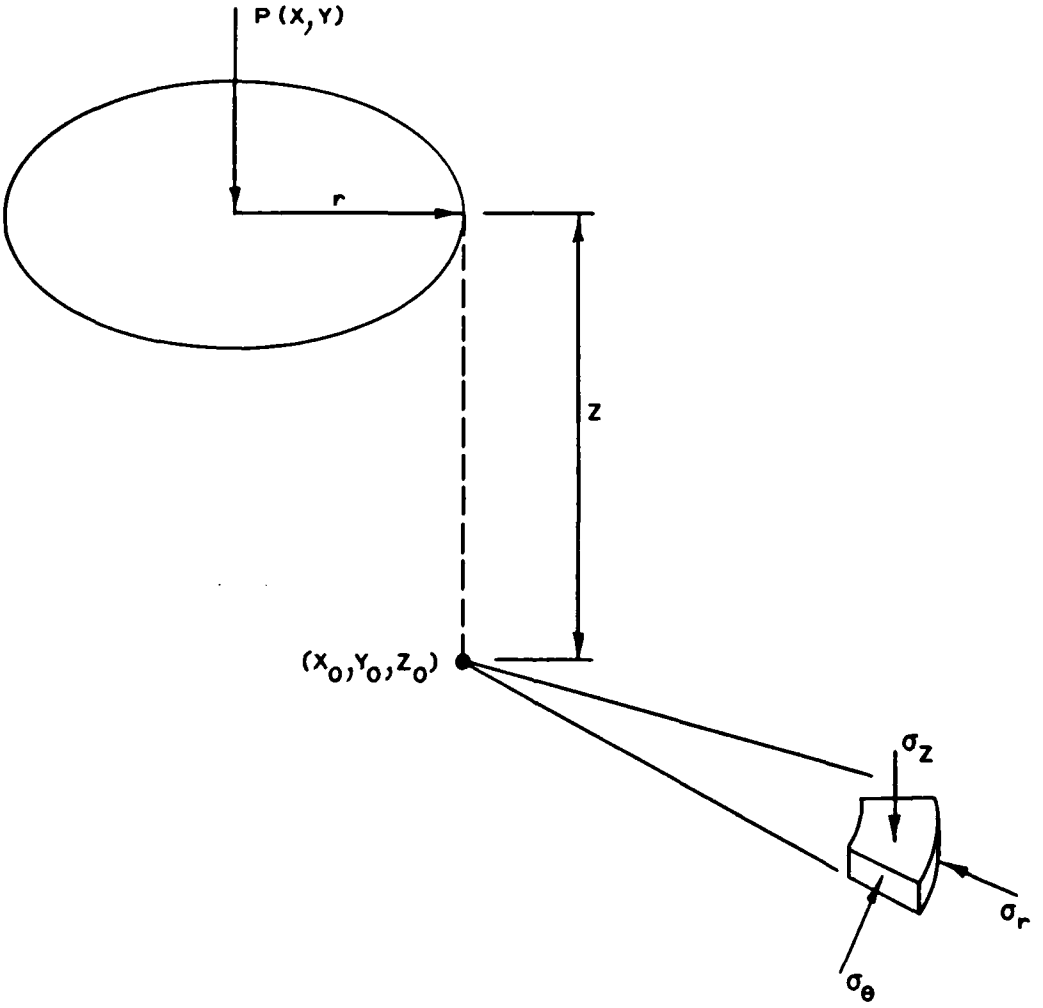

Figure B1. Stresses in elastic half-space due to point load on surface (shearing stress τ_{zr} not shown)

Writing Skempton's equation in the axisymmetric form

$$\Delta u = B\left[\frac{1}{2}\,(\Delta\sigma_\theta + \Delta\sigma_r)\right] + A\left[\Delta\sigma_z + \frac{1}{2}\,(\Delta\sigma_\theta + \Delta\sigma_r)\right] \qquad \text{(B4)}$$

the integrand for Equation B2 can be obtained by combining Equations B1, B3, and B4.

3. The Boussinesq equation is valid for isotropic materials and involves only one material parameter, Poisson's ratio ν. Stress formulas for anisotropic materials are more complex and involve four independent constants. A number of formulas have been developed for determining the stresses caused by a point load (Gerrard and Wardle 1973). The Westergaard solution assumes extreme anisotropy in which lateral strains (ε_r,ε_θ) are not permitted (Craig 1978). Also, Barden (1963) presented a solution for orthotropic materials in which the stresses $\Delta\sigma_r$ and $\Delta\sigma_\theta$ were determined approximately. However, it was found that $\Delta\sigma_r$ and $\Delta\sigma_\theta$ had a significant influence on the computed pore pressure and using approximate solutions introduced unnecessary uncertainty into the analysis. Therefore, the following rigorous solution for the point load problem presented by Lekhnitskii (1963) was used:

$$\frac{\sigma_\theta + \sigma_r}{2} = \frac{-P_Z}{4\pi(s_1 - s_2)}\left\{\frac{\sqrt{d}}{ac - d}\left[-\frac{s_1^2 q_2}{\left(r^2 + s_1^2 Z^2\right)^{3/2}} + \frac{s_2^2 q_1}{\left(r^2 + s_2^2 Z^2\right)^{3/2}}\right]\right.$$

$$\left. + \frac{1}{\sqrt{d}}\left[\frac{s_1^2}{\left(r^2 + s_1^2 Z^2\right)^{3/2}} - \frac{s_2^2 q_2}{\left(r^2 + s_2^2 Z^2\right)^{3/2}}\right]\right\} \qquad \text{(B5)}$$

$$\sigma_Z = \frac{P_Z}{2\pi\sqrt{d}(s_1 - s_2)}\left[\frac{1}{\left(r^2 + s_1^2 Z^2\right)^{3/2}} - \frac{1}{\left(r^2 + s_2^2 Z^2\right)^{3/2}}\right]$$

where

$$s_1 = \sqrt{\frac{a + c + \sqrt{(a + c)^2 - 4d}}{2d}}$$

$$s_2 = \sqrt{\frac{a + c - \sqrt{(a + c)^2 - 4d}}{2d}}$$

$$q_1 = \left(b - as_2^2\right)\left(1 - as_1^2\right)$$

$$q_2 = \left(b - as_1^2\right)\left(1 - as_2^2\right)$$

and

$$a = - \frac{v_2(1 + v_1)}{1 - \eta v_2^2}$$

$$b = \frac{v_2\eta(G_{13}v_2 - E_1) + v_1G_{13}}{G_{13}\left(1 - \eta v_2^2\right)}$$

$$c = \frac{\frac{E_1}{G_{13}} - (v_1 + v_2)}{1 - \eta v_2^2}$$

$$d = \frac{\left(\eta^2 - v_1^2\right)}{\left(\eta\ 1 - \eta v_2^2\right)}$$

$$\eta = \frac{E_3}{E_1}$$

$$G_{13} = 0.4E_1 \text{ (assumed)}$$

4. The integrand in Equation B2 is quite complex for fill shapes

(described by $h(x,y)$) , which are of practical interest, and a numerical integration scheme was used to determine Δu . To simplify the numerical integration process, the function $h(x,y)I(x,y)$ was mapped into a reference square by using a coordinate transformation of the form

$$x = \sum_{i=1}^{k} N_i(\alpha,\beta)X_i$$

$$y = \sum_{i=1}^{k} N_i(\alpha,\beta)Y_i \qquad \text{(B6)}$$

where

X_i, Y_i = coordinates of selected points on fill boundaries corresponding to s_i , t_i

s_i, t_i = coordinates of selected points inside the reference square

α, β = coordinates of location within unit square

$N_i(\alpha,\beta)$ = interpolation factors.

5. Using the transformation Equation B6, the integral B2 can be written as

$$\Delta u = \int_{-1}^{1} \int_{-1}^{1} B\gamma_t h'(\alpha,\beta)I'(\alpha,\beta)\left|J\right| d\alpha\, d\beta \qquad \text{(B7)}$$

where

$\left|J\right|$ = Jacobian of Transformation

$$= \frac{\partial x}{\partial s}\frac{\partial y}{\partial t} - \frac{\partial x}{\partial t}\frac{\partial y}{\partial s}$$

Equation B7 can be evaluated numerically by the quadrature formula

$$\Delta u = B\gamma_t \sum_{i=1}^{k}\sum_{j=1}^{k} H_i H_j h'(\alpha_i,\beta_j)I'(\alpha_i,\beta_j)\left|J\right|_{ij} \qquad \text{(B8)}$$

where

h', I' = $h(x,y)$ and $I(x,y)$ evaluated at $x(\alpha_i,\beta_j)$, $y(\alpha_i,\beta_j)$

α_i, β_i = coordinates of integration sampling points

H_i, H_j = weighting functions

$\left|J\right|_{ij}$ = Jacobian at α_i , β_j

Evaluation of Equation B8 requires only that the fill height h and the influence factor I be expressed as a function of x and y. The influence factor can, of course, be determined from combining Equation B4 with either Equation B3 or B5. The function describing fill height can be expressed in the form of an interpolation function similar to the coordinate transformation formulae. That is,

$$h'(\alpha,\beta) = \sum_{i=1}^{k} N_i(\alpha,\beta)t_i \qquad \text{(B9)}$$

where

$h'(\alpha,\beta)$ = fill height at α , β

t_i = fill height at X_i , Y_i in Equation B6

The sampling locations α_i and β_j and the weighting function H_i and H_j are determined analytically to give the best trade-off between accuracy, economy, and simplicity of application (see for example, Hornbeck (1975)). The general integration procedure described above is commonly used in the evaluation of stiffness matrices in the finite element method, and a detailed description of the procedure is given by Zienkiewicz (1977).

6. A computer code was developed to evaluate Equation B8 for linear interpolation factors (Equations B6 and B9), using Gauss integration formulae for H_i , H_j , α_i , and β_j . For a given order of integration, the Gauss integration procedure specifies fixed values of H_i , H_j , α_i , and β_j , which greatly simplifies the computer code. However, little advantage is gained from the well-known efficiency of Gauss integration formula since Equations B3 and B5 are not well behaved for the small values of r/z typically found in the embankment problem. The "shape" of the function to be integrated is determined by the location (x_o,y_o,z_o), and none of the commonly used integration formulae, which specify fixed values of α_i , β_i , are particularly well suited for integrating the problem formulated in Equation B7. Thus, the integration required a large number of sampling points α_i , β_i at a

relatively large computational cost. Problems involving deep foundation layers, relative to the size of loaded areas, could be solved at a greatly reduced cost since fewer sampling points would be required to evaluate the integral accurately.

7. As an alternative to the numerical integration of Equation B2, a graphical method based on the influence chart technique was developed. The influence chart consists of a series of concentric circles, equally subdivided by radial lines, which are drawn to scale with the center of the circles located over the point for which the pore pressure is to be computed. The radii of the concentric circles are determined so that if an infinite uniform load is placed over the ground surface, each annular loaded region between consecutive circles makes an equal contribution to the induced pore water pressure. Thus, each influence area created by subdividing the circles with radial lines makes an equal contribution to the induced pore pressure. By the principle of superposition, the pore pressure induced by an irregularly loaded area can be determined by summing the contribution of each unit area. That is,

$$\Delta u = B\gamma_t \, I \sum_{i=1}^{n} t_i \, f_i \qquad \text{(B10)}$$

where

B = Skempton's B value

γ_t = total unit weight of fill

$I = 1/n$

n = number of subdivided influence areas

t_i = average height of fill in i^{th} influence area

f_i = fraction of influence area covered by fill

The influence chart for pore pressure is similar to Newmark's chart for computation of vertical stress distribution below foundations.

8. To illustrate the use of the chart, the pore pressure induced by a fill layer of the test berm constructed at the Hillsdale damsite

is computed for a point 34.9 ft below the current ground surface. To determine the radial distance of each influence circle, a plot is first made of r/z versus $\Delta u/\gamma_t t$, then r/z values corresponding to 10 equal increments of $\Delta u/\gamma_t t$ are determined from the plot in Figure B2. The values of $\Delta u/\gamma_t t$ and r/z used to construct the plot were computed by the computer code CURLS described in Appendix C. The radial distances used in the scale drawing (Figure B3) are computed by multiplying each r/z value by 34.9 ft. The circles are further subdivided by 10 equally spaced radial lines that give an influence value I of 0.01. A circular broken line is also drawn corresponding to $\Delta u/\gamma_t t = 0.85$ to facilitate subdividing the larger influence areas. Using the estimated values of f_i and t_i shown in Figure B3, the pore pressure is computed as follows:

$$\sum_{i=1}^{n} f_i t_i = (70)(1)(17) + (1)(17) + (1)(17) + (1)(17) + (1)(17)$$
$$+ (1)(17) + (1)(17) + (1)(17) + (1)(16) + (1)(15)$$
$$+ (1)(16) + (1/2)(17) + (1/2)(17) + (1/2)(17)$$
$$+ (1/2)(17) + (1/2)(17) + (1/2)(17) + (1/2)(17)$$
$$+ (1/2)(13) + (1/2)(10) + (1/2)(13) + (1/4)(13)$$
$$+ (3/8)(15) + (1/4)(12) + (1/8)(7) + (1/4)(12)$$
$$+ (1/2)(17) + (1/2)(13) + (1/8)(6) + (1/8)(6)$$
$$+ (1/16)(16) + (1/16)(14)$$
$$= 1467.6 \text{ ft}$$

For

$B = 1.0$ (assumed)

$\gamma_t = 126.0$ (assumed)

$I = 0.01$

$$\Delta u = (1.0)(0.01)(126.0)(1467.6) = 1850 \text{ psf}$$

Change in piezeometric level = $\frac{1850}{62.4} = 29.6$ ft.

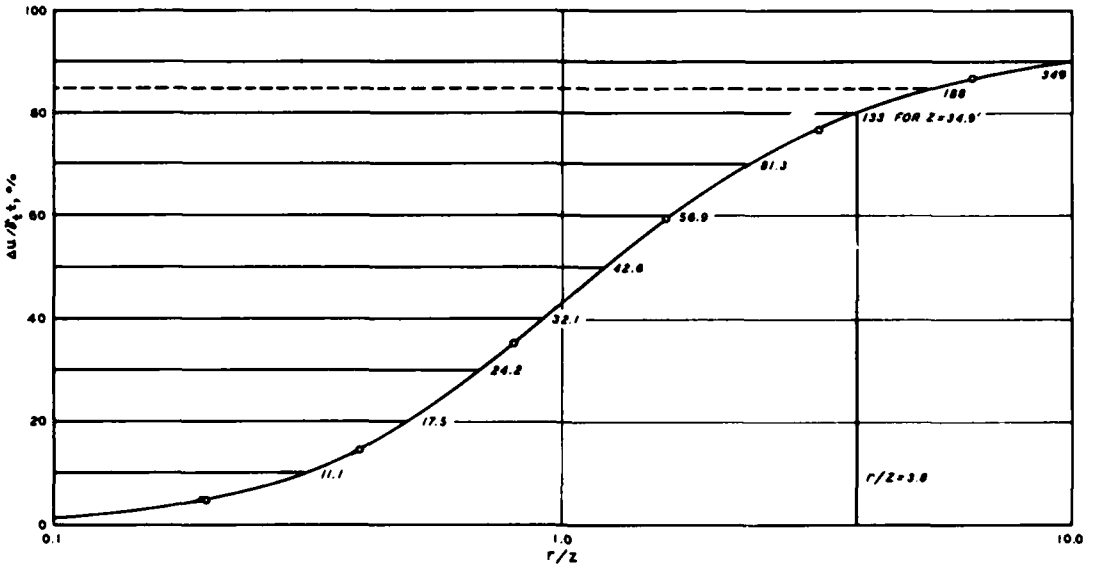

Figure B2. $\Delta u/\gamma_t t$ values versus r/z ratios used for example problem, A = 0.7 and η = 2.5

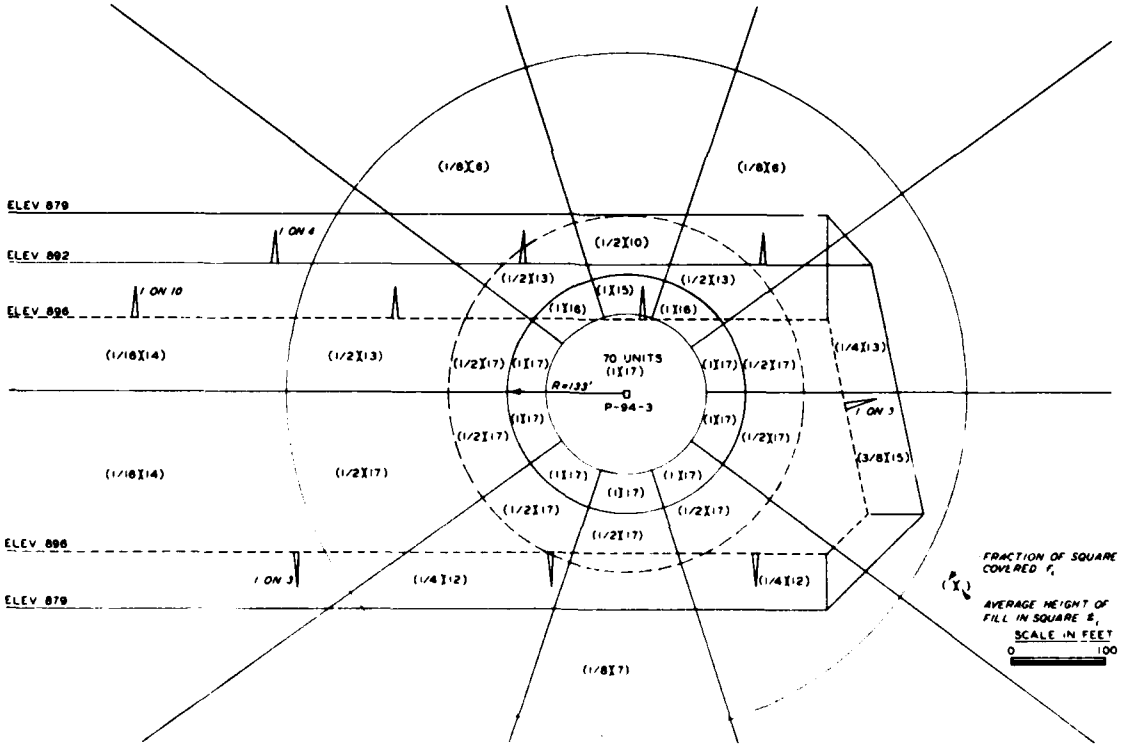

Figure B3. Example problem showing the use of the influence chart

9. The computed value of 29.6 ft compares well with the observed value of 27.0 ft. The value computed directly by CURLS was 29.0 ft.

10. Data to construct influence charts for other values of A and η can be computed using CURLS as described in Appendix C. However, values of $\Delta u/\gamma_t t$ for various values of r/z and A are tabulated in Table B1 and plotted in Figure B4. Also shown in Table B1 are values of $\Delta\sigma_v$ for various r/z ratios. Thus, these data can be used to construct influence charts for computing vertical stresses.

Table B1

$\Delta u/\gamma_t t$ Values for Selected r/z Ratios and A Parameters

r/z	0.33	0.50	0.55	0.60	0.65	0.70	0.75	1.00	$\Delta\sigma_v$
0.2	2.1	3.1	3.3	3.6	3.9	4.2	4.5	5.9	5.92
0.4	7.2	10.3	11.3	12.2	13.1	14.1	15.0	19.8	19.77
0.8	18.6	26.1	28.3	30.6	32.8	35.1	37.3	48.5	48.52
1.6	35.2	46.1	49.4	52.7	56.0	59.2	62.5	78.9	78.94
3.2	54.0	64.2	67.3	70.3	73.4	76.4	79.5	94.8	94.80
6.4	70.5	77.7	79.8	82.0	84.1	86.3	88.4	99.1	99.12
12.8	81.1	85.8	87.2	88.6	90.0	91.4	92.8	99.9	99.86
25.6	86.7	90.0	91.0	92.0	93.0	94.0	95.0	100.0	99.96
51.2	89.6	92.2	93.0	93.8	94.5	95.3	96.1	100.0	99.97
102.4	91.1	93.3	94.0	94.6	95.3	96.0	96.6	100.0	99.98

Note: B = 1.0 , η = 2.5 , ν_1 = 0.2 , and ν_2 = 0.1 .

$\Delta u/\gamma_t t$ is in percent; σ_v is in pounds per square foot.

Example:

For r/z = 3.2 , A = 0.70

$\Delta u/\gamma_t t$ = 76.4 percent.

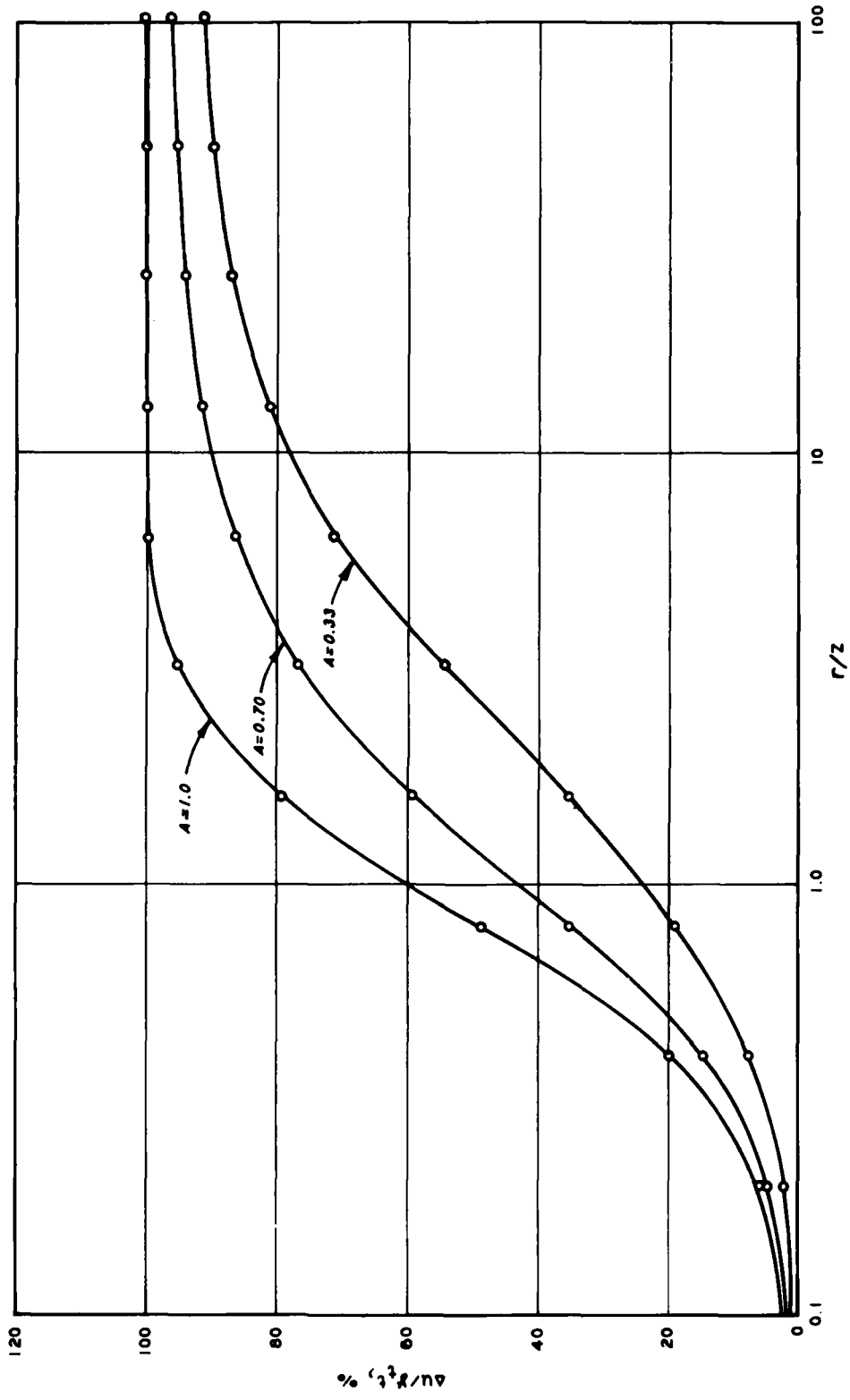

Figure B4. $\Delta u/\gamma_t$ values versus r/z ratios for values of the pore pressure A parameter, $\eta = 2.5$

APPENDIX C: COMPUTER PROGRAM CURLS

1. This appendix presents input instructions and computer code for the program CURLS with examples of its use. The code is documented with the appropriate equation numbers as found in Appendix B. The computer program can be used either for determination of pore-water pressure induced by an embankment load or to produce the information necessary for construction of an influence chart.

Input Instructions

* Card 1 (8A8)		
Col 5-69:	Title	Any information that is to be printed as a title for the influence chart or problem analysis
* Card 2 (free format)		
	ITYPE	Type of problem: 0 - problem analysis 1 - influence chart
* Card 3 (free format)		
	XN	Ratio of the horizontal modulus to the vertical modulus (see paragraphs 39 and 54)
* Card 4 (free format)		
	A	Value of Skempton's A parameter
	B	Value of Skempton's B parameter
Card 5 (free format)		
	PX	x coordinate of point where pore pressure prediction is to be computed (feet)
	PY	y coordinate of point where pore pressure prediction is to be computed (feet)
	PZ	Elevation of point where pore pressure prediction is to be computed (feet)

* Only cards 1-4 are needed to obtain data for the influence chart.

Card 6 (free format)

GAMMA	Total unit weight of fill material (pounds per cubic feet)
NTIMES	Total number of fill increments (integer)

* Card 7 (I5)

NAREA	Number of fill areas per fill increment

** Card 8 (free format)

XYH(1,1) XYH(1,2) XYH(1,3) XYH(1,4)	X coordinates of a quadrilateral fill area input in a clockwise direction

** Card 9 (free format)

XYH(2,1) XYH(2,2) XYH(2,3) XYH(2,4)	Y coordinates of a quadrilateral fill area input in a clockwise direction

** Card 10 (free format)

XYH(3,1) XYH(3,2) XYH(3,3) XYH(3,4)	Height of fill at each corner of a quadrilateral fill area input in a clockwise direction

** Card 11 (free format)

GRADE	Grade elevation before placement of fill increment (feet)

* Card 7 is repeated for each fill increment (see input data for field problem).

** Cards 8-11 are repeated for each fill area per fill increment (see input data for field problem).

AD-A121 448 ENGINEERING PROPERTIES OF CLAY SHALES REPORT 4 2/2
LABORATORY AND COMPUTATION.. (U) ARMY ENGINEER WATERWAYS
EXPERIMENT STATION VICKSBURG MS D A LEAVELL ET AL.
UNCLASSIFIED SEP 82 WES/TR/S-71-6-4 F/G 8/13 NL

END

FILMED
DTIC

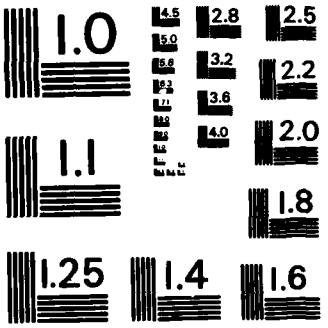

MICROCOPY RESOLUTION TEST CHART
NATIONAL BUREAU OF STANDARDS-1963-A

Recommended Material Parameters

(Prespecified in Program)

XMU = 0.2 — Poisson's coefficient in the plane of isotropy in a transversely isotropic material (line 220)

XMU1 = 0.1 — Poisson's coefficient transverse to the plane of isotropy in a transversely isotropic material (line 230)

Computer-Unique Variables

NF — The unit that the computer reads input data from (line 260)

LNB — Sequential data line numbers (located in each read statement)

Program Listing

```
C       ************************************************
C       *                                              *
C       *                    CURLS                     *
C       *                                              *
C       *     PROGRAM TO DETERMINE P.W.P. INDUCED IN   *
C       *     A FLAT LYING, LAYERED MATERIAL DUE TO    *
C       *     EMBANKMENT LOADING. PREPARED BY J.F.     *
C       *     PETERS AT THE U.S.A.E. WATERWAYS EX-     *
C       *     PERIMENT STATION, VICKSBURG, MS. 1981    *
C       *                                              *
C       ************************************************
C
      DIMENSION STATE(50),WAIT(50),XYH(3,4),FACT(4)
      COMMON /PROP/GAMMA,A,B,IS0,XN,XMU,XMU1
C
      CHARACTER FNA(4) /'/   ',33','33',' ; '/
      CHARACTER TITLE(10)
C
C SAMPLING POINTS AND WEIGHTING FACTORS FOR EQ. B8
      DATA STATE /0.032380,0.097005,0.161222,0.224764,0.287362
     &,0.348756,0.408686,0.466903,0.523161,0.577225,0.629867,0.677872,
     & 0.724034,0.767159,0.807066,0.843588,0.8765720,0.905879,
     & 0.931387,0.952988,0.970592,0.984125,0.993530,0.998771,26*0.0/
C
      DATA WAIT /0.064738,0.064466,0.063924,0.063114,0.062039,
     & 0.060704,0.059115,0.057277,0.055200,0.052890,0.050359,0.047617,
     & 0.044675,0.041545,0.038241,0.034777,0.031167,0.027427,0.023571,
     & 0.019616,0.015579,0.011477,0.007328,0.003153,26*0.0/
C
C PROGRAM VERSION FOR HONEYWELL SERIES 60 LEVEL 66, TSS
C RECOMMENDED MATERIAL PARAMETERS
      XMU= 0.2
      XMU1= 0.1
C
C PROGRAM READS FROM UNIT 12
      NF=12
C
C THE VARIABLE LNB IS THE DATA SET LINE NUMBER
C
C***********
C FOLLOWING USED TO RUN FROM TIME SHARING
C SET UP ACCESS  TO FILE
      PRINT, 'WHAT IS YOUR DATA FILE NAME?'
      READ 1492,FNA(2),FNA(3)
 1492 FORMAT(2A4)
      CALL ATTACH(12,FNA,3,0,ISTAT,)
      CALL FPARAM(1,132)
C***********
C
C FILL IN OTHER HALF OF ARRAY
```

```
510           N12=24
520           N=2*N12
530           DO 2 I=1,N12
540              WAIT(I+N12)=WAIT(I)
550              STATE(I+N12)=-STATE(I)
560 2         CONTINUE
570C
580 9999   FORMAT(//)
590 1000   FORMAT(V)
600C
610        WRITE(6,9999)
620        READ(NF,1100) LNB,(TITLE(I),I=1,8)
630        WRITE(6,1200) (TITLE(I),I=1,8)
640 1100   FORMAT(I4,8A8)
650 1200   FORMAT(1X,66("*")/,1X,"*",64X,"*"/,1X,"*",8A8,"*"/,1X,
660&       "*",64X,"*"/,1X,66("*"))
670        READ(NF,1000) LNB,ITYPE
680        READ(NF,1000) LNB,XN
690        ISO= 0
700        XB= ABS(XN-1)
710        IF(XB.GT.0.001) ISO= 1
720        READ(NF,1000) LNB,A,B
730C
740C CHECK FOR TYPE OF PROBLEM
750        IF(ITYPE.GT.0) GO TO 6
760C
770C DATA FOR FILL
780        READ(NF,1000) LNB,PX,PY,PZ
790        READ(NF,1000) LNB,GAMMA,NTIMES
800        WRITE(6,9999)
810        WRITE(6,2000) PX,PY,PZ
820        WRITE(6,3100) GAMMA,A,B
830        IF(ISO.EQ.0) WRITE(6,2100)
840        IF(ISO.GT.0) WRITE(6,2200) XN
850        WRITE(6,4000) NTIMES
860        WRITE(6,4001)
870        GO TO 7
880C
890C DATA FOR INFLUENCE CHART
900 6      PX=0.0
910        PY=0.0
920        PZ=0.0
930        NTIMES= 17
940        GAMMA=1.0
950        WRITE(6,9999)
960        WRITE(6,3000) A,B
970        IF(ISO.EQ.0) WRITE(6,2100)
980        IF(ISO.GT.0) WRITE(6,2200) XN
990        WRITE(6,9999)
```

```
1000        WRITE(6,4050)
1010        WRITE(6,4100)
1020C
1030C**********
1040C BEGIN LOOP FOR TIME
1050C
1060        XM= 0.0
1070        NAREA=1
1080 7      CONTINUE
1090C
1100        TPWP= 0.0
1110        THEAD= 0.0
1120        TSV= 0.0
1130        DO 45 IT=1,NTIMES
1140C CHECK FOR TYPE OF PROBLEM
1150        IF(ITYPE.GT.0) GO TO 11
1160C
1170C DATA FOR FILL
1180        READ(NF,1000) LNB,NAREA
1190C
1200 11         PWP = 0.0
1210               SV=0.0
1220            DO 5 KOUNT=1,NAREA
1230C
1240C CHECK FOR PROBLEM TYPE
1250        IF(ITYPE.EQ.0) GO TO 9
1260C
1270C CALCULATE DATA FOR INFLUENCE CHART
1280        IF(XM.LT.1.0) XINC= 0.1
1290        IF(XM.GE.1.0) XINC= XM
1300        XM= XM+XINC
1310        IF(XM.GT.100.0) XM= 100.0
1320           XYH(1,1)=0.0
1330           XYH(1,2)=-0.1736*XM
1340           XYH(1,3)=0.0
1350           XYH(1,4)=-XYH(1,2)
1360           XYH(2,1)=0.0
1370           XYH(2,2)=0.9848*XM
1380           XYH(2,3)=XM
1390           XYH(2,4)=XYH(2,2)
1400C
1410C 1800.0 GIVES FACTORS IN % OF GAMMA*H
1420              DO 12 I=1,4
1430                 XYH(3,I)=1800.0
1440 12           CONTINUE
1450C
1460C VARIABLE XM EQUALS R/Z
1470              GRADE = 1.0
1480        GO TO 8
1490C
```

```
1500C READ DATA FOR EACH AREA OF FILL FOR TIME IT
1510 9      CONTINUE
1520              DO 10 I=1,3
1530                READ(NF,1000) LNB,(XYH(I,J),J=1,4)
1540 10           CONTINUE
1550              READ(NF,1000) LNB,GRADE
1560 8      CONTINUE
1570C
1580C BEGIN GAUSS INTEGRATION
1590C
1600C DOUBLE SUMMATION, EQ. B8
1610              DO 20 K=1,N
1620              DO 20 L=1,N
1630                 XI=STATE(K)
1640                 ETA=STATE(L)
1650C FACT IS INTERPOLATION FACTOR NI(S,T); EQ. B6
1660                 FACT(1)=(1.-XI)*(1.+ETA)*0.25
1670                 FACT(2)=(1.+XI)*(1+ETA)*0.25
1680                 FACT(3)=(1.+XI)*(1.-ETA)*0.25
1690                 FACT(4)=(1.-XI)*(1.-ETA)*0.25
1700C
1710C COMPUTE X,Y, AND H AT EACH INTEGRATION STATION.
1720C USE EQ. B6
1730                 X=0.
1740                 Y=0.
1750                 H=0.
1760                 DO 30 I=1,4
1770                    X=X + XYH(1,I)*FACT(I)
1780                    Y=Y + XYH(2,I)*FACT(I)
1790                    H=H + XYH(3,I)*FACT(I)
1800 30              CONTINUE
1810C
1820C COMPUTE P.W.P DUE TO UNIT LOAD AT STATION(K,L)
1830C
1840                 CALL PRES(X,Y,H,PX,PY,PZ,GRADE,DELU,SIGZ)
1850C
1860C COMPUTE JACOBIAN AT STATION(K,L)
1870C
1880                 ALLX=XYH(1,2)+XYH(1,4)-XYH(1,1)-XYH(1,3)
1890                 ALLY=XYH(2,2)+XYH(2,4)-XYH(2,1)-XYH(2,3)
1900C
1910                 XXI=XYH(1,2)+XYH(1,3)-XYH(1,1)-XYH(1,4)+ETA*ALLX
1920                 YXI=XYH(2,2)+XYH(2,3)-XYH(2,1)-XYH(2,4)+ETA*ALLY
1930                 XETA=XYH(1,1)+XYH(1,2)-XYH(1,3)-XYH(1,4)+XI*ALLX
1940                 YETA=XYH(2,1)+XYH(2,2)-XYH(2,3)-XYH(2,4)+XI*ALLY
1950C
1960                 XJAKE=XXI*YETA-XETA*YXI
1970                 XJAKE=0.0625*XJAKE
1980C
```

```
1990C ADD INTO WEIGHTED SUM FOR INTEGRAL EVALUATION.
2000C
2010                SV=SV + SIGZ*XJAKE*WAIT(K)*WAIT(L)
2020                PWP=PWP + DELU*XJAKE*WAIT(K)*WAIT(L)
2030 20          CONTINUE
2040 5        CONTINUE
2050           HEAD=0.016*PWP
2060C WRITE OUT RESULT
2070          IF(ITYPE.GT.0) WRITE(6,4200) XM,PWP,SV
2080          IF(ITYPE.EQ.0) WRITE(6,5000) IT,NAREA,PWP,HEAD,SV
2090C
2100C SUM VARIABLES PWP, HEAD AND SV
2110        TPWP= TPWP+PWP
2120        THEAD= THEAD+HEAD
2130        TSV= TSV+SV
2140 45    CONTINUE
2150C
2160C WRITE OUT SUMMATION OF PWP, HEAD AND SV
2170        IF(ITYPE.EQ.0) WRITE(6,4300) TPWP,THEAD,TSV
2180C
2190C**************
2200 2000   FORMAT(1X,'PORE PRESSURE INDUCED AT
2210& LOCATION X= ',F10.2,' FT.  Y= ',F10.2,' FT.'/,5X,'AT ELEVATION= ',
2220& F8.2,' FT.')
2230 2100   FORMAT(1X,'MATERIAL TYPE= ISOTROPIC')
2240 2200   FORMAT(1X,'MATERIAL TYPE= ANISOTROPIC, N= ',F5.2)
2250 3000   FORMAT(1X,'A PARAMETER= ',F5.3/,1X,'B PARAMETER= ',F5.3)
2260 3100   FORMAT(1X,'UNIT WEIGHT OF FILL= ',F7.1,' LB/CF'/,1X,
2270&       'A PARAMETER= ',F5.3/,1X,'B PARAMETER= ',F5.3)
2280 4000   FORMAT(1X,'COMPUTATION FOR', I5,' TIME INCREMENTS'//)
2290 4001   FORMAT(3X,'TIME',5X,'NUMBER OF',7X,'PORE',8X,'STATIC',4X,
2300&       'VERTICAL'/,1X,'INCREMENT',2X,'FILL AREAS',2X,'PRESSURE(PSF)'
2310&       ,2X,'HEAD(FT)',2X,'STRESS(PSF)'/,1X,9('-'),2X,10('-'),2X,
2320&       13('-'),2X,8('-'),2X,11('-'))
2330 4050   FORMAT(12X,'INFLUENCE FACTORS(% OF GAMMA*H)'/,12X,31('-')/)
2340 4100   FORMAT(3X,'R/Z',5X,'PORE PRESSURE',5X,'VERTICAL STRESS'/,
2350&       2X,5('-'),4X,13('-'),5X,15('-'))
2360 5000   FORMAT(1X,I6,5X,I6,9X,F7.1,6X,F7.2,4X,F7.1)
2370 4200   FORMAT(1X,F6.1,7X,F6.1,13X,F7.2)
2380 4300   FORMAT(24X,13('-'),2X,8('-'),2X,11('-')/,16X,'TOTAL=',
2390&       4X,F8.1,7X,F6.2,3X,F8.1)
2400        STOP
2410        END
2420C
2430C********** SUBROUTINE PRES **********
2440C
2450        SUBROUTINE PRES(X,Y,H,PX,PY,PZ,GRADE,DELU,SIGZ)
2460C
2470C  SUBROUTINE TO  FIND P.W.P INDUCED IN A TRANSVERSELY ANISOTROPIC
2480C CLAY SHALE DUE TO UNIFORM LOAD ON UNIT AREA.
```

```
2490C
2500        COMMON /PROP/GAMMA,A,B,ISO,XN,XMU,XMU1
2510        REAL*4 LANDA
2520C
2530C
2540C COMPUTE COMMON FACTORS
2550C
2560        SMALR=(X-PX)*(X-PX) + (Y-PY)*(Y-PY)
2570        Z=ABS(GRADE-PZ)
2580        R=SMALR + Z*Z
2590        R=SQRT(R)
2600        SMALR=SQRT(SMALR)
2610        RATIO=SMALR/Z
2620C
2630C USE BOUSSINESQ EQ. B3
2640C
2650        Q=H*GAMMA*0.1591549
2660C
2670        IF(ISO.EQ.1) GO TO 10
2680        LANDA=3.0*Q*(Z*Z/R**5)
2690        SIGZ=LANDA*Z
2700        TAU=LANDA*SMALR
2710        AVE=SIGZ*(3.0*SMALR*SMALR-R*R*(1.0-2.0*XMU))/(6.0*Z*Z)
2720        GO TO 20
2730C
2740C USE ANISOTROPIC EQUATIONS FROM LEKHNITSKII; EQ. B5
2750 10     CONTINUE
2760        X1=-XMU1*(1.0+XMU)/(1.0-XN*XMU1**2)
2770        X2=(1.0-XMU**2)/(XN*(1.0-XN*XMU1**2))
2780        X3=(0.4*XMU1*(1.0+XMU)+1.0)/(0.4*(1.0-XN*XMU1**2))
2790        X0=(XMU*XN*(XMU1-2.5)+XMU)/(1.0-XN*XMU1**2)
2800        S3=SQRT((X1+X3)**2-4.0*X2)
2810        S1=SQRT((X1+X3+S3)/(2.0*X2))
2820        S2=SQRT((X1+X3-S3)/(2.0*X2))
2830        Q1=(X0-X1*S2**2)*(1.0-X1*S1**2)
2840        Q2=(X0-X1*S1**2)*(1.0-X1*S2**2)
2850        X9=(SMALR*SMALR+S1*S1*Z*Z)**1.5
2860        X6=(SMALR*SMALR+S2*S2*Z*Z)**1.5
2870C
2880        SIGZ=(Q*Z/((S1-S2)*SQRT(X2)))*(1.0/X9-1.0/X6)
2890        AVE=-Q*0.5*Z*((SQRT(X2)/(X1*X3-X2))*(1.0/(S1-S2))*(-S1*S1*Q2/X9
2900&       +S2*S2*Q1/X6)+(1.0/((S1-S2)*SQRT(X2)))*(S1*S1/X9-S2*S2/X6))
2910C
2920C LEKHNITSKII ASSUMED COMPRESSION TO BE NEGATIVE; SO ........
2930        SIGZ=-SIGZ
2940        AVE=-AVE
2950 20     CONTINUE
2960C
2970C COMPUTE PORE PRESSURE INCREMENT FROM EQ. B4
2980        DELU=B*(AVE + A*(SIGZ-AVE))
2990        RETURN
3000        END
```

Input data for field problem

```
10          EXAMPLE PROBLEM FROM HILLSDALE DAM - TEST BERM
20 0
30 2.5
40 0.7 .999
50 1380 350 844.1
60 126.0 7
70 3
80 0.0 125.0 185.0 185.0
90 240.0 490.0 550.0 115.0
100 3.0 3.0 3.0 3.0
110 879.0
120 185.0 185.0 1650.0 1650.0
130 115.0 550.0 560.0 125.0
140 3.0 3.0 3.0 3.0
150 879.0
160 1650.0 1650.0 1680.0 1760.0
170 125.0 560.0 500.0 250.0
180 3.0 3.0 3.0 3.0
190 879.0
200 3
210 10.0 135.0 185.0 185.0
220 240.0 490.0 535.0 135.0
230 5.0 5.0 5.0 5.0
240 882.0
250 185.0 185.0 1650.0 1650.0
260 135.0 535.0 540.0 140.0
270 5.0 5.0 5.0 5.0
280 882.0
290 1650.0 1650.0 1680.0 1760.0
300 140.0 540.0 500.0 250.0
310 5.0 5.0 5.0 5.0
320 882.0
330 3
340 40.0 160.0 185.0 185.0
350 240.0 490.0 515.0 150.0
360 4.0 4.0 4.0 4.0
370 887.0
380 185.0 185.0 1650.0 1650.0
390 150.0 515.0 520.0 160.0
400 4.0 4.0 4.0 4.0
410 887.0
420 1650.0 1650.0 1665.0 1740.0
430 160.0 520.0 500.0 250.0
440 4.0 4.0 4.0 4.0
450 887.0
460 3
470 60.0 180.0 185.0 185.0
480 240.0 490.0 500.0 165.0
490 5.0 5.0 5.0 5.0
500 891.0
```

```
510 185.0 185.0 1650.0 1650.0
520 165.0 500.0 505.0 175.0
530 5.0 5.0 5.0 5.0
540 891.0
550 1650.0 1650.0 1655.0 1730.0
560 175.0 505.0 500.0 250.0
570 5.0 5.0 5.0 5.0
580 891.0
590 3
600 80.0 185.0 185.0 185.0
610 240.0 445.0 445.0 180.0
620 2.0 2.0 2.0 2.0
630 896.0
640 185.0 185.0 1650.0 1650.0
650 180.0 445.0 450.0 185.0
660 2.0 2.0 2.0 2.0
670 896.0
680 1650.0 1650.0 1650.0 1715.0
690 185.0 450.0 450.0 250.0
700 2.0 2.0 2.0 2.0
710 896.0
720 3
730 90.0 185.0 185.0 185.0
740 240.0 420.0 420.0 185.0
750 4.0 4.0 4.0 4.0
760 898.0
770 185.0 185.0 1650.0 1650.0
780 185.0 420.0 430.0 190.0
790 4.0 4.0 4.0 4.0
800 898.0
810 1650.0 1650.0 1650.0 1705.0
820 190.0 430.0 430.0 250.0
830 4.0 4.0 4.0 4.0
840 898.0
850 6
860 120.0 185.0 185.0 185.0
870 240.0 390.0 390.0 240.0
880 0.0 0.0 0.0 14.0
890 902.0
900 185.0 185.0 1650.0 1650.0
910 240.0 390.0 395.0 250.0
920 14.0 0.0 0.0 14.0
930 902.0
940 1650.0 1650.0 1650.0 1695.0
950 250.0 395.0 395.0 250.0
960 14.0 0.0 0.0 0.0
970 902.0
980 1650.0 1650.0 1650.0 1695.0
990 205.0 250.0 250.0 250.0
1000 0.0 14.0 14.0 0.0
```

```
1010 902.0
1020 185.0 185.0 1650.0 1650.0
1030 200.0 240.0 250.0 205.0
1040 0.0 14.0 14.0 0.0
1050 902.0
1060 120.0 185.0 185.0 185.0
1070 240.0 240.0 240.0 200.0
1080 0.0 14.0 14.0 0.0
1090 902.0


*
```

Output data for field problem

```
**************************************************************************
*                                                                        *
*        EXAMPLE PROBLEM FROM HILLSDALE DAM - TEST BERM                  *
*                                                                        *
**************************************************************************


PORE PRESSURE INDUCED AT LOCATION X=    1380.00FT.  Y=     350.00 FT.
    AT ELEVATION=   844.10 FT.
UNIT WEIGHT OF FILL=   126.0 LB/CF
A PARAMETER= 0.700
B PARAMETER= 0.999
MATERIAL TYPE= ANISOTROPIC, N=  2.50
COMPUTATION FOR    7 TIME INCREMENTS
```

TIME INCREMENT	NUMBER OF FILL AREAS	PORE PRESSURE(PSF)	STATIC HEAD(FT)	VERTICAL STRESS(PSF)
1	3	351.6	5.63	398.0
2	3	571.2	9.14	651.5
3	3	440.5	7.05	509.6
4	3	535.0	8.56	627.3
5	3	200.1	3.20	241.5
6	3	383.0	6.13	468.1
7	6	450.5	7.21	541.1
	TOTAL=	2931.9	46.91	3437.1

Input data for influence chart

```
10        EXAMPLE PROBLEM FOR PRODUCING INFLUENCE CHART FACTORS
20 1
30 1.0001
40 .7 .999
```

Output data for influence chart

```
**************************************************************************
*                                                                        *
*      EXAMPLE PROBLEM FOR PRODUCING INFLUENCE CHART FACTORS             *
*                                                                        *
**************************************************************************

A PARAMETER= 0.700
B PARAMETER= 0.999
MATERIAL TYPE= ISOTROPIC
```

	INFLUENCE FACTORS(% OF GAMMA*H)	
R/Z	PORE PRESSURE	VERTICAL STRESS
0.1	1.0	1.47
0.2	3.8	5.68
0.3	8.1	12.07
0.4	13.5	19.87
0.5	19.3	28.33
0.6	25.3	36.81
0.7	31.1	44.87
0.8	36.5	52.23
0.9	41.5	58.78
1.0	45.9	64.49
2.0	69.8	90.98
4.0	81.4	98.54
8.0	86.3	99.78
16.0	88.6	99.95
32.0	89.8	99.97
64.0	90.3	99.97
100.0	90.5	99.97

In accordance with letter from DAEN-RDC, DAEN-ASI dated 22 July 1977, Subject: Facsimile Catalog Cards for Laboratory Technical Publications, a facsimile catalog card in Library of Congress MARC format is reproduced below.

Leavell, Daniel A.
Engineering properties of clay shales : Report 4 : laboratory and computational procedures for predictions of pore pressures in clay shale foundations / by Daniel A. Leavell, John F. Peters, Frank C. Townsend (Geotechnical Laboratory, U.S. Army Engineer Waterways Experiment Station). -- Vicksburg, Miss. : The Station ; Springfield, Va. ; available from NTIS, 1982.
104 p. in various pagings : ill. ; 27 cm. -- (Technical report ; S-71-6, Report 4)
Cover title.
"September 1982."
"Prepared for Office, Chief of Engineers, U.S. Army under CWIS 31244."
Bibliography: p. 57-58.

1. Clay shales. 2. Foundations. 3. Shales. 4. Soils--Testing. I. Peters, John F. II. Townsend, Frank C. III. United States. Army. Corps of Engineers. Office of the Chief of Engineers. IV. U.S. Army

Leavell, Daniel A.
Engineering properties of clay shales : ... 1982.
(Card 2)

Engineer Waterways Experiment Station. Geotechnical Laboratory. V. Title VI. Series: Technical report (U.S. Army Engineer Waterways Experiment Station) ; S-71-6, Report 4.
TA7.W34 no.S-71-6 Report 4